CHAPTER 3

CEY-1 attenuates *let-7* microRNA-mediated gene silencing in *C. elegans*

AUTHORS

Alessi AF, Khivansara K, Han T, Freeberg MA, Montoye E, Karp X, and Kim JK

AUTHOR CONTRIBUTIONS

AFA and JKK contrived all experiments. AFA prepared all text. TH designed and performed CEY-1 HITS-CLIP. MAF performed computational analysis for HITS-CLIP. DY and MAF provided HITS-CLIP experimental methods. VK performed CEY-1 RIPs. XK and EM designed and performed *mir-48 mir-241* assay and post-dauer assays. AFA performed all other experiments.

ABSTRACT

MicroRNAs (miRNAs) function in the miRNA-induced silencing complex (miRISC) to trigger translational repression and destabilization of target mRNAs. The miRISC is guided to targets by its bound miRNA that binds to partially complementary sequences in target 3'UTRs. Recent studies suggest miRISC activity is modulated by accessory factors, including RNA binding proteins that affect miRISC binding to its targets. Here we report that the conserved RNA binding protein, CEY-1 (*C. elegans* Y-box protein-1), is a negative regulator of the *let-7* miRNA gene silencing pathway. *let-7* is a broadly conserved miRNA that regulates cellular differentiation in animals. *C. elegans let-7* controls developmental timing, including temporal specification of cell fate. Using a

genetic approach, we discovered loss of *cey-1* potently suppresses both the hypodermal seam cell hyperplasia and the highly penetrant, lethal vulval defects of *let-7* hypomorphic mutants. Intriguingly, loss of *cey-1* does not suppress defects associated with loss of a panel of other miRNAs, including the highly similar *let-7* family miRNAs. However our data suggest that, unlike its well-characterized paralog, LIN-28, which specifically acts to negatively regulate *let-7* biogenesis, the function of CEY-1 in the *let-7* miRNA pathway may interfere with *let-7* miRISC target silencing. Specifically, loss of *cey-1* in *let-7* mutants suppresses up-regulation of the key *let-7* target, *lin-41*, but does not increase mature *let-7* levels, indicating CEY-1 antagonizes *let-7* miRISC activity, not *let-7* biogenesis. Furthermore, RNA immunoprecipitation (RIP) of CEY-1 recovers *lin-41* transcripts and high-throughput sequencing of RNA isolated by crosslinking and immunoprecipitation (HITS-CLIP) identifies CEY-1 binding sites in the 3'UTRs of *let-7* target mRNAs. Taken together, our data suggest a model in which mRNA binding by CEY-1 antagonizes *let-7*-mediated silencing by attenuating *let-7* miRISC activity.

INTRODUCTION

MiRNAs are a conserved family of ~22 nt non-coding RNAs that post-transcriptionally regulate genes involved in fundamental biological processes, such as developmental timing, organogenesis, body patterning, stem cell maintenance and differentiation [1,2,3]. The majority of miRNAs are transcribed by RNA Polymerase II and successively processed into their precursor and mature forms by the RNase III enzymes Drosha and Dicer, respectively [4,5]. Mature miRNAs are incorporated into the miRNA-induced silencing complex (miRISC), which minimally contains a core miRNA-binding Argonaute

protein and a GW182 family protein. In animals, mature miRNAs guide miRISC to mRNAs in a sequence-specific manner by base pairing to partially complementary sequences that are located in the 3'UTR of target mRNAs [6,7]. It is through association with miRISC that miRNAs elicit translational repression and degradation of target mRNAs through miRISC interaction with co-factors and downstream effectors involved in these processes [3,8].

In *C. elegans, alg-1/-2* [9,10] and *ain-1/-2* [11,12] encode the core miRISC Argonaute and GW182 proteins, respectively. Additional conserved miRISC co-factors facilitate miRISC activity, including the fly Vasa Intronic Gene ortholog, VIG-1, and the Tudor domain protein, TSN-1, which were shown to be required for silencing of a *let-7* target 3' UTR reporter [13]. The DEAD-box RNA helicase CGH-1, and the TRIM-NHL ubiquitin ligase NHL-2, were also demonstrated to be required for effective miRISC silencing and are thought to function by promoting miRISC interaction with targets [14]. The human ortholog of CGH-1, DDX6, has been shown to promote miRISC by interaction with the CCR4-NOT deadenylase complex and mRNA degradation machinery [15,16,17].

While the mechanisms of miRNA biogenesis and target silencing have been extensively characterized, regulation of mRNA silencing activity, specifically regulation of miRISC is less well understood. Recent studies suggest miRISC activity is modulated by RNA binding proteins (RBP). RBPs can indirectly alter miRISC function by affecting mRNA stability, degradation, and translation, or function directly, affecting miRISC target binding or interactions with downstream effectors, like translational repressors, deadenylation and/or decapping factors [18]. Notably, FMRP (fragile X mental

retardation protein) [19,20], and the Pumillio protein PUM1 [21] have been shown to promote miRISC silencing, while DND1 (DND microRNA-mediated repression inhibitor 1) [22] and HuR/ELAV [23,24] antagonize miRISC silencing.

This chapter will describe work characterizing the role of the *C. elegans* cold-shock domain/Y-box protein, CEY-1, in antagonizing *let-7* microRNA silencing. Genetic and molecular data that suggest that CEY-1 mRNA binding uniquely antagonizes *let-7* miRNA-mediated silencing by limiting *let-7* miRISC function, a previously unknown interface between cold-shock domain/Y-box proteins and miRNA silencing in the context of *C. elegans* development.

RESULTS

CEY-1 is a member of the conserved Y-box binding/Cold-Shock Domain family of proteins

The cold-shock domain (CSD) represents one of the most highly conserved protein domains, retaining ~40% amino acid identify and ~60%, similarity from bacteria to vertebrates [25]. The CSD contains characteristic, nucleic acid binding motifs, or RNPs, that are capable of binding of single-stranded RNA and/or DNA [26]. In *C. elegans*, there are five members CSD-containing proteins: four *C. elegans* Y-box proteins, CEY-1 to -4, and LIN-28 (Fig 3-1A).

Y-box proteins (YBP) are a subfamily of CSD-containing proteins, first named for their ability to bind the Y-box DNA motif in vitro [27]. In addition to the CSD, many Y-box proteins have additional motifs including alternating patches of positively and negatively charged amino acids, glycine-rich regions, and arginine/glycine-rich (RG) regions that

are thought to contribute to substrate affinity and specificity [28,29,30] and/or to facilitate protein-protein interactions [31]. Among the CEYs, only CEY-1 and CEY-4 have RG-rich regions (Fig 3-1B). In particular, the C-terminal region of CEY-1 is highly RG-rich, composed of ~27% arginines and ~52% glycines arranged in serial RG and RGG motifs.

YBPs function in a variety of cellular processes that involve the regulation of mRNA stability, translational state, and localization. They are essential for proper gametogenesis, as characterized in a host of model organisms, including YB1 in human [32], YBX2/MSY2 in mouse [33,34], FRGY2 in frog [35], Ypsilon schachtel (Yps) in fly [36], Ybx1 in fish [37], and CEY-2/-3 in worm [38] (Fig 3-1A).

The most thoroughly studied of the *C. elegans* cold-shock domain protein is LIN-28, which has a conserved role in the negative regulation of *let-7* biogenesis [39,40,41,42]. In *C. elegans,* LIN-28 prevents premature accumulation of mature *let-7* in early larval stages by binding to, and stimulating degradation of, the *let-7* precursor RNA [39,40]. LIN-28 differs structurally from the other CEYs, containing a C-terminal CCHC-type zinc finger domain that is required for recognition of the terminal loop of precursor *let-7* [43] (Fig 3-1b). Until recently, little was known about the function of the CEY proteins. A recent publication reported that CEY-2 and CEY-3 are functionally redundant and required for fertility and accumulation of mRNAs in the germline, CEY-1 and CEY-4 have a novel, yet seemingly dispensable, function in promoting accumulation of large polysomes in both the germline and soma [38].

We first identified the CEY proteins through mass spectrometry of immunopurified miRISC (our unpublished data). Since the relationship between miRISC function and RNA binding proteins that modulate miRNA target stability, degradation,

and translation is currently an area of interest in our lab, we investigated whether the CEYs affect miRNA function.

Since miRNA regulation is primarily characterized in the soma, and CEY proteins have known roles in the *C. elegans* germline [38,44], we confirmed somatic expression of the CEYs. We examined the relative somatic expression of each *cey* transcript by comparing its expression in wild-type animals versus those treated with *glp-1* RNAi. *glp-1* encodes a *C. elegans* Notch family receptor [45] required for proliferation and maintenance of germline stem cells [46]. Hence, *glp-1* RNAi severely disrupts early germline development, producing adults that are primarily composed of somatic cells. In agreement with a recent report [38], we find that the highly homologous *cey-2* and *cey-3* (Fig 3-1A-B) are primarily expressed in the *C. elegans* germline, while *cey-1* and *cey-4* expression is highly enriched in the soma (Fig 3-1C).

CEY-1 antagonizes *let-7* miRNA function

To assess if the CEYs impact the miRNA pathway, we began with genetic assays that employ the hypomorphic *let-7* mutation, *let-7(n2853)*. *let-7(n2853)* is a point mutation that alters the mature *let-7* miRNA [2], which destabilizes target interactions and leads to up-regulation of *let-7* targets [47,48]. In *C. elegans, let-7* controls the developmental timing of the transition from the last larval stage (L4) to adult. Consistent with the prominent roles of *let-7* in terminal differentiation of diverse tissues, *let-7* mutants exhibit several well-characterized cell specification defects, including hyperproliferation of hypodermal seam cells and loss of structural integrity of the vulva, which results in animals that herniate and rupture through the vulva (Rup) [2] (Fig 3-2A). *let-(n2853)*

mutants exhibit Rup at nearly 80% penetrance (Fig 3-2B). RNAi of *cey-2, cey-3,* or *cey-4* has no significant effect on Rup, while RNAi of *cey-1* results in a nearly 4-fold suppression of Rup, similar in magnitude to RNAi of the primary *let-7* target *lin-41* [49] (Fig 3-2B). Consistent with suppression of vulval defects, GFP-tagged CEY-1 expresses robustly in the vulva at the L4 stage, as well as in a number of other somatic tissues in which miRNA regulation occurs, including the body muscle and neurons (Fig 3-1D).

To confirm the striking *cey-1* RNAi phenotype, we examined *let-7(n2853)* Rup in two *cey-1* deletion mutants *(tm4347)* and *(ok1805)* (Fig 3-3A). Similar to *cey-1* RNAi, both *cey-1* mutants significantly suppress Rup in *let-7(n2853)* (Fig 3-3B). Concordantly, FLAG::CEY-1 expressed from a single copy integrated transgene generated using Mos1-mediated transgene insertion (MosSCI) [50], significantly rescues the suppression of Rup in *cey-1; let-7* double mutants (indicated as "WT", Fig 3-3C). CEY-1::GFP expressed from an integrated high-copy array (HC) also significantly rescues Rup in *cey-1; let-7* double mutants in a manner dependent on CEY-1::GFP expression (Fig 3-3D). To test the requirement of the RNP motifs and the RG-rich regions of CEY-1 in *let-7* function, we examined the ability of RNPΔ and RGΔ versions of FLAG::CEY-1 to rescue *let-7(n2853)* Rup. Neither the RNPΔ that harbors site specific mutations in both RNP domains of the CSD (Fig 3-3A), nor the RGΔ that has a truncated RG-rich region, rescue Rup suppression in *cey-1; let-7* double mutants (Fig 3-3C), suggesting that both the RNP motifs and RG regions of CEY-1 are required for *let-7* suppression. Stable expression of mutant proteins was confirmed by Western analysis (data not shown).

Next, we examined if loss of *cey-1* also suppressed a *let-7(n2853)* phenotype in another tissue. Hypodermal seam cells are generated through stem cell-like divisions

during larval transitions, terminally differentiating in the adult to yield 16 laterally distributed seam cells on each side of the body [51] that can be visualized using a seam cell-specific GFP reporter [52]. Terminal differentiation of these cells depends on *let-7*. In comparison to wild-type or *cey-1(ok1805)* mutant, both of which exhibit the wild-type number of seam cells, *let-7(n2853*) displays a significantly increased number of seam cells (Fig 3-3E). This seam cell hyperplasia in *let-7* mutants is significantly suppressed by loss of *cey-1*, to a similar degree as RNAi of the *let-7* target *lin-41* (Fig 3-3E).

Taken together, these data indicate that wild-type CEY-1 antagonizes the function of the *let-7* miRNA pathway. Furthermore, CEY-1 transgenic analysis suggests that key domains required for RNA binding and for substrate and/or protein interaction are required for this effect. Since the depletion of CEY-2, CEY-3 and CEY-4 did not have observable phenotypes in our preliminary analyses (Fig 3-2B), we focused our subsequent studies on CEY-1.

cey-1 mutant does not suppress other miRNA mutant phenotypes

Loss of most individual miRNAs in *C. elegans* has no detectable phenotypes [53], suggesting that miRNAs have redundant functions. However, mutants of several well-characterized individual miRNAs or family of miRNAs exhibit robust phenotypes that can be exploited for genetic suppression analyses. To examine if CEY-1 function is specific to the *let-7* pathway or generally antagonizes miRISC function, we explored the affect of *cey-1* depletion in these sensitized mutant backgrounds. To our great surprise, we find that *cey-1* mutants fail to significantly suppress any other miRNA mutant phenotypes that we examined.

miR-1 is a conserved muscle-specific miRNA that regulates targets that affect pre- and post- synaptic function at neuromuscular junctions in *C. elegans*, including subunits of levamisole-sensitive nicotinic acetylcholine receptors [54]. Consequently, the *mir-1(gk276)* loss of function mutant displays resistance to whole-body paralysis induced by the acetylcholine agonist levamisole [54]. Our data suggest that while wild-type and *cey-1* mutants alone display nearly completely penetrant paralysis on levamisole at the terminal assay time point, both *mir-1* mutants and *cey-1; mir-1* double mutants display statistically indistinguishable paralysis resistance (Fig 3-4A). These data suggest CEY-1 does not antagonize miR-1 function at the neuromuscular junction.

Loss of *cey-1* also failed to rescue phenotypes associated with loss of the miRNA *lin-4*. *lin-4* promotes the L1-to-L2 transition through the temporal down-regulation of its target *lin-14* [1]. *lin*-14 encodes a protein which regulates a wide range of developmental events including, stage-specific hypodermal seam cell division and differentiation [55,56], cell division of vulval precursor cells and the competence of these cells to adopt proper vulval cell fate [56], and neuronal remodeling [57]. Thus *lin-4(e912)* null mutants display a variety of phenotypes including “bag of worms” (Bag), in which an improperly formed vulva results in progeny hatching inside of the body of the adult, and an elongated body plan [55,56]. Bag is significantly suppressed in *lin-4(e912)* by *lin-14* RNAi, but not by *cey-1* mutants (Fig 3-4B, Right). Similarly, the elongated body plan of *lin-4(e912)* is qualitatively decreased by *lin-14* RNAi, but not by *cey-1* mutants (Fig 3-4B, Left). These data suggest CEY-1 does not antagonize *lin-4* function.

The miRNA *lsy-6* functions to specify the fate of ASEL, one of two morphologically similar, bilaterally symmetric ASE neurons (ASEL and ASER), which

can be monitored by expression of an ASEL-specific P*lim-6*::*gfp* reporter [58] (image in Fig 3-4C). In both *lsy-6* null and hypomorphic alleles, *(ot71)* and *(ot150),* respectively, loss of *cey-1* fails to significantly alter the penetrance of ASEL mis-specification (Fig 3-4C). Although regulation of *lim-6* expression is downstream of the *lsy-6* target *cog-1*, these data are consistent with CEY-1 not antagonizing the function of *lsy-6* in neuronal specification.

The miR-35 family of miRNAs (miR-35-42) control *C. elegans* embryonic development [53]. Deletion of *miR-35-41* leads to semi-penetrant, temperature-sensitive, late embryonic lethality [53]. First, we confirmed that loss of *cey-1* does not substantially alter embryonic lethality (Emb) by examining baseline levels of Emb in wild-type and *cey-1* mutants (Fig 3-4D). Next, we examined Emb in *miR-35-41(nDf50)* at 20°C and 25°C, and observe no significant change in *miR-35-41* mutants versus *cey-1; miR-35-41* double mutants (Fig 3-4D). In contrast both wild-type and *miR-35-41(nDf50)* animals subjected to *alg-1* RNAi (a positive control for enhanced Emb) display an expected increase in embryonic lethality at 20°C (Fig 3-4D). *miR-35-41(nDf50)* subjected to *alg-1* RNAi at 25°C failed to lay eggs, so Emb could not be scored. These data suggest CEY-1 does not antagonize the function of the miR-35 family in embryonic development.

The mir-51/miR-100 family of miRNAs is also required for embryonic viability in *C. elegans.* Individual deletions of miRNAs in this family are superficially wild-type, but deletions of increasing numbers of the family yield synthetic phenotypes of varying severity, including several deletion combinations that exhibit significant delay the rate of larval development [59]. Three partial deletions of the mir-51/miR-100 family with mild, modest, and severe growth delay were examined for evidence of phenotype

suppression on *cey-1* RNAi versus vector control RNAi. No substantial difference between RNAi conditions was observed (data not shown).

Collectively, genetic analyses using a variety of null and hypomorphic miRNA alleles suggest that CEY-1 does not have any detectable affect on the function several miRNA/miRNA families that mediate a range of biological processes in multiple *C. elegans* tissues.

Loss of *let-7* family activity is differentially suppressed by *cey-1* mutants

Our data indicate that *cey-1* depletion strongly suppresses phenotypes associated with the *let-7(n2853)* mutant but not several other miRNA mutants. We next asked if phenotypic suppression mediated by *cey-1* mutation could suppress phenotypes associated with mutations in other members in the *let-7* family. *C. elegans* has four *let-7* family miRNAs that regulate developmental timing: *let-7* and three "sisters", miR-48, miR-241, and mir-84 [60]. All four share the same seed sequence, conserved in human, with varying degrees of nucleotide conservation outside of the seed (Fig 6A). The *let-7* "sisters" act together to promote the early L2 to L3 larval transition, while *let-7* acts later, promoting the transition from L4 to adult (Fig 1-1B) [61].

First, we examined the ability of *cey-1* mutants to suppress the multiple, ectopic vulva (Muv) phenotype associated with *let-60(ga89),* a gain of function mutation of the miR-84 target *let-60/RAS* [62]. miR-84 regulates vulval precursor cell (VPC) fate specification by attenuating *let-60/RAS* [63,64]. Failure to repress LET-60 activity in specific VPCs leads to vulval cell misspecification and semi-penetrant Muv [63].

Consistent with observations in *let-7(n2853), cey-1* mutants significantly suppress Muv, nearly four fold, versus *let-60(ga89)* alone (Fig 3-5B).

Next, we examined the ability of *cey-1* mutants to suppress semi-penetrant Rup of the *mir-48 mir-241 (nDf51)* mutant. *cey-1; mir-48 mir-241* triple mutants did not significantly suppress Rup compared to the *mir-48 mir-241* mutant (Fig 3-5C). To confirm a lack of suppression, we also examined adult alae defects in the *mir-48 mir-241* mutant. Alae are cuticle protrusions that run longitudinally along the left and right sides of the animals; synthesis of alae in adult animals is dependent on *let-7* family miRNA activity [2,61]. Alae defects in *mir-48 mir-241* mutants can be divided by severity: ~15% of have no alae and ~4% have breaks in alae continuity, called gaps. Comparatively, *cey-1; mir-48 mir-241* triple mutants do not have significantly different proportions of no alae, gapped alae, or total alae defects.

Taken together, these data indicate that loss of *cey-1* differentially suppresses *let-7* sister phenotypes. However, suppression of the *let-60(ga89)* phenotype may be attributed to *let-7* rather than miR-84. Genetic evidence suggests that the miR-84 target *let-60/RAS* may be co-regulated by *let-7,* as RNAi of *let-60/RAS* suppresses the Rup phenotype of *let-7* mutants [63]. Thus, *cey-1* mutants may not suppress *let-7* sister mutant phenotypes since the *cey-1* mutant did not suppress the mutant phenotypes of *mir-48 mir-241.*

***cey-1* mutant does not suppress the *let-7* null mutant**

Considering our differing results among the *let-7* sisters. We decided to examine the effect of *cey-1* depletion in another allele of *let-7*. We chose to examine the *let-*

7(mn112) null [2]. Since *let-7* is essential for viability, the strain carrying *let-7(mn112)* is maintained by a rescue plasmid carrying wild-type copies of *let-7* that partially ameliorate null lethality. Since transmission of the plasmid is less than 100%, and the rescue is not complete (animals exhibit attenuated *let-7* mutant phenotypes), we scored animals with and without the rescue plasmid. As a control, we ran parallel experiments with the hypomorphic *let-7(n2853)* allele. Consistent with previous observations, both *cey-1* and *lin-41* RNAi significantly suppress adult lethality in *let-7(n2853)* (Fig 3-5D). In contrast, only *lin-41* RNAi, not *cey-1* RNAi, significantly suppresses lethality in *let-7(mn112)* that lack the rescue plasmid (Fig 3-5D). Remarkably, *cey-1* RNAi does significantly suppress lethality in *let-7(mn112)* when the mutant harbors the plasmid expressing wild-type *let-7*. Thus, it appears that the *let-7* expressed from the rescue plasmid enables *cey-1* RNAi to suppress *let-7(mn112)* lethality. Based on these data, we hypothesized that suppression of *let-7* mutant phenotypes caused by the loss of *cey-1* may require at least a minimal amount of functional *let-7*. To address this hypothesis we turned to molecular analyses of *let-7* and its targets.

CEY-1 does not negatively affect mature *let-7* accumulation

One explanation of the strong suppression of *let-7* mutant phenotypes only when a minimal amount of *let-7* is present is that CEY-1 acts directly on *let-7* itself. In this case, CEY-1 might function like LIN-28, the single non-CEY, CSD protein in *C. elegans* (Fig 3-1A-B). As previously described, *C. elegans* LIN-28 functions by preventing premature accumulation of mature *let-7* in early larval stages by binding to, and stimulating degradation of, the *let-7* precursor RNA. If, like LIN-28, CEY-1 negatively regulates

precursor *let-7*, we would predict that loss of *cey-1* would result in increased levels of mature *let-7*. During the L3 larval stage, *let-7* rapidly accumulates, reaching its peak levels in L4, when it is most actively silencing targets to promote the L4 to adult transition. Examination of mature *let-7* at four time points during L3 and L4 in both wild-type and *let-7(n2853)* indicate that loss of *cey-1* does not result in a significant increase in *let-7* levels (Fig 3-6). In fact, at late L3 and L4 stages, loss of *cey-1* in *let-7(n2853)* significantly decreases mature *let-7* (Fig 3-6). These data suggest that CEY-1 does not negatively affect the accumulation of mature *let-7*. While measurement of only mature *let-7* does not specifically interrogate accumulation of primary and precursor *let-7* species, these results largely exclude the possibility that CEY-1 acts in concert with LIN-28, or functions to negatively regulate *let-7* biogenesis or stability.

Loss of *cey-1* may attenuate *let-7* target levels at a critical time point

To investigate if CEY-1 might be negatively regulating *let-7* activity, we examined levels of the primary *let-7* target *lin-41* [49]. In wild-type and *cey-1* mutants, *lin-41* is rapidly degraded during the L4 stage (Fig 3-7). In contrast, the *let-7(n2853)* mutant has substantially higher levels of *lin-41* throughout early and mid-L4 stages (Fig 3-7). Interestingly *cey-1; let-7* double mutants have similar *lin-41* profiles to the *let-7* mutant, with the exception of one L4 time point (highlighted, Fig 3-7) where *lin-41* is significantly decreased ~1.6 fold versus the *let-7* mutant alone. These data suggest that loss of *cey-1* may suppress *let-7(n2853)* phenotypes by attenuating the elevated *lin-41* levels in *let-7(n2853)* mutants.

Global Analysis of CEY-1 bound RNAs identifies *let-7* targets

To further explore if and how CEY-1 might be antagonizing *let-7* activity we performed a global analysis of RNAs bound to CEY-1 by High-Throughput Sequencing of RNA isolated by Crosslinking and Immunoprecipitation (HITS-CLIP) (Fig 3-8A). Since our data suggest that the RNA binding capacity of CEY-1 may be important for its function in the miRNA pathway (Fig 3-8C), we reasoned that CEY-1 might affect *let-7* activity by binding to *let-7*-targeted mRNAs. Therefore, we examined CEY-1 binding in L4 stage wild-type and "soma enriched" animals (somatically enriched samples were generated by treating wild-type animals with *glp-1* RNAi to prevent germline proliferation).

In both samples, CEY-1 binds over 6,000 genes, which encompasses approximately a third of the annotated *C. elegans* coding genes expressed at this stage in development [65,66] (Fig 3-8A). Separation of binding sites by functional region suggests that CEY-1 primarily binds coding RNAs in the 3'UTR (45-47%) or exons (46-48%) (Fig. 3-8B-C). Interestingly, while miRNA regulation is thought to occur primarily via binding in the 3'UTR, the miRISC Argonaute, ALG-1, also binds a significant portion of mRNAs in exonic regions, although the functional relevance of this association is unclear [65]. Additionally, CEY-1 binds a large component of non-coding RNAs (Fig 3-8B-C); the majority of these are ribosomal RNAs (~82% in wild-type and ~87% in *glp-1* RNAi).

Consistent with a previous report [38], we did not identify any enriched primary sequence motifs bound by CEY-1 among all binding sites, binding sites only in the 3'UTR, or among *let-7* targets using sequence analysis tools [66,67]. Since bacterial cold shock domain proteins bind RNA to reduce the formation of secondary structure,

we also performed secondary structure predictions on a subset of miRNA targets using RNAfold from the ViennaRNA Package 2.0 [68]. However, these analyses remain inconclusive. We did notice that CEY-1 binding sites appear AU-rich. While further analysis is required to confirm this observation, a host of well-characterized RNA binding proteins engaged in mRNA regulatory functions bind AU-rich elements (ARE), including HuR/ELAV, which affects miRISC binding at co-targeted mRNAs [69,70,71].

To specifically address CEY-1 binding in relationship to the miRNA pathway, we examined CEY-1 binding sites in the 3'UTR of known *let-7* and *let-7* family targets. In both CEY-1 libraries, we identified binding sites in *lin-41, hbl-1, let-60,* and *daf-12* (Fig 3-8D-G). CEY-1 binding sites were also identified in the 3'UTR of miRNA targets for which loss of *cey-1* did not affect the miRNA mutant phenotype, including the mir-1 target, *mef-2*, the *lin-4* target, *lin-14*, and the *lsy-6* target, *cog-1*.

Interestingly, when CEY-1 binding sites are compared to either experimentally derived ALG-1 binding sites [65] or miRNA complementary sequences, there appears to be direct overlap or adjacency with *let-7* binding sites that is not observed in the non-*let-7* targets *mef-2* or *cog-1* (compare Fig 3-8D-G with 3-8H). Binding in *lin-14* is overlapping, however, biologically relevant regulation by *lin-4* occurs before the L4 stage, making the relationship of ALG-1 and CEY-1 binding on this target more difficult to interpret. Although additional analysis is required to confirm the significance of these observations, they are nonetheless intriguing, as recent studies of the miRISC-antagonizing, RNA binding proteins HuR/ELAVL1 and MOV10 suggest that the proximity of RBP and miRISC binding sites can dictate the nature of the RBP's effect on miRISC silencing [20,72,73].

CEY-1 RNA-Immunoprecipitation supports CEY-1 association with *let-7* targets

To validate HITS-CLIP findings on *let-7* targets, we performed CEY-1 RNA-Immunoprecipitation (RIP). The relative enrichment of *lin-41* bound by CEY-1 in L4 stage animals is over 30-fold increased versus *eft-2*, a non-miRNA targeted mRNA expressed at similar levels (Fig 3-9A). Similarly, but less robustly, the *let-7* target *daf-12* is also ~2.6 fold enriched versus *eft-2* (Fig 3-9A).

Next we asked if CEY-1 association with *lin-41* was dependent on key RNA binding residues in the RNP motifs of the cold-shock domain. Consistent with CEY-1 acting as an RNA binding protein, CEY-1 association with *lin-41* in animals expressing only the RNA binding mutant transgene, FLAG::CEY-1 RNPΔ, is decreased over 100 fold versus the wild-type transgene expressed from high or single copy plasmids (Fig 3-9B). Together, these findings suggest that CEY-1 associates with the *let-7* target, *lin-41*, in an RNA binding dependent manner during the critical *let-7* regulatory period in L4 stage.

Validating CEY-1 binding sites

To continue our analysis of CEY-1 binding to *let-7* targets, we have generated *C. elegans* strains that express a *gfp* reporter with a variety of different mutations in the *lin-41* 3'UTR. First, to test if the HITS-CLIP-identified CEY-1 binding sites (CBS) are required for CEY-1 binding and regulation of *lin-41*, we generated CBS mutant reporters (Fig 3-10A). In addition to being a primary *let-7* target, *lin-41* has the advantage of having experimentally validated *let-7* binding sites in the 3'UTR [48]. Therefore, to test

the requirement of *let-7* binding in CEY-1 regulation, we also generated strains carrying reporters with mutagenized *let-7* binding sites, including mutation of the primary regulatory site, LCS1 (Fig 3-10A). We also mutated LCS4 since it is the *let-7* binding site most proximal to the strongest HITS-CLIP identified CBS (Fig 3-10A). Initial analysis of the wild-type *lin-41* reporter versus the LCS1 mutant suggest that the mutant reporter is, less responsive to *let-7* regulation, evidenced by a relative lack of down-regulation by the young adult stage when the wild-type reporter has been substantially repressed (Fig 3-10B). Thus, these reporters may be useful tools to further investigate the dynamics of CEY-1 and *let-7* miRISC interaction on the *lin-41* 3'UTR. Discussion of their use in future studies in elaborated on in CHAPTER 4: Future Directions.

DISCUSSION

Recent studies have identified mRNA binding proteins that affect the ability of the miRNA effector complex, miRISC to effectively silence target mRNAs. Here we characterize the role of *C. elegans* cold-shock domain/Y-box protein, CEY-1, in antagonizing *let-7* miRNA silencing. Genetically, we find that loss of *cey-1,* but not other *ceys,* potently suppresses defects associated with a *let-7(n2853)* hypomorphic mutant. Intriguingly, *cey-1* mutants do not suppress defects associated with loss of a panel of other miRNAs, including the *let-7* sisters *mir-48* and *mir-241*.

Molecular analyses suggest that CEY-1 functions downstream of the cold-shock domain containing protein, LIN-28, which negatively regulates *let-7* biogenesis. Instead, *cey-1* affects *let-7* miRISC target silencing activity: loss of *cey-1* in *let-7(n2853)* does not lead to an increase in mature *let-7* accumulation but attenuates up-regulation of the

primary *let-7* target, *lin-41.* Furthermore, immunopurification of CEY-1 recovers *lin-41* transcripts, and High-Throughput Sequencing of RNA isolated by Crosslinking and Immunoprecipitation (HITS-CLIP) identifies CEY-1 binding sites in the 3'UTRs of *let-7* targets. Taken together, our data suggest a model in which CEY-1 mRNA binding antagonizes *let-7* miRNA-mediated silencing by limiting the activity of *let-7* miRISC.

How does CEY-1 affect *let-7* miRISC silencing?

CEY-1 and CEY-4 globally promote accumulation of somatic mRNAs, facilitate the formation of large polysomes, and may directly promote ribosome formation [38]. In light of these data, a simple model to explain our observations can be invoked: CEY-1 binds *let-7* targets and promotes their stability by preventing miRISC binding. This antagonism could occur directly by CEY-1 binding in the miRISC footprint, and/or indirectly by CEY-1 thwarting miRISC access via promoting polysome formation. In this model, the concurrent loss of *cey-1* and *let-7* balances the up-regulation of *let-7* targets by destabilizing and/or decreasing translation of target transcripts. However this model fails to account for the unique effect that loss of *cey-1* has on *let-7* mutant phenotypes. Our HITS-CLIP data support CEY-1 association with a large pool of transcripts, including a target mRNAs for a number of miRNAs, where the miRNA mutant phenotype is not suppressed by loss of *cey-1* (including miR-1 and target *mef-2*; *lin-4* and target *lin-14*; and *lsy-6* and target *cog-1*) (Fig 3-4A-C, Fig 3-8D-H).

One possibility is that *let-7* target regulation has some unique quality that sensitizes it to loss of *cey-1*. Translational dynamics of *lin-41* during the critical *let-7* regulatory period has been reported to differ from other *let-7* targets. *let-7* regulation occurs in a narrow time window in development. *let-7* activity reaches its peak in the L4

stage when it rapidly down-regulates its targets to promote the L4-to-adult transition [74]. Despite the essential nature of *let-7* down-regulation of *lin-41* activity [49], high-throughput ribosome profiling of *lin-41* suggests that ribosome-protected fragments on *lin-41* remain largely unchanged from L3 to L4, when *lin-41* activity is substantially down-regulated by *let-7* [75]. There is also no indication that *lin-41* translation is reduced by ribosomal drop-off or translational pausing [75]. Ribosome loading on *lin-41* was actually observed to increase ~1.6 fold from L3 to L4. In contrast, two other *let-7* targets, *daf-12* and *hbl-1,* both exhibit decreased ribosome-protected fragments and ribosome loading from L3 to L4. Taken together, these data suggest that regulation of *lin-41* may be particularly sensitive to changes in mRNA stability and translation.

We observe a ~1.6 fold repression of *lin-41* mRNA up-regulation in *cey-1; let-7* double mutants versus the *let-7* mutant alone (Fig 3-7). This upregulation, which is of the same magnitude as the increase in ribosome loading observed on *lin-41* from L3 to L4 in wild-type animals [75], might be accounted for by loss of *cey-1*-mediated polysome formation. But, since *cey-1* mutants do not suppress *let-7* null lethality, it appears that loss of polysome formation cannot singly account for the rescue of *let-7* hypomorphic phenotypes. As *let-7* nulls carrying a partial *let-7* rescue plasmid were phenotypically suppressed by *cey-1* mutants, we hypothesize that some amount of functional *let-7* miRISC is required for the lack of *cey-1* to have a biological effect. Recent reports have indicated that miRISC binding can be compromised by the occupancy of other RBPs [20,72,73]. HITS-CLIP-identified CEY-1 binding sites in *lin-41,* and in other *let-7* targets, are in close proximity to some ALG1-1 binding sites (Fig. 3-8D-G), indicating that loss of CEY-1 binding in *let-7(n2853)* may increase *let-7* miRISC

target accessibility. We propose a model in which loss of *cey-1* in the *let-7* hypomorph exhibits phenotypic suppression when the effect of the loss of *cey-1* on mRNA stability and/or translation is complemented by attenuated, but still effective, *let-7* miRISC activity.

An "observable" effect to accompany the loss of *cey-1* may be context dependent. Thus far, our data suggest that loss of *cey-1* results in a decrease in target mRNA levels, which in some sensitized backgrounds, like *let-7(n2853),* may also result in a decrease in protein levels. Based on this model, we hypothesize that loss of *cey-1* would enhance phenotypes of a hypomorphic allele of *lin-41.* The LIN-41 protein represses adult cell fates until their proper expression time in L4 through negative regulation of LIN-29, a transcription factor that promotes adult cellular fates (Fig 1-1B). Thus, *lin-41* mutants prematurely adopt adult fates, including formation of alae in the L3 stage, due to precocious expression of LIN-29 [74,76]. Unexpectedly, we observe that loss of *cey-1* significantly suppresses precocious alae formation in *lin-41(ma161)* (Fig 3-12). However, if we consider that (1) loss of *cey-1* is not reported to have any effect on global protein level [38], and (2) that we only observe that loss of *cey-1* affects *lin-41* levels when *lin-41* is upregulated and *let-7* miRISC is compromised (*i.e*. in the *let-7(n2853)* hypomorph), then it may be possible that loss of *cey-1* would not effect the expression of the LIN-41 protein in a background where there is low levels of *lin-41* and wild-type miRISC. Likewise, if we consider the scenario of *lin-29* regulation in the *lin-41* mutant, we find the following parallels with *lin-41* up-regulation in *let-7(n2853)*: the post-transcriptional regulator, *let-7* or LIN-41, is below optimum biological concentrations, and the target mRNA, *lin-41* or *lin-29*, respectively, is up-regulated. Based on our model of *let-7*

regulation of *lin-41* in the *cey-1* mutant, we would then hypothesize that in a *cey-1; lin-41* double mutant, *lin-29* levels would be decreased and precocious alae defects suppressed, which is what we observe. Consistent with CEY-1 functioning as an RNA binding protein, both wild-type and soma enriched CEY-1 HITS-CLIP libraries identify CEY-1 binding sites in the *lin-29* mRNA. Thus we propose that the *lin-41(ma161)* phenotype in *cey-1* mutants is not unexpected if one considers that loss of *cey-1* may only have an "observable" effect when the CEY-1 target meets specific context-dependent criteria, which in this case, are partial loss of a negative regulator and/or target mRNA up-regulation during a critical regulatory period.

Consequently, future studies into the mechanism of CEY-1 function and/or validation of potential CEY-1 targets will likely require a sensitized background to detect a physiological or molecular phenotype. Fortunately, our discovery that the loss of *cey-1* is tractable in animals that have reduced *let-7* function provides a genetic background to elucidate the molecular dynamics of CEY-1, miRISC, and the translational machinery.

MATERIALS AND METHODS

Phylogenetic Analysis. Sequences for non-nematode proteins were obtained from uniprot.org, sequences for nematode proteins were obtained from wormbase.org. Sequence alignment and phylogenetic tree (neighbor joining with no distance correction) were constructed using T-Coffee and ClustalW2 Phylogeny (http://www.ebi.ac.uk/Tools/msa/tcoffee/). NJplot (http://pbil.univ-lyon1.fr/software/njplot.html) was used to modify the phylogenetic tree.

***C. elegans* Strains and Maintenance.** All strains used in this study are listed in Table 3-1. *C. elegans* were grown and maintained under standard laboratory conditions [77] except where indicated.

Feeding RNAi. All RNAi clones are from the Ahringer RNAi library [78]. Induced bacterial cultures were fed to synchronized L1s at the indicated temperature.

Phenotypic Assays. All assays conducted with synchronized populations, attained by plating arrested L1s, generated by alkaline-hypochlorite embryo extraction and overnight hatching in M9, unless noted. Vulval rupture (Rup) in *let-7(n2853)* was scored in adults grown at 22.5°C unless indicated. Dauer larvae for post-dauer Rup analysis were selected by 1% SDS incubation from starved stock plates at 15˚C. After SDS selection, dauers were allowed to resume growth on seeded plates and were scored as adults. Adult lethality/Rup in *let-7(mn112)* was scored in adults grown 80h on indicated

RNAi from starved L1 at 20°C. Hypodermal seam cell number was scored on a Leica MZ16 F fluorescence stereomicroscope using *[Pscm::gfp]* to indicate seam cells in young adults grown at 25°C. Multiple vulva (Muv) was scored in adults grown at 25°C. Levamisole resistance was scored at late L4 on NGM plates freshly seeded with OP50 mixed with 100uM levamisole. Paralysis was defined as inability to reverse in response to a single, gentle "nose tap" with a worm pick [79]. ASE neuron misspecification was scored in adults at 25°C using *otIs114 [Plim-6::gfp]* to indicate ASEL using a Leica MZ16 F fluorescence stereomicroscope. Embryonic lethality was scored by allowing adult worms fed RNAi from L1 to lay eggs on new RNAi, after 3-4 hr adults were removed and the number of eggs counted, approximately 48h later the number of viable offspring was scored. Full Strength RNAi of *alg-1* results in death and sterility, therefore RNAi was diluted 1:1 with vector to obtain adults for egg lay. At 25°C even a 1:1 dilution was not sufficient to obtain eggs in *mir-34-51(nDf50).* Bagging of *lin-4* mutants was scored through day 4 of adulthood (144h post-L1) at 20°C. Body length of *lin-4* mutants was qualitatively assessed of on the first day of gravid adulthood (80h) at 20°C. Images were taken at the same magnification using Handycam HDR-SR1 camcorder attached to a Leica MZ9.5 microscope. Rup and alae defects in *mir-48 mir-241 (nDf51)* were scored in adults grown at 20°C and synchronized by ~2-3 hr egg lay. Alae formation was scored on one side of each animal by DIC optics.

Microscopy. GFP and DIC images were captured on an Olympus BX61 epifluorescence compound microscope with a Hamamatsu ORCA ER camera using

Slidebook 4.0.1 digital microscopy software (Intelligent Imaging Innovations) and processed using ImageJ.

Reporter Plasmids and Transgenic Strains. The endogenous *cey-1::gfp* plasmid was generated by introducing the following fragments into a Fire-derived vector containing a C-terminal *gfp* coding region (0.9 kb fragment with synthetic introns and termination codon): *cey-1* promoter and genomic coding region (4 kb fragment with mutated termination codon) and *cey-1* 3′UTR (1 kb fragment immediately downstream of *cey-1* termination codon). The endogenous *flag::cey-1* plasmid was generated by introducing the following fragments into pJK225, a house vector with N-terminal 6x flag: *cey-1* promoter (~4 kb fragment upstream of the start codon), *cey-1* genomic coding region, and *cey-1* 3′UTR (~1 kb fragment immediately downstream of *cey-1* termination codon). RNP I + II mutant has non-synonymous nucleotide changes, generated by SOE-PCR, that alter RNP 1 from GYGFI to GAGAI, and RNP 2 from IFVHQ to IAVAQ.). The endogenous *mcherry::prmt-1* plasmid was generated by introducing the following fragments into pJK206, a house vector with N-terminal mCherry: *prmt-1* promoter (~3 kb fragment upstream of the start codon), *cey-1* genomic coding region, and *prmt-1* 3′UTR (~1 kb fragment immediately downstream of *cey-1* termination codon). Reporter plasmids were used to generate multi-copy integrated transgenes as described [80], single-copy site directed insertions were generated by subcloning transgenes into pCFJ151 and applying the MosSCI technique at the chrII locus [50]. The *flag::cey-1* RG truncation mutant was serendipitously generated as a result of an incomplete MosSCI insertion. Sequencing of the locus suggests ~125nt region of the RG-rich domain of

flag::cey-1 is absent in this strain. Expression of transgenics was verified by fluorescence microscopy and/or Western analysis.

Antibody Production. Custom polyclonal antibody to CEY-1 was generated by immunizing rabbits with the synthetic antigenic peptide KNDVAEQPADKPVKATKVKG-C conjugated to KLH (Proteintech). Antisera were affinity purified using Affi-Gel 15 gel (Bio-Rad). CEY-1 antibody was pre-absorbed in *cey-1(ok1805)* lysate.

Western Blotting. Protein samples from synchronized populations were prepared by direct boiling in Novex Tris-Glycine SDS sample buffer (Invitrogen), supplemented with 0.1 M DTT. Proteins were resolved on Novex Tris-Glycine gels (Invitrogen), and immobilized on Immobilon-FL transfer membrane (Millipore) according to the manufacturer protocols. Membranes were probed with custom rabbit polyclonal antibody to CEY-1 (1:1000) or Y-tubulin (Sigma LL-17) (1:2000). Peroxidase-AffiniPure goat anti-rabbit IgG secondary antibody was used at 1:10000 (Jackson ImmunoResearch Laboratories) for detection using Pierce ECL western Blotting Substrate (Thermo Scientific). SDS PAGE for analysis of CEY-1 in *prmt-1(ok2710)* was run for an extended time (120min) at 130V on a 10-20% gel. Sample for *Ex[prmt-1::mch];prmt-1* blot was collected by selectively picking transgenic animals.

RNA extraction and RT-qPCR. Samples were lysed by three rounds of freeze/thaw lysis and RNA was extracted in TriReagent (Ambion) following the vendor's protocol, with the following alterations: RNA was precipitated in isopropanol at 80C; RNA was

pelleted by centrifugation at 4C for 30 min at high speed; the pellet was washed three times in 75% ethanol; the pellet was resuspended in water. For quantification of mRNA levels, total RNA were converted into cDNA with Multiscribe Reverse Transcriptase (Applied Biosystems) following the vendor's protocol with the following changes: 25 units of RT and 7.6 units of RNAse OUT (Invitrogen) were used per reaction. cDNAs were analyzed using Power Sybr Green PCR Master Mix (Applied Biosystems). RT-qPCR primers are listed in Table 3-2. For quantification of miRNA levels, TaqMan assays and probes (hsa-let-7a cat#4427975, U18 cat#4427975) (Applied Biosystems) were used according to the vendors' protocol with modifications as described in [81]. Relative RNA levels were calculated based on the ΔΔ2Ct method [82] using *act-1* or *eft-2* for normalization of mRNA and U18 for normalization of miRNAs. For *lin-41* target analysis *ssp-16* and *glp-1* mRNA levels were measured to assess developmental delay.

RNA Immunoprecipitation (RIP). For each RIP, antibody was cross-linked to Protein A Dynabeads (Invitrogen) and incubated at 4°C for 1 hr with homogenized sample. Beads were washed with RIP wash buffer (50 mM Tris-HCl pH 7.5, 200 mM KCl, 0.05% NP-40), then split for protein and RNA analyses. For protein analyses, SDS sample buffer (Novex Tris-Glycine, Invitrogen), was added directly to beads and incubated at 50°C for 10 min. Eluted proteins were supplemented with 0.1 M DTT, and incubated at 90°C for 5 min prior to western blotting. For RNA analysis, 1 ml of TRI-Reagent (Ambion) was directly added to beads and extracted as described in RNA Analyses, with extended RNA precipitation for 2 hr at -30°C. cDNA and miRNA taqmans were synthesized in technical replicates and analyzed as described in RNA Analyses. CEY-1::GFP was

immunoprecipitated with anti-GFP antibody (3E6). FLAG::CEY-1 was immunoprecipitated with anti-FLAG antibody (Sigma). For RNA analysis of FLAG::CEY-1 only, 10 ng of Firefly Luciferase RNA (Promega) was directly added to beads prior to extraction. RT-qPCR analyses for IP were normalized to firefly luciferase.

HITS-CLIP. CEY-1::GFP HITS-CLIP was performed as described for Puf3p PAR-CLIP (Freeberg *et al*., 2013) with modifications for application in *C. elegans*:

UV crosslinking of protein & RNA. Live synchronized L4s were washed once with water, resuspended in 10ml water on 15cm glass cell culture dishes and placed on ice. Samples were irradiated with 254nm UV at 150 mJ/cm^2 four times in a Stratalinker 2400 (Stratagene). Samples were centrifuged for 1 min at 3000xg and water was removed. Samples were flash frozen in liquid nitrogen and ground to a fine powder in a ball-mill homogenizer (Retsch MM400).

Extract preparation. 100mg of frozen sample powder was resuspended in 1ml Lysis Buffer (1xPBS, 0.5%NP-40, 1xComplete Mini Protease Inhibitor, EDTA-free). Lysates were cleared by sequential spins at 1,300Xg for 5 min and 20,000Xg for 10 min at 4°C. 500µl of clarified lysate was passed through a Costar Spin-X filter (Corning), mixed with RNase T1 (Fermentas) to 1 U/µl, and incubated at 24°C for 15 min in an Eppendorf Thermomixer (with 15 s shaking at 1,000 rpm followed by a 2 min rest interval) followed by a 5 min incubation on ice.

RNP immunoprecipitation and RNase T1 treatment. Lysates were mixed with 25µl anti-GFP magnetic bead slurry (prepared by DMP-mediated crosslinking of 5ug monoclonal anti-GFP antibody (Invitrogen clone 3E6) to 100µl Protein A Dynabeads

(Invitrogen) and resuspended in 200µl Lysis Buffer) to pull down PUF-9-GFP or GFP-ALG-1 at 4°C for 1 hr. Beads were washed twice with 1x PBS + 0.1% NP-40, then incubated with 20 µl of 50 U/µl RNase T1 (Fermentas, 1:20 dilution in 1× PBS) at 24°C for 15 min on a Thermomixer (15 s shaking at 1,000 rpm followed by a 2 min rest interval), followed by a 5 min incubation on ice. Beads were washed twice with wash buffer (1× PBS, 0.1% SDS, 0.5% deoxycholate, 0.5% NP-40), twice with high-salt wash buffer (5× PBS, 0.1% SDS, 0.5% deoxycholate, 0.5% NP-40) and twice with 1× PNK buffer (50 mM Tris pH 7.4, 10 mM $MgCl_2$, 0.5% NP-40).

On-bead CIP treatment. Beads were incubated with 20 µl of CIP mix (50 mM Tris pH 7.9, 100 mM NaCl, 10 mM $MgCl_2$, 0.5 U/µl calf intestinal alkaline phosphatase (CIP); NEB) at 37°C for 15 min, with 15 s shaking at 1,000 rpm followed by a 2 min rest interval on a Thermomixer. After CIP treatment, beads were washed twice with 1× PNK+EGTA buffer (50 mM Tris pH 7.4, 20 mM EGTA, 0.5% NP-40) and twice with 1× PNK buffer.

On-bead 3' DNA linker ligation. Beads were incubated with 20 µl of ligation mix (50 mM Tris pH 7.4, 10 mM $MgCl_2$, 0.5 mM DTT, 2 µM pre-adenylated 3' DNA linker, 25% PEG-8000, 10 U/µl T4 RNA ligase 2, truncated K227Q; NEB M0351S) at 16°C overnight (≥16 h), with 15 s shaking at 1,000 rpm followed by a 2 min interval on a Thermomixer. After linker ligation, beads were washed three times with 1× PNK+EGTA buffer.

SDS-PAGE and nitrocellulose transfer. Beads were mixed with 15 µl of 1× PNK+EGTA buffer and 15 µl of 4× NuPAGE LDS sample buffer (Invitrogen NP0007), and incubated at 70°C for 10 min. Beads were removed, and the supernatant was

loaded onto NuPAGE 4-12% Bis-Tris gel (Invitrogen) and run at 150 V for 1 hr. The gel was transferred to Protran BA 85 nitrocellulose membrane (pore size 0.45 µm, Whatman) using Novex wet transfer at 30 V for 1 hr. A membrane band corresponding to each RNP was excised and transferred to a microfuge tube. (See next section.)

On-bead ^{32}P labeling of RNA 5' ends identifies membrane regions for excision. A diagnostic CLIP experiment was performed in parallel, for the sole purpose of identifying RNP bands on nitrocellulose membranes. Extract preparation, RNP immunoprecipitation, and RNase T1 digestion were performed as described above. 5' end phosphorylation was performed on-bead in 15 µl of PNK mix (70 mM Tris pH 7.6, 10 mM $MgCl_2$, 5 mM DT, 0.75 µl P32 rATP (6000 Ci/mmol 10 mCi/ml Perkin Elmer BLU502Z500UC), 1 U/µl T4 polynucleotide kinase (NEB)) and incubated at 37°C for 15 min. After SDS-PAGE and transfer, crosslinked RNAs were visualized by autoradiography.

RNA isolation and purification. Non-radioactive membrane bands were excised for RNA isolation and library construction. Excised membranes were incubated with 200 µl of 4 mg/ml Proteinase K prepared in 1× PK buffer (100 mM Tris pH 7.5, 50 mM NaCl, 10 mM EDTA) for 20 min at 37°C on a Thermomixer. We added 200 µl of 7 M urea prepared in 1× PK buffer to the tube followed by another 20 min incubation at 37°C. The Proteinase K digestion reaction was mixed with 1 ml of phenol:chloroform:isoamyl alcohol 25:24:1 (Sigma-Aldrich P2069) by vortexing and spun for 5 min at 20,000Xg. The liquid phase was transferred into a new tube, mixed with 50 µl of 3 M NaOAc, 1 ml of 100% ethanol and 1 µl of 15 mg/ml Glycoblue (Invitrogen), and precipitated for 2 h at

-80°C. RNAs were collected by centrifugation for 20 min at 20,000Xg at room temperature followed by two washes with cold 75% ethanol.

RNA 5' end phosphorylation. RNA pellets were air-dried briefly, resuspended in 10 µl of PNK mix (70 mM Tris pH 7.6, 10 mM $MgCl_2$, 5 mM DTT, 1 mM ATP, 1 U/µl T4 polynucleotide kinase (NEB)) and incubated at 37°C for 30 min. The reaction was combined with 90 µl of H_2O and 100 µl of phenol:chloroform:isoamyl alcohol 25:24:1, mixed well and spun for 5 min at 20,000Xg. The liquid phase was mixed with 12.5 µl of 3 M NaOAc, 250 µl of 100% ethanol, 1 µl of 15 mg/ml glycoblue and precipitated for 2 h at -80°C. RNAs were collected by centrifugation for 20 min at 20,000Xg at room temperature, followed by two washes with cold 75% ethanol.

5' RNA linker ligation. RNA pellets were resuspended in 10 µl of ligation mix (50 mM Tris pH 7.5, 10 mM $MgCl_2$, 10 mM DTT, 1 mM ATP, 0.1 mg/ml bovine serum albumin, 2 µM 5' RNA linker, 1 U/µl T4 RNA ligase (Fermentas EL0021), 10% DMSO) and incubated at 15°C for 2 h.

RNA size selection. Ligation reaction was terminated by adding 10 µl of 2× formamide gel loading buffer (Invitrogen AM8546G), heated for 2 min at 70°C and then quickly chilled on ice. Samples were loaded onto a 6% TBE UREA gel (Invitrogen EC6865) and run at 150 V for 45 min. After staining with 1× Sybr Gold Stain (Invitrogen S-11494), a gel piece corresponding to a 70 to 90 nucleotide RNA (80 to 100 nucleotide single-stranded DNA) was excised, crushed, and soaked in 400 µl of 0.3 M NaOAc overnight at room temperature. After removing gel pieces, the solution was combined with 1 ml of 100% ethanol and 1 µl of 15 mg/ml glycoblue and precipitated for 2 h at -80°C. RNAs were collected by centrifugation for 20 min at 20,000Xg at room temperature, followed

by two washes with cold 75% ethanol. After brief drying, RNAs were resuspended in 15 µl of H_2O.

RT-PCR. The ligated RNA (10 µl) was combined with 2 µl of 5 µM RT primer, heated at 65°C for 5 min, and then quickly chilled on ice, and followed by the addition of 1 µl of water, 1 µl of 10 mM dNTP, 1 µl of 0.1 M DTT, 4 µl of 5× First strand buffer, and 0.5 µl of SuperScript III Reverse transcriptase (Invitrogen, 200 U/µl). The RT reaction was kept at 50°C for 45 min, 55°C for 15 min and 90°C for 5 min. A test PCR was performed with 2.5 µl of RT product in 20 µl PCR mix: 1× AccuPrime PCR buffer I, 0.5 µM P5 long primer, 0.5 µM P7 primer, 0.2 µl AccuPrime Taq High Fidelity (Invitrogen, 5 U/µl). PCR was carried out with an initial 3 min denaturation at 98°C, followed by 14 to 22 cycles of 80 s denaturation at 98°C, 90 s annealing and extension at 65°C, and termination with a final 5 min extension at 65°C. PCR product (15 µl) was collected after 14, 18, and 22 cycles and analyzed on a 10% TBE gel (Invitrogen) at 150 V for 1 h to determine the optimal amplification cycles (the lowest cycle number required to generate 96 to 116 bp amplicons detected by Sybr Gold staining).

Preparation of sequencing libraries. A 50µl PCR reaction was carried out with the determined cycle number. Amplicons were purified using DNA clean and concentrator-5 (Zymo D4013; Irvine, CA, USA), run on 10% TBE gels at 150 V for 1 h and stained with Sybr Gold. A gel piece corresponding to 96 to 116 bp DNA was excised, crushed, and soaked overnight in 400 µl 0.3 M NaOAc at room temperature. After removing gel pieces, the solution was combined with 1 ml of 100% ethanol and 1 µl of 15 mg/ml glycoblue and precipitated for 2 h at -80°C. DNAs were collected by centrifugation for 20 min at 20,000Xg at room temperature, followed by two washes with cold 75% ethanol.

After brief drying, amplicons were resuspended in 20 µl of H_2O. Purified amplicons (5 µl) were used to seed a second round of PCR in 50 µl: 1× AccuPrime PCR buffer I, 0.5 µM Illumina Primer A, 0.5 µM Illumina Primer B, 0.2 µl AccuPirme Taq High Fidelity for 6 to 12 cycles. Second PCR amplicons were purified with DNA clean and concentrator-5 (Zymo) and sequenced on an Illumina HiSeq 2000 sequencer.

Sequence read processing. HITS-CLIP reads were processed to remove linkers and low-quality reads. Reads >15nt were aligned to the masked C. elegans genome version WS220 using BWA 0.6.2 (Li:2009). Only single optimal alignments were kept based on mismatches (mm) per read length: <2mm per 20nt, <3mm per 30nt, and <4mm per 40nt. Read clusters were generated from single nucleotide overlapping reads, and Gaussian smoothing was applied to resolve multi-peak clusters as described (Freeberg:2013). Read clusters were annotated to genic regions from WS220, including predicted 3'UTRs which we defined as 1.5kb downstream from any ORF with no annotated 3'UTR. Clusters mapping anti-sense to annotated genes were removed from downstream analyses. Cluster read counts were normalized to the total number of million mapped reads in each library (RPM) and additionally to gene RPKM values determined by the modENCODE group (Hillier:2009hr) for the gene to which each cluster was aligned.

Functional category enrichment analysis. DAVID (Huang:2009b,Huang:2009) was used to derived enriched functional categories for genes targeted by CEY-1 in each stage. Background gene lists were restricted to genes expressed in each specific stage as determined by the modENCODE group (Hillier:2009hr). Identification of sequence motifs MEME (Bailey:1994aa) was used to search 3'UTR CEY-1 binding sites in each

stage for over-represented sequence motifs. The following parameters were used: -zoops -minw 6 -maxw 9.

RNA structure prediction. RNAfold from the ViennaRNA Package 2.0 (Lorenz:2011) was used to determine optimal minimum free energy (MFE) scores for all CEY-1 binding sites. Each binding site was extended 15nt in either direction for prediction. As matched controls for each binding site, RNA regions immediately upstream and downstream of each site were chosen, with the same length, and used as input to RNAfold to derive MFE scores. The RNAfold web server (http://rna.tbi.univie.ac.at/cgi-bin/RNAfold.cgi) was used to generate example RNA structures for select CEY-1 binding sites.

Figure 3-1. CEY-1 is a member of the conserved Y-box binding/Cold-Shock Domain family of proteins. (A) Phylogenetic tree (neighbor joining with no distance correction) of the 5 *C.elegans* CSD proteins (CEY-1,-2,-3,-4, and LIN-28) and Y-box proteins in other organisms. Branch length indicates the number of amino acid substitutions as a proportion of the length of the alignment. CEY-1 (red) has diverged from other CEYs. (B) Protein domains in *C.elegans* Y-box proteins. CEY-1 has a RG-rich C-terminal. CSD = Cold Shock Domain (red) with two RNP motifs (yellow stripes) required for nucleic acid binding. RG-rich = enriched with RG/RGG repeats (blue). CCHC = retroviral-type Cys-Cys-His-Cys zinc finger-containing domain (grey). CEY-1 is the most RG rich CEY. (C) Relative somatic enrichment of *cey* mRNAs. RT-qPCR analysis of *cey* mRNA normalized to *act-1* in germline-depleted *glp-4(bn2)* versus wild-type adults at 25°C. Data are from one experiment, a replicate analysis yielded similar trends. CEY-2/-3 are expressed primarily in germline. CEY-1/-4 are expressed in soma and germline. (D) CEY-1::GFP driven by the *cey-1* promoter is broadly expressed in the soma of L4 larva [neurons (N), body muscle (M), vulva (V)].

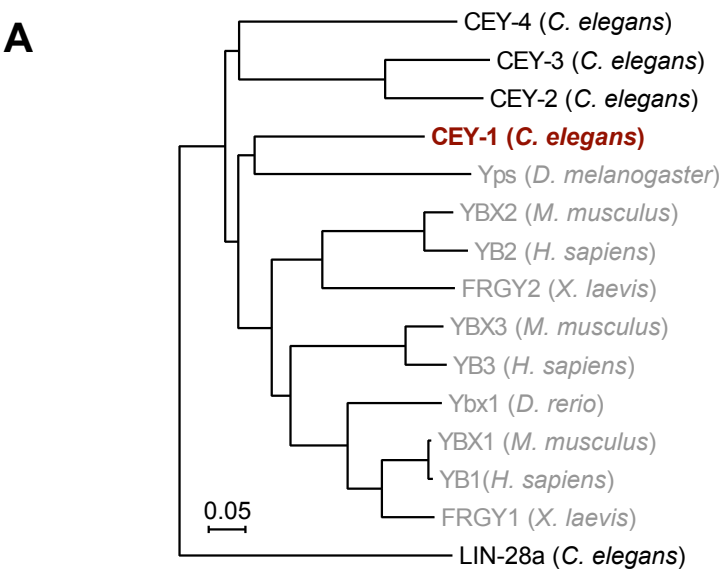
A
CEY-4 (C. elegans)
CEY-3 (C. elegans)
CEY-2 (C. elegans)
CEY-1 (C. elegans)
Yps (D. melanogaster)
YBX2 (M. musculus)
YB2 (H. sapiens)
FRGY2 (X. laevis)
YBX3 (M. musculus)
YB3 (H. sapiens)
Ybx1 (D. rerio)
YBX1 (M. musculus)
YB1(H. sapiens)
FRGY1 (X. laevis)
0.05
LIN-28a (C. elegans)

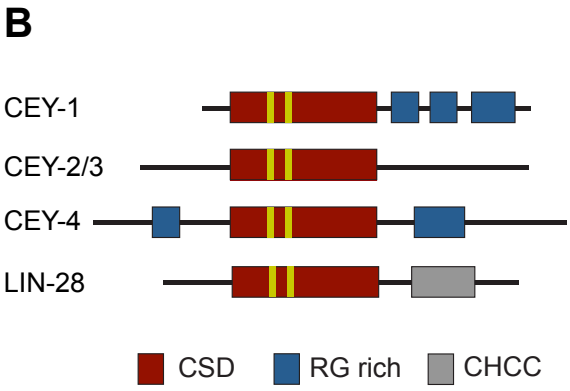
B
CEY-1
CEY-2/3
CEY-4
LIN-28
CSD
RG rich
CHCC

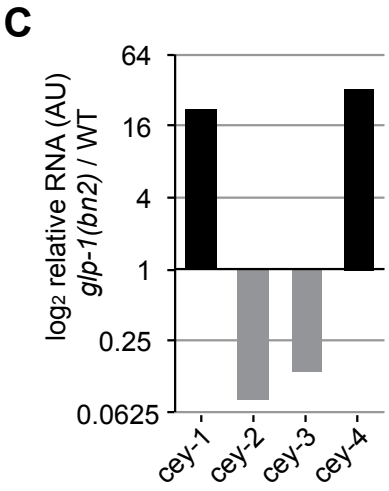
C
log2 relative RNA (AU)
glp-1(bn2) / WT
64
16
4
1
0.25
0.0625
cey-1
cey-2
cey-3
cey-4

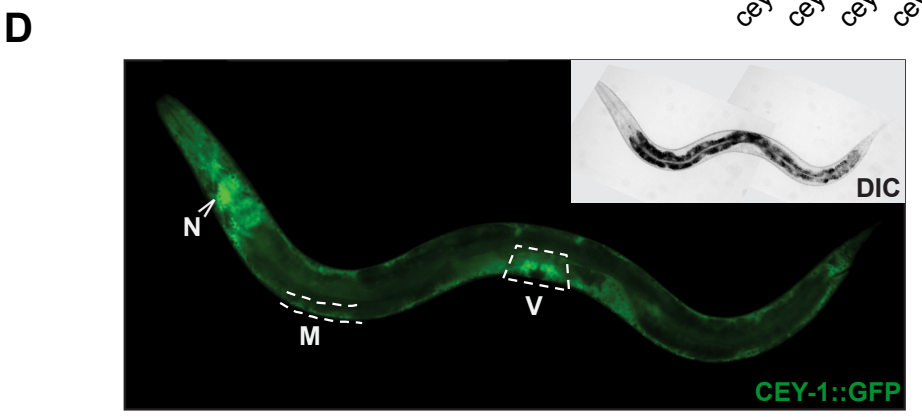
D
N
M
V
DIC
CEY-1::GFP

Figure 3-2. CEY-1 depletion, but not CEY-2/-3/-4 depletion suppresses *let-7(n2783)* vulval rupture (Rup). (A) DIC image of wild-type vulva, indicated by black arrow (top), and *let-7(n2853)* vulval rupture (Rup) with herniated contents of animal delineated by the yellow dotted line (bottom). (B) *cey-1* RNAi significantly suppresses Rup versus vector control to similar degree as RNAi of the *let-7* target, *lin-41*. RNAi of *cey-2/-3/-4* do not significantly alter Rup. (asterisk: $p<0.05$ by one-tailed Student's *t*-test, mean and standard deviation are plotted for replicate experiment, n>65/assay).

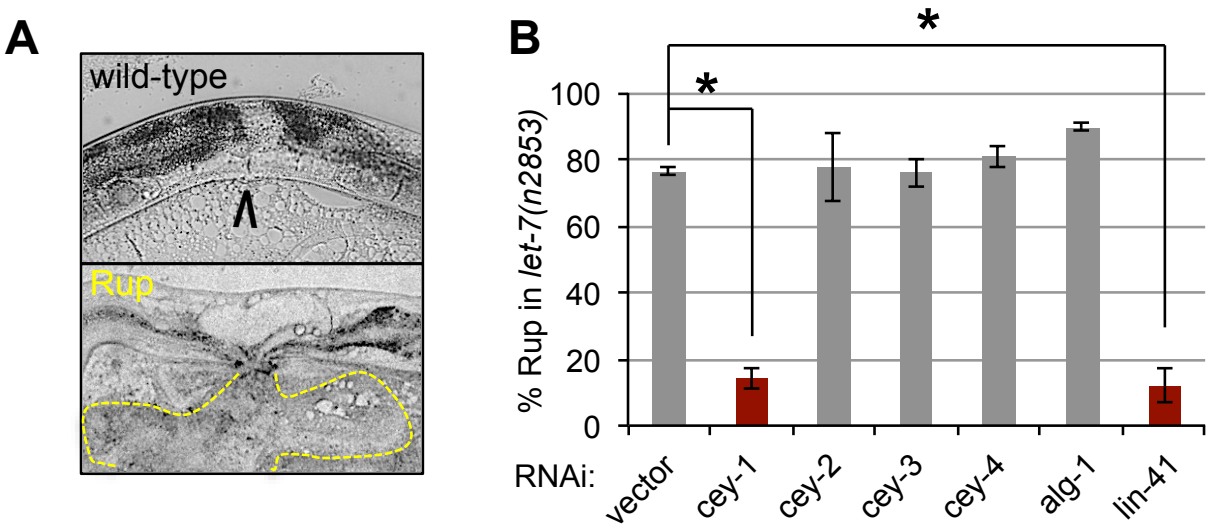

Figure 3-3. CEY-1 antagonizes *let-7* miRNA function. (A) CEY-1 protein and *cey-1* gene structure with annotated GFP and FLAG transgenics and *(ok1850)* and *(tm4347)* deletion mutants. (B) *cey-1* mutants significantly suppress phenotypes of the hypomorphic *let-7(n2853)* allele (asterisk: $p<0.05$ by two-tailed Student's *t*-test, mean and standard deviation are plotted for experimental triplicates, n>113/assay). (C-D) Endogenous *cey-1* transgenics rescue *cey-1; let-7* Rup. (asterisk: $p<0.05$ by two-tailed Student's *t*-test, mean and standard deviation are plotted for experimental replicates, n≥122/assay) (C) Single copy MosSCI insertion of WT *flag::cey-1* significantly rescues Rup suppression; *flag::cey-1* with either RNP1+2 mutation or RG-rich region truncation do not rescue. (D) High Copy (HC) WT *cey-1::gfp* significantly rescues Rup suppression. *gfp* RNAi attenuates rescue. (E-F) Hypodermal seam cell hyperplasia. (E) GFP and DIC images of animals expressing *Pscm::GFP*. Wild-type seam cells indicated with white arrowheads. Supernumerary seam cells in *let-7(n2853)* indicted with yellow arrowheads. (F) Seam cell number quantitation. P*scm::gfp* reporter was used to identify seam cells. (asterisk: $p<0.001$ by two-tailed Student's *t*-test, mean and standard deviation are plotted n≥68/assay).

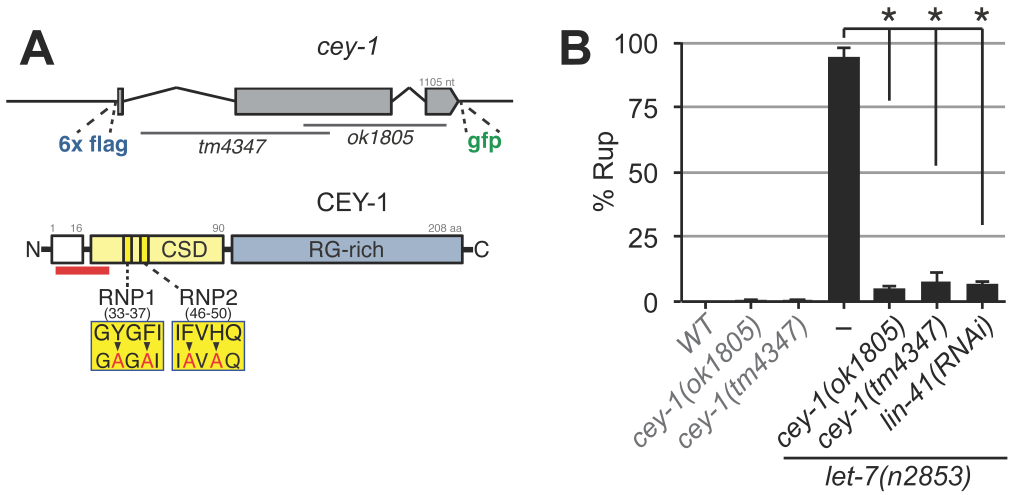
A
cey-1
1105 nt
6x flag
tm4347
ok1805
gfp
CEY-1
1
16
90
208 aa
N
CSD
RG-rich
C
RNP1
(33-37)
RNP2
(46-50)
GYGFI
GAGAI
IFVHQ
IAVAQ
B
% Rup
100
75
50
25
0
*
*
*
WT
cey-1(ok1805)
cey-1(tm4347)
–
cey-1(ok1805)
cey-1(tm4347)
lin-41(RNAi)
let-7(n2853)

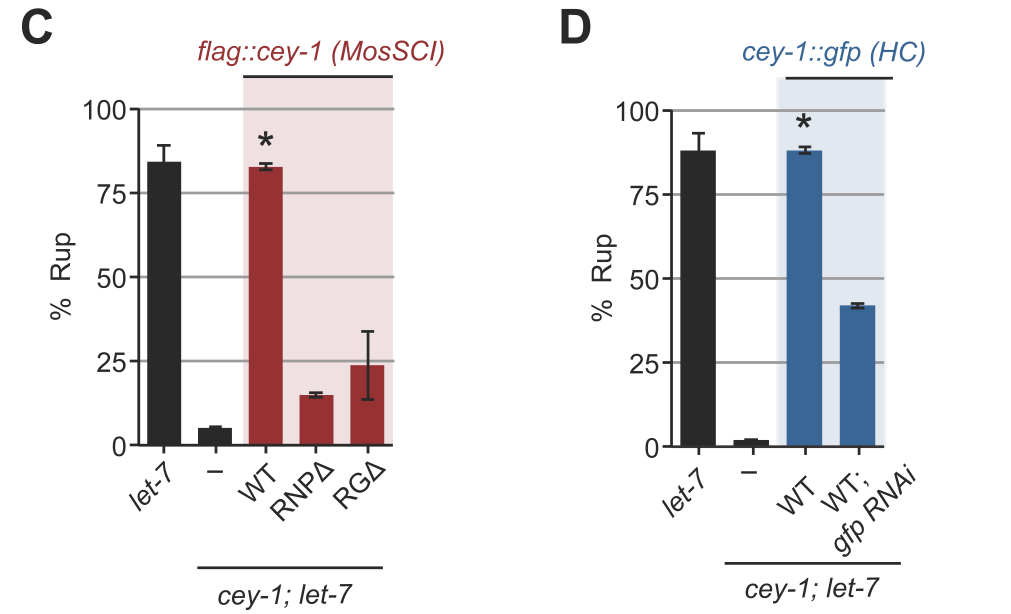
C
flag::cey-1 (MosSCI)
% Rup
100
75
50
25
0
*
let-7
–
WT
RNPΔ
RGΔ
cey-1; let-7
D
cey-1::gfp (HC)
% Rup
100
75
50
25
0
*
let-7
–
WT
WT;
gfp RNAi
cey-1; let-7

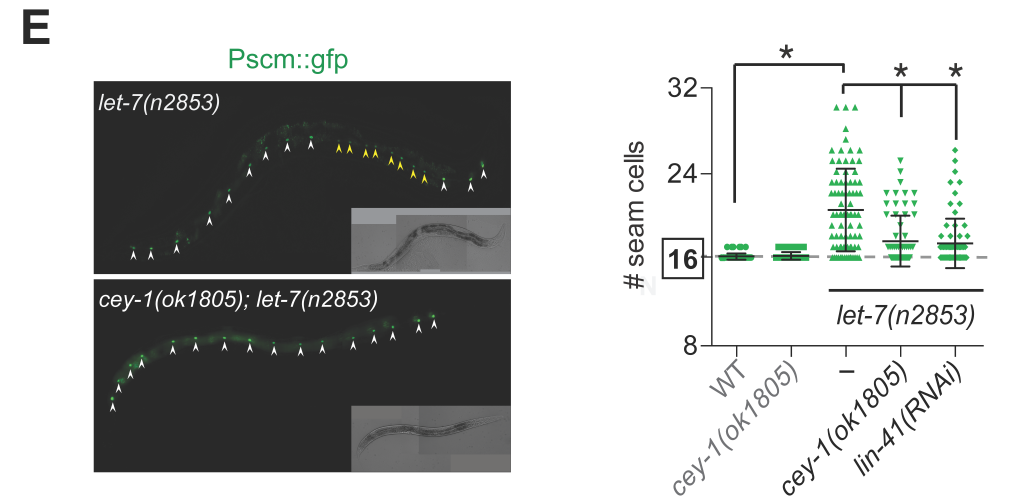
E
Pscm::gfp
let-7(n2853)
cey-1(ok1805); let-7(n2853)
seam cells
32
24
16
8
*
*
*
let-7(n2853)
WT
cey-1(ok1805)
–
cey-1(ok1805)
lin-41(RNAi)

Figure 3-4. *cey-1* mutant does not suppress other miRNA mutant phenotypes. (A) *cey-1(ok1508)* does not suppress levamisole resistance of *miR-1(gk276)* (p>0.05 at all points by two-tailed Student's *t*-test, mean and standard deviation are plotted for experimental triplicates, n≥25/assay). (B) *cey-1(ok1508)* does not suppress bagging phenotype (Bag) of *lin-4(e912).* (p>0.05 by two-tailed Student's *t*-test, mean and standard deviation are plotted for experimental replicates, n≥100/assay). Qualitative images of adults suggest *cey-1(ok1805)* does not appreciably suppress elongated body phenotype (Lon). *lin-14* RNAi was used as a positive control for suppression. [Similar results were obtained using *cey-1* RNAi in *lin-4(e912)* and the hypomorphic *lin-4(ma161)* allele (data not shown)]. (C) *cey-1(ok1508)* does not significantly suppress ASEL misspecification in the *lsy-6(ot71)* null or *(ot150)* hypomorph (n.s.: p>0.05 by two-tailed Student's *t*-test, mean and standard deviation are plotted for experimental triplicates, n=300/assay). (D) *cey-1* RNAi does not significantly suppress embryonic lethality of *miR-35-41(nDf50)* at 20° or 25°C. (n.s.: p>0.05 by two-tailed Student's *t*-test, mean and standard deviation are plotted for experimental replicates, n≥150/assay). *alg-1* RNAi at 25°C was not scored (n.d), see text and methods.

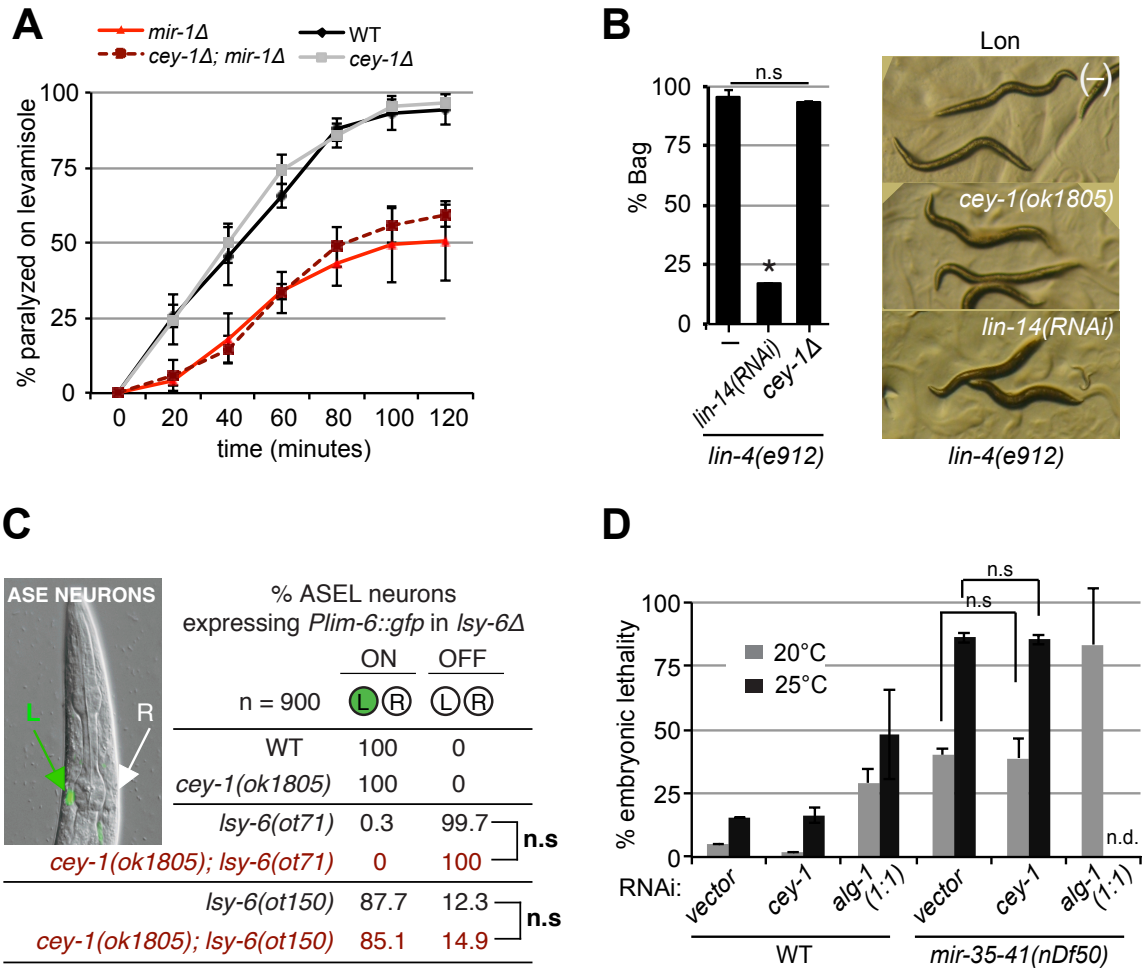

Figure 3-5. CEY-1 depletion does not suppress *let-7* sister phenotypes or *let-7(mn112)* null lethality. (A) Mature sequences of *let-7* family miRNAs in *C. elegans* and human *let-7a*. Conserved seed in red letters. (B) (Left) DIC image of wild-type vulva and Muv. Vulva indicated by white arrowhead, ectopic vulvae by yellow arrowhead. (Right) *cey-1(ok1805)* significantly suppresses multiple ectopic vulvae (Muv) in *let-60*(*ga89*), a gain-of-function mutant of the miR-48 target *let-60*. (asterisk: p<0.001 by two-tailed Student's *t*-test, mean and standard deviation are plotted for experimental triplicates, n=200/assay). (C) *cey-1(ok1508)* does not significantly suppress Rup or alae defects of *let-7* sister mutant *mir-48 mir-241(nDf51)*. Comparisons of gapped only, none only, and total alae defects are not significant (n.s.: p>0.05 by two-tailed Fisher's Exact test, n≥55). (D) (Left) *cey-1* RNAi significantly suppresses lethality of *let-7(n2853)* hypomorph (Mid) *cey-1* RNAi does not significantly suppress lethality of *let-7(mn112)* null. (Right) *cey-1* RNAi significantly suppresses lethality of *let-7(mn112)* null expressing a *let-7* rescue plasmid. For all, RNAi of *let-7* target, *lin-41,* significantly suppresses lethality. (asterisk: p<0.05 compared to vector control by Fisher's exact test, mean and standard deviation are plotted for replicate experiments, n>38/assay).

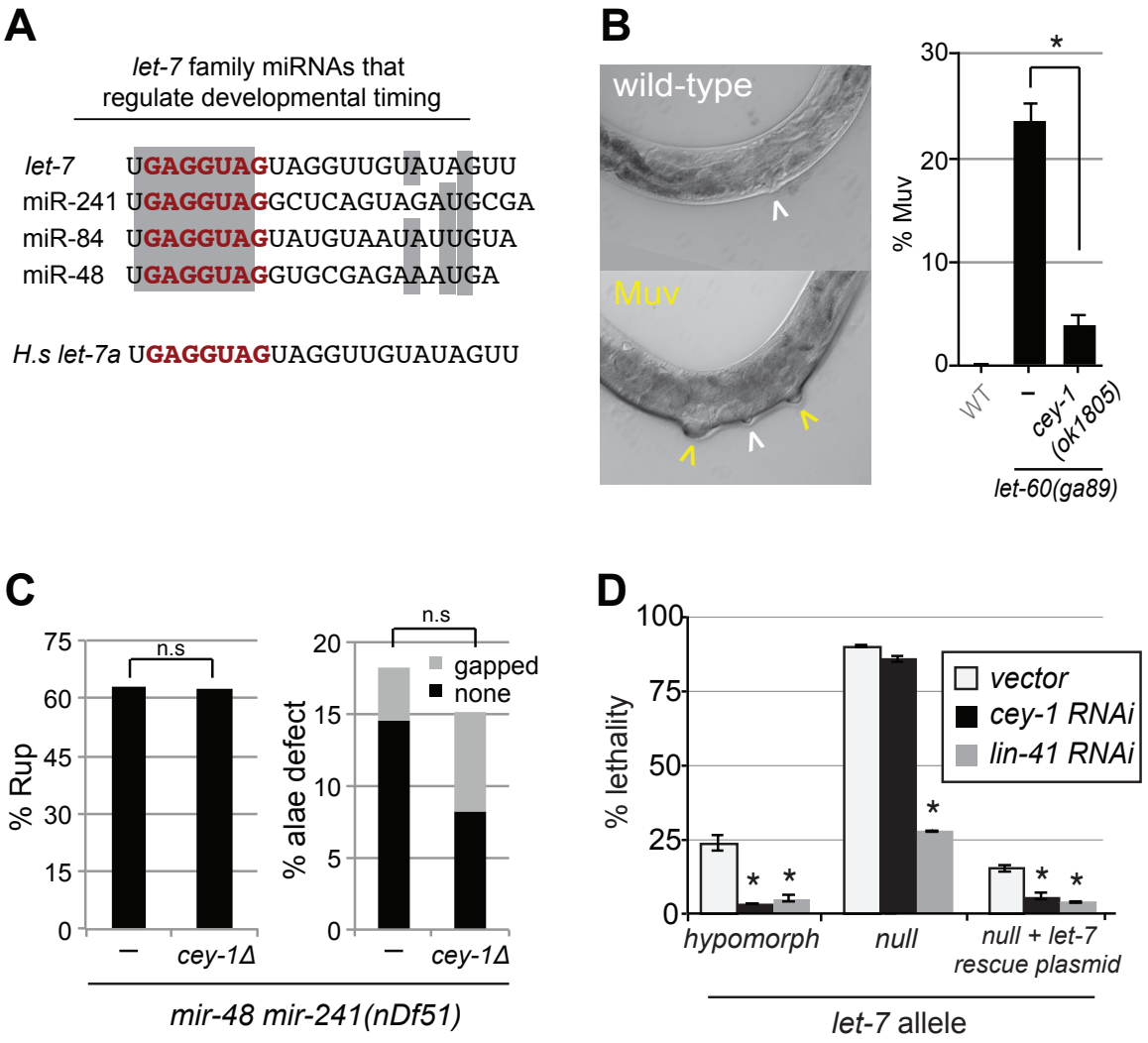

Figure 3-6. CEY-1 does not affect mature *let-7* accumulation. Detection of mature *let-7* by Taqman RT-qPCR suggests that loss of *cey-1* in a wild-type background does not result in substantial loss of mature *let-7* during the key developmental period of let-7 accumulation during L3 and L4 larval stages. Loss of *cey-1* in the sensitized *let-7(n2853)* hypomorph does show a significant difference only at late L3 and L4 timepoints. (asterisk: $p<0.05$ compared to *cey-1* (+/+) control by Student's *t*-test test, mean and standard deviation are plotted for technical replicates, experiment was repeated at least one time).

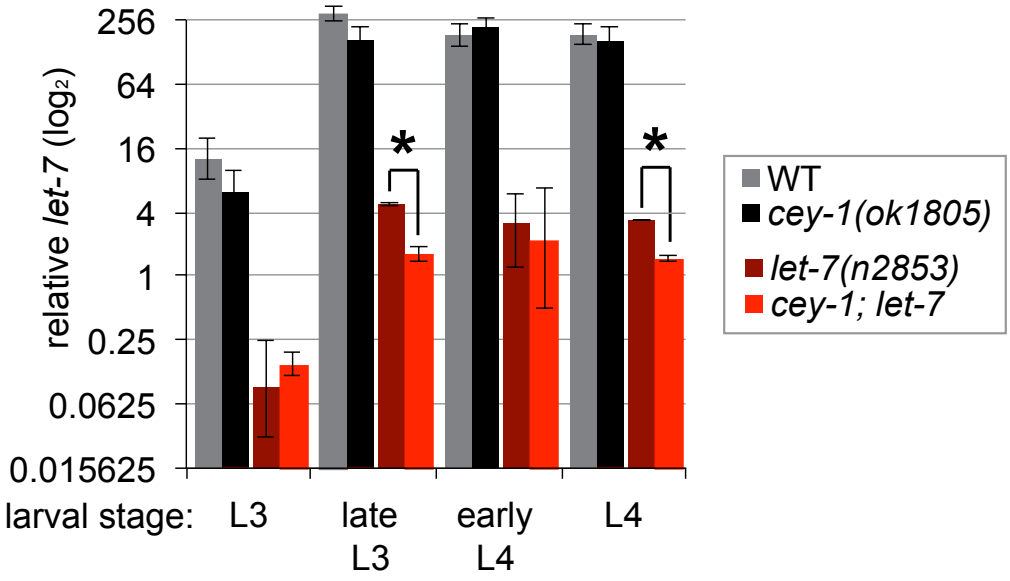

Figure 3-7. *cey-1* attenuates up-regulation of the primary *let-7* target, *lin-41, in let-7(n2853).* *lin-41* mRNA levels are rapidly down-regulated in wild-type animals during L4. *let-7(n2853)* display up-regulated levels of *lin-41* at the majority of L4 time points. *cey-1;let-7* has a slight but significant decrease in *lin-41* levels versus *let-7* at the early L4 time point (highlighted in grey). (asterisk: $p<0.05$ by two-tailed Student's *t*-test, mean and standard deviation are plotted for technical replicates, experiment was performed at least three times with similar trends, at least one experiment was performed where no difference was observed between *cey-1; let-7 and let-7*).

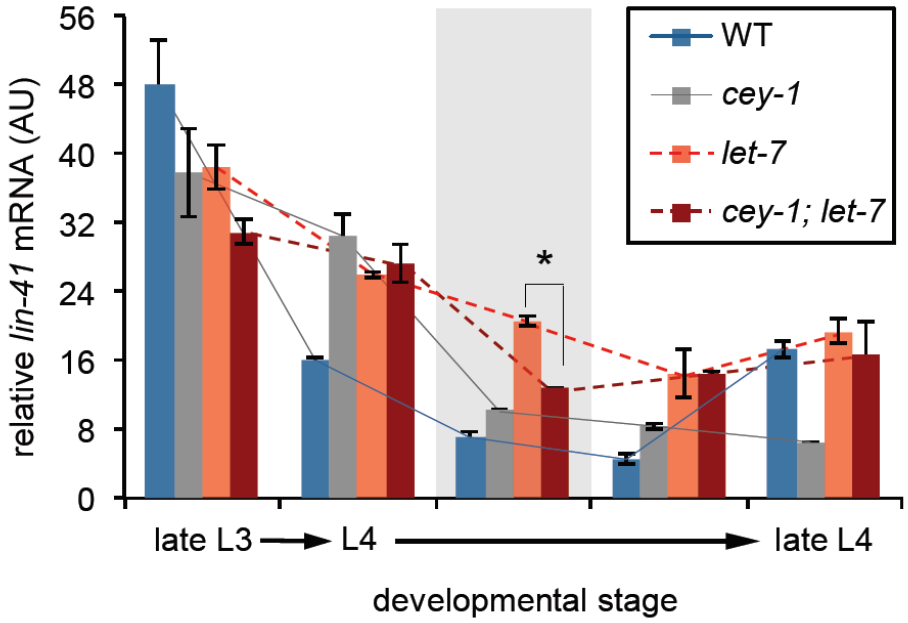

Figure 3-8. Global Analysis of RNAs bound to CEY-1 identifies *let-7* targets. (A) FLAG::CEY-1 HITS-CLIP (high-throughput sequencing of RNA isolated by crosslinking and immunoprecipitation) computational workflow to identify CEY-1 binding sites in L4 staged wild-type or "soma enriched" animals that were fed *glp-1* RNAi to prevent germline development. (B-C) CEY-1 binding sites divided by functional region. CEY-1 binding sites are globally enriched in 3'UTRs and exons. (D-H) Examples of CEY-1 binding in the 3'UTR of miRNA targets: (D-G) Four *let-7*/*let-7* family targets, (H) Three non-*let-7* targets: *mef-2* mRNA is a target of miR-1. *cog-1* mRNA is a target of *lsy-6*. *lin-14* mRNA is a target of *lin-4*. For all CEY-1 binding sites are indicated as high confidence (filled box) or low confidence (empty box) based on read coverage.

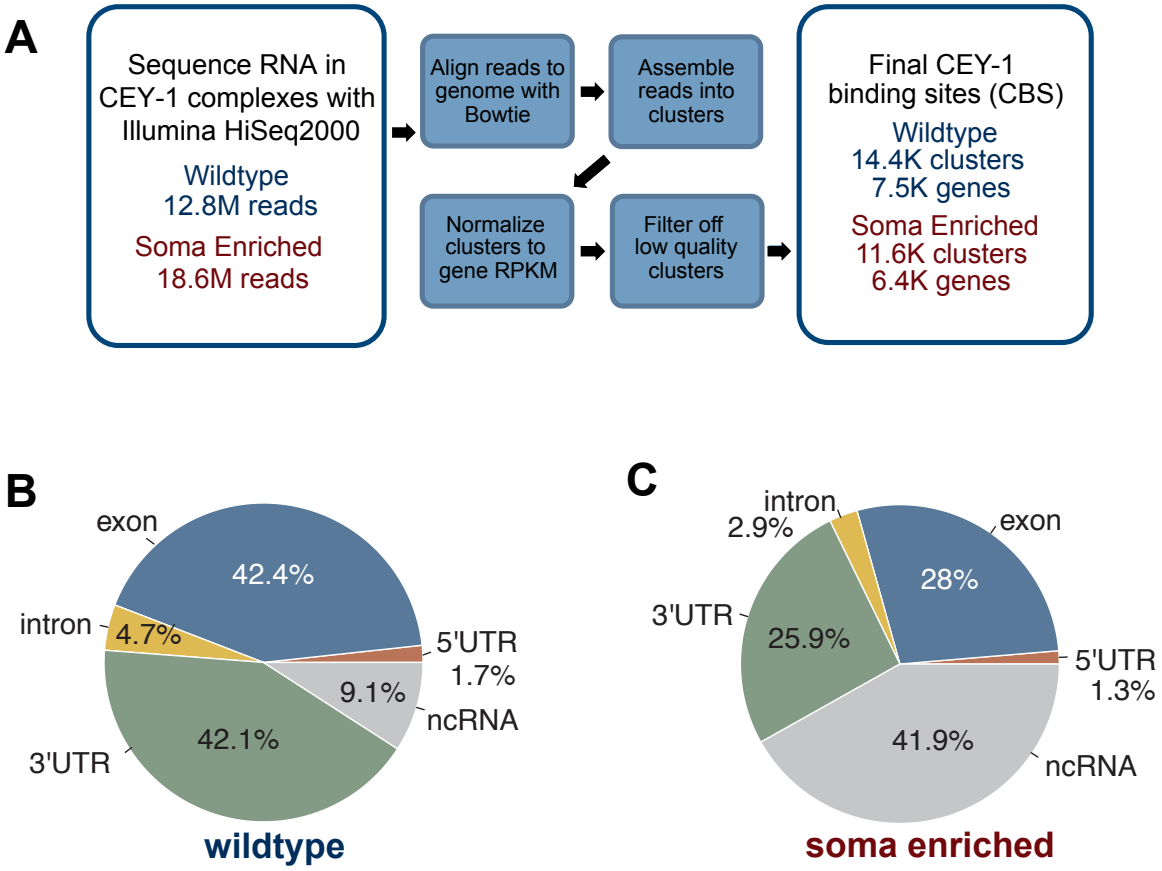

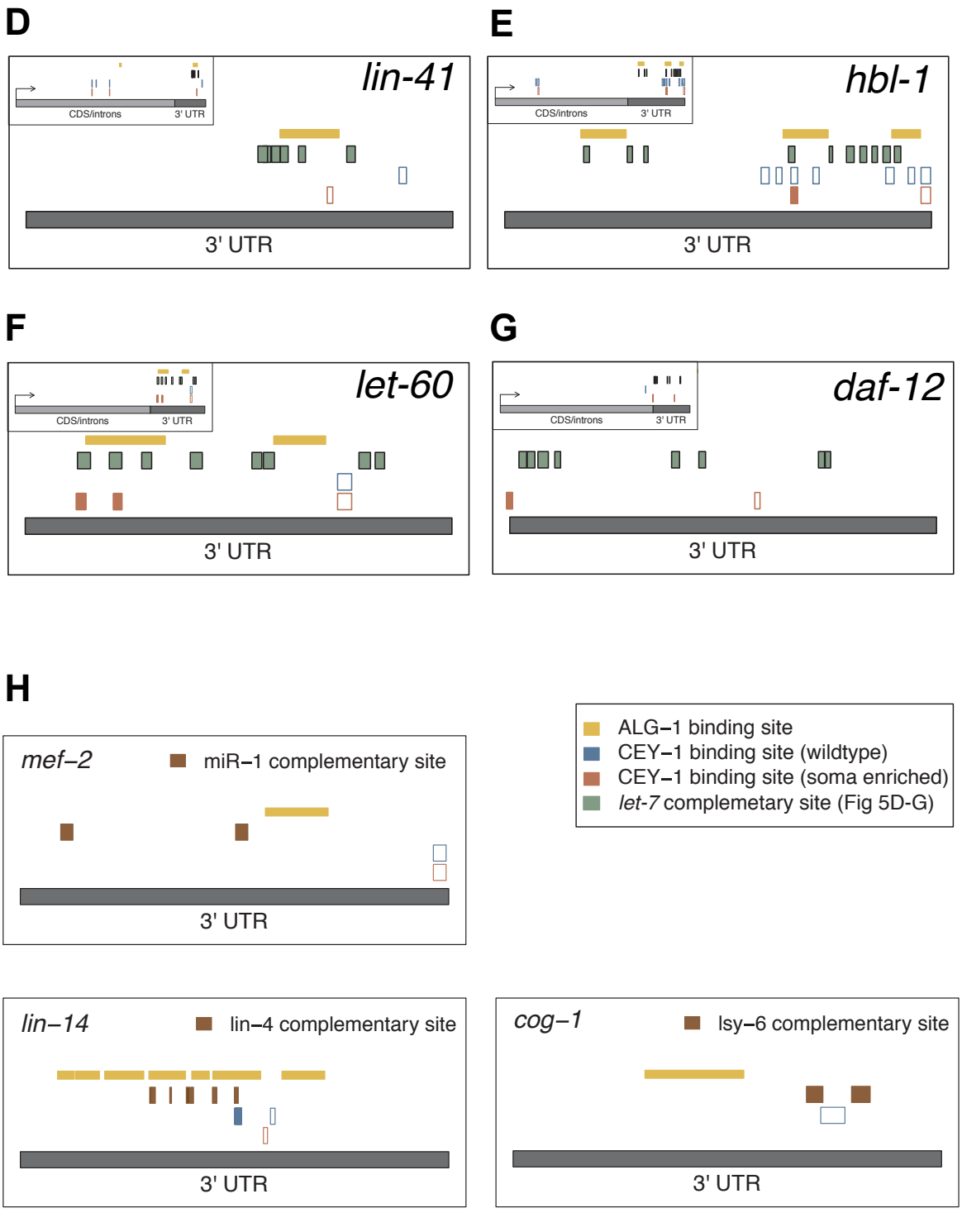
D
lin-41
CDS/introns
3' UTR
3' UTR
E
hbl-1
CDS/introns
3' UTR
3' UTR
F
let-60
CDS/introns
3' UTR
3' UTR
G
daf-12
CDS/introns
3' UTR
3' UTR
H
mef–2
miR–1 complementary site
3' UTR
ALG–1 binding site
CEY–1 binding site (wildtype)
CEY–1 binding site (soma enriched)
let-7 complemetary site (Fig 5D-G)
lin–14
lin–4 complementary site
3' UTR
cog–1
lsy–6 complementary site
3' UTR

Figure 3-9. CEY-1 binds *let-7* targets in an RNP-dependent manner. RNA bound to transgenic CEY-1 was isolated from L4 stage animals by RNA immunoprecipitation (RIP) and quantified by RT-qPCR. (A) CEY-1::GFP RIP. Compared to crude lysate (input) *let-7* mRNA target *lin-41* is statistically enriched versus the non-miRNA target *eft-2.* The *let-7* family target *daf-12* is also substantially enriched versus *eft-2*. (asterisk: $p<0.05$ by one-tailed Student's *t*-test, mean and standard deviation are plotted for technical replicates). (B) FLAG::CEY-1 RIP. Two transgenic lines expressing FLAG::CEY-1 indicate WT FLAG::CEY-1 binds *lin-41* at significantly higher levels than RNPΔ FLAG::CEY-1 that has non-conservative amino acid substitutions in the RNA binding RNP motifs of the Cold Shock Domain. (asterisk: $p<0.05$ by one-tailed Student's *t*-test, mean and standard deviation are plotted for technical replicates). HC = high-copy transgenic. Mos = MosSCI single copy transgenic insertion.

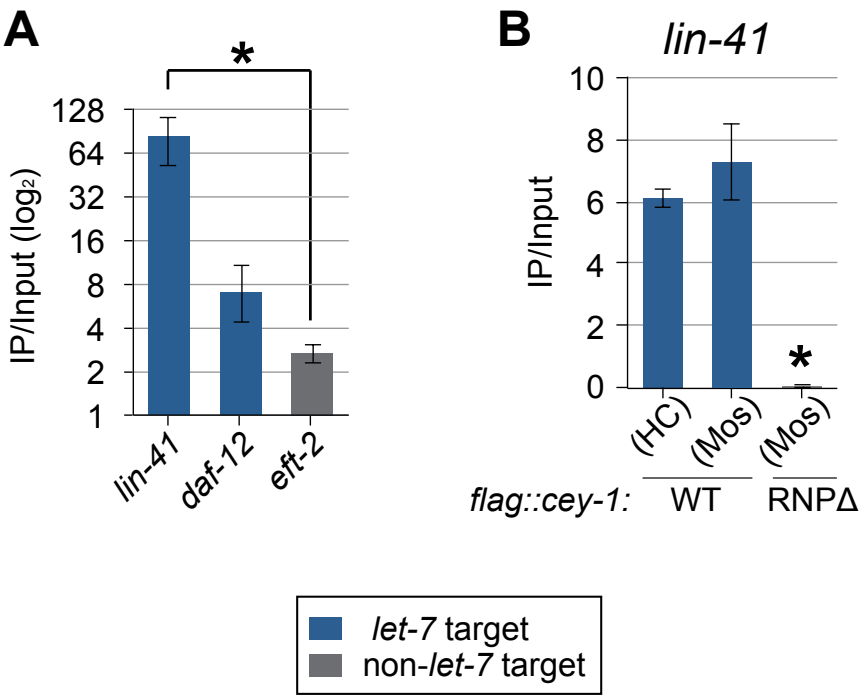

Figure 3-10. Validation of CEY-1 binding sites in *let-7* target, *lin-41*. (A) Schematic of *lin-41* 3'UTR GFP reporter. Mutations were made to abrogate HITS-CLIP identified CEY-1 binding sites (CBS, blue) and/or experimentally validated *let-7* sites (LCS, red). (B) Synchronized, young adults expressing the wild-type (WT) or LCS1 mutant versions the *lin-41* UTR reporter imaged with the same exposure time at the same magnification. Preliminary analysis suggest reporters are sensitive to miRNA regulation: relative to the WT reporter the GFP intensity of the LCS1 mutant reporter was not substantially down-regulated during the L4 to adult transition.

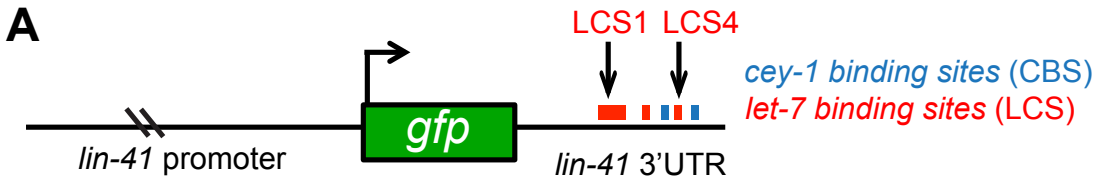

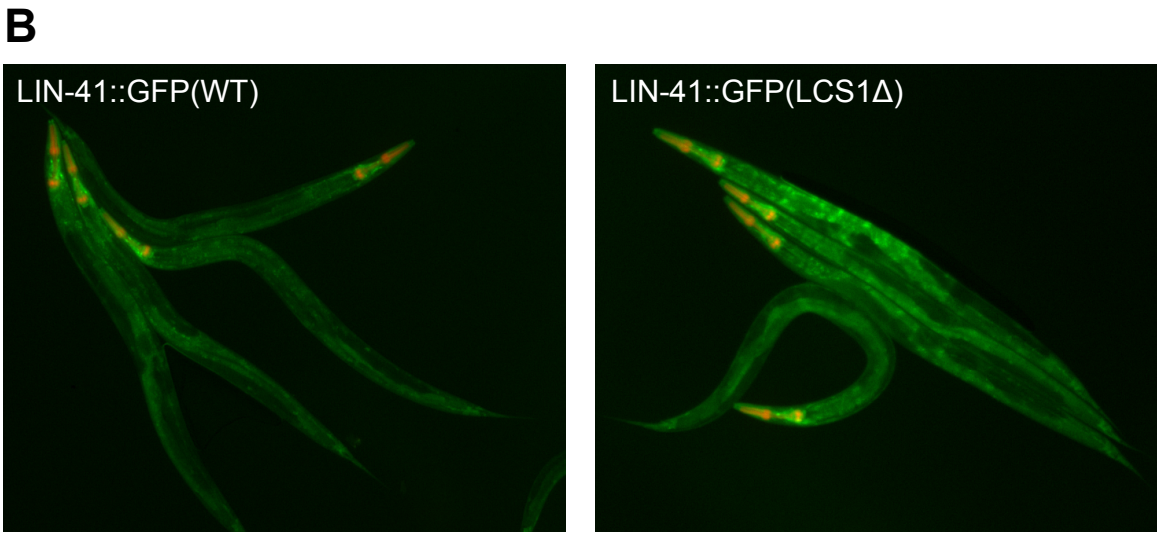

Figure 3-11. Loss of *cey-1* suppresses precocious alae in *lin-41* mutants. *cey-1* mutants suppress precocious alae formation in the *lin-41(ma161)* hypomorphic mutant. (asterisk: p<0.01 by Fisher's exact test, n=57, replicate experiments were pooled).

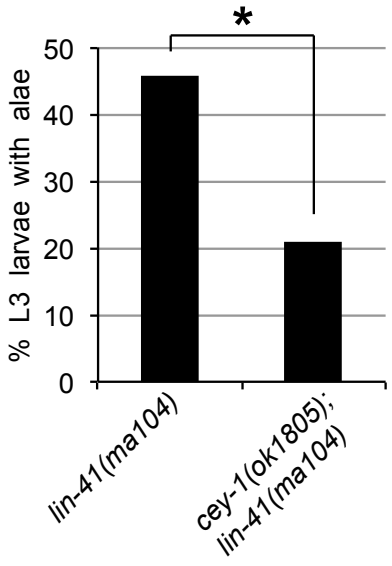

Table 3-1. *C. elegans* strains used in this study.

Strain ID	Genotype
N2	*C. elegans* wild isolate; wild-type reference strain (WT)
QK054	*cey-1(ok1805) II*
QK055	*cey-1(tm4347) II*
QK030	*cey-1(ok1805) II; let-7(n2853) X*
	cey-1(tm4347 II; let-7(n2853) X
QK031	*xkIs24 [cey-1p::cey-1::gfp::cey-1 3UTR]; cey-1 (ok1805) II*
	xkIs24[cey-1p::cey-1::gfp::cey-1 3UTR]; cey-1(ok1805) II; let-7(n2853) X
	xkSi30[cey-1p::flag::cey-1 genomic coding::cey-1 3UTR] II; cey-1(ok1805) II; let-7(n2853) X
	xkSi31[cey-1p::flag::cey-1 with RNP I+II mutated::cey-1 3UTR] II; cey-1(ok1805) II; let-7(n2853) X
	xkSi32 [cey-1p::flag::cey-1 with RG truncation::cey-1 3UTR] II; cey-1(ok1805) II; let-7(n2853) X
SS104	*glp-4(bn2) I*
GR1452	*veIs13 [col-19::GFP + rol-6(su1006)] V; let-7(mn112) unc-3(e151) X; mgEx725 [lin-4::let-7 + ttx-3::RFP]*
MT7626	*let-7(n2853) X*
SD551	*let-60(ga89) IV*
QK058	*cey-1(ok1805) II; let-60(ga89) IV*
CT8	*lin-41(ma104) I*
	lin-41(ma104) I; cey-1 (ok1805) II
VC576	*mir-1(gk276) I*
	mir-1(gk276) I; cey-1(ok1805) II
MT14119	*mir-35-41(nDf50) II*
XV4	*mir-48 mir-241(nDf51) V*
XV3	*cey-1 (ok1805) II; mir-48 mir-241(nDf51) V*
RB2047	*prmt-1 (ok2710) V*
	xkEx[prmt-1p::mcherry::prmt-1 genomic coding::prmt-1 3'UTR]; prmt-1 (ok2710) V
OH812	*otIs114 [Plim-6::gfp] I*
	otIs114 [Plim-6::gfp] I; cey-1(ok1805) II
	otIs114 [Plim-6::gfp] I; lsy-6(ot71) V
	otIs114 [Plim-6::gfp] I; cey-1(ok1805) II; lsy-6(ot71) V
OH3646	*otIs114 [Plim-6::gfp] I; lsy-6(ot150) V*
	otIs114 [Plim-6::gfp] I; cey-1(ok1805) II; lsy-6(ot150) V
JR672	*wIs54 (scm::gfp)*
QK057	*wIs54 (scm::gfp); cey-1(ok1805) II*
QK036	*wIs54 (scm::gfp); let-7(n2853) X*
QK056	*wIs54 (scm::gfp); cey-1(ok1805) II; let-7(n2853) X*
	xkIs[lin-41p::gfp::lin-41 3'UTR]
	xkIs[lin-41p::gfp::lin-41 3'UTR with LCS1 mutated]

*CGC - Caenorhabditis Genetics Center, University of Minnesota, Minneapolis, MN.
**NBRP - National Bioresource Project for *C. elegans*, Tokyo Women's Medical University School of Medicine, Japan.

Table 3-2. qPCR primers used in this study

cey-1	F	GAAGGGAACAGTGAAATGGTTCAA
	R	TCTTCGTTGGTGTCAGTGCG
cey-2	F	CAACAGCGAAGAGAAGATGCGTA
	R	GGTGGTAATGGCTGTCTTCG
cey-3	F	AAGCAAGGATGATACAAGCAAGCA
	R	CCAGCGGTAAGAACAATCTTCG
cey-4	F	GGACAAAGTTGCCGAGGTGAC
	R	CGTTCGCCTCGTTGGTAGTG
act-1	F	GATCGTATGCAGAAGGAAATCAC
	R	GTTTCCTTGTTGCACAAAAATATG
daf-12	F	GATCCTCCGATGAACGAAAA
	R	CTCTTCGGCTTCACCAGAAC
eft-2	F	ACGCTCGTGATGAGTTCAAG
	R	ATTTGGTCCAGTTCCGTCTG
lin-41	F	GGTTCCAAATGCCACAAGAG
	R	AGGTCCAACTGCCAAATCAG

REFERENCES

1. Lee RC, Feinbaum RL, Ambros V (1993) The C. elegans heterochronic gene lin-4 encodes small RNAs with antisense complementarity to lin-14. Cell 75: 843-854.
2. Reinhart BJ, Slack FJ, Basson M, Pasquinelli AE, Bettinger JC, et al. (2000) The 21-nucleotide let-7 RNA regulates developmental timing in Caenorhabditis elegans. Nature 403: 901-906.
3. Bartel DP (2009) MicroRNAs: target recognition and regulatory functions. Cell 136: 215-233.
4. Kim VN (2005) MicroRNA biogenesis: coordinated cropping and dicing. Nat Rev Mol Cell Biol 6: 376-385.
5. Kim VN, Han J, Siomi MC (2009) Biogenesis of small RNAs in animals. Nat Rev Mol Cell Biol 10: 126-139.
6. Lewis BP, Shih IH, Jones-Rhoades MW, Bartel DP, Burge CB (2003) Prediction of mammalian microRNA targets. Cell 115: 787-798.
7. Olsen PH, Ambros V (1999) The lin-4 regulatory RNA controls developmental timing in Caenorhabditis elegans by blocking LIN-14 protein synthesis after the initiation of translation. Developmental biology 216: 671-680.
8. Huntzinger E, Izaurralde E (2011) Gene silencing by microRNAs: contributions of translational repression and mRNA decay. Nature reviews Genetics 12: 99-110.
9. Grishok A, Pasquinelli AE, Conte D, Li N, Parrish S, et al. (2001) Genes and mechanisms related to RNA interference regulate expression of the small temporal RNAs that control C. elegans developmental timing. Cell 106: 23-34.
10. Tops BB, Plasterk RH, Ketting RF (2006) The Caenorhabditis elegans Argonautes ALG-1 and ALG-2: almost identical yet different. Cold Spring Harb Symp Quant Biol 71: 189-194.
11. Ding L, Spencer A, Morita K, Han M (2005) The developmental timing regulator AIN-1 interacts with miRISCs and may target the argonaute protein ALG-1 to cytoplasmic P bodies in C. elegans. Mol Cell 19: 437-447.
12. Zhang L, Ding L, Cheung TH, Dong MQ, Chen J, et al. (2007) Systematic identification of C. elegans miRISC proteins, miRNAs, and mRNA targets by their interactions with GW182 proteins AIN-1 and AIN-2. Mol Cell 28: 598-613.
13. Caudy AA, Ketting RF, Hammond SM, Denli AM, Bathoorn AM, et al. (2003) A micrococcal nuclease homologue in RNAi effector complexes. Nature 425: 411-414.
14. Hammell CM, Lubin I, Boag PR, Blackwell TK, Ambros V (2009) nhl-2 Modulates microRNA activity in Caenorhabditis elegans. Cell 136: 926-938.
15. Rouya C, Siddiqui N, Morita M, Duchaine TF, Fabian MR, et al. (2014) Human DDX6 effects miRNA-mediated gene silencing via direct binding to CNOT1. RNA 20: 1398-1409.
16. Mathys H, Basquin J, Ozgur S, Czarnocki-Cieciura M, Bonneau F, et al. (2014) Structural and biochemical insights to the role of the CCR4-NOT complex and DDX6 ATPase in microRNA repression. Molecular cell 54: 751-765.

17. Chen Y, Boland A, Kuzuoglu-Ozturk D, Bawankar P, Loh B, et al. (2014) A DDX6-CNOT1 complex and W-binding pockets in CNOT9 reveal direct links between miRNA target recognition and silencing. Molecular cell 54: 737-750.
18. Krol J, Loedige I, Filipowicz W (2010) The widespread regulation of microRNA biogenesis, function and decay. Nature reviews Genetics 11: 597-610.
19. Alpatov R, Lesch BJ, Nakamoto-Kinoshita M, Blanco A, Chen S, et al. (2014) A chromatin-dependent role of the fragile X mental retardation protein FMRP in the DNA damage response. Cell 157: 869-881.
20. Kenny PJ, Zhou H, Kim M, Skariah G, Khetani RS, et al. (2014) MOV10 and FMRP regulate AGO2 association with microRNA recognition elements. Cell reports 9: 1729-1741.
21. Kedde M, van Kouwenhove M, Zwart W, Oude Vrielink JA, Elkon R, et al. (2010) A Pumilio-induced RNA structure switch in p27-3' UTR controls miR-221 and miR-222 accessibility. Nature cell biology 12: 1014-1020.
22. Kedde M, Strasser MJ, Boldajipour B, Oude Vrielink JA, Slanchev K, et al. (2007) RNA-binding protein Dnd1 inhibits microRNA access to target mRNA. Cell 131: 1273-1286.
23. Lebedeva S, Jens M, Theil K, Schwanhausser B, Selbach M, et al. (2011) Transcriptome-wide analysis of regulatory interactions of the RNA-binding protein HuR. Molecular cell 43: 340-352.
24. Kim HH, Kuwano Y, Srikantan S, Lee EK, Martindale JL, et al. (2009) HuR recruits let-7/RISC to repress c-Myc expression. Genes & development 23: 1743-1748.
25. Sommerville J (1999) Activities of cold-shock domain proteins in translation control. BioEssays : news and reviews in molecular, cellular and developmental biology 21: 319-325.
26. Landsman D (1992) RNP-1, an RNA-binding motif is conserved in the DNA-binding cold shock domain. Nucleic acids research 20: 2861-2864.
27. Dorn A, Bollekens J, Staub A, Benoist C, Mathis D (1987) A multiplicity of CCAAT box-binding proteins. Cell 50: 863-872.
28. Kohno K, Izumi H, Uchiumi T, Ashizuka M, Kuwano M (2003) The pleiotropic functions of the Y-box-binding protein, YB-1. BioEssays : news and reviews in molecular, cellular and developmental biology 25: 691-698.
29. Bouvet P, Matsumoto K, Wolffe AP (1995) Sequence-specific RNA recognition by the Xenopus Y-box proteins. An essential role for the cold shock domain. The Journal of biological chemistry 270: 28297-28303.
30. Matsumoto K, Meric F, Wolffe AP (1996) Translational repression dependent on the interaction of the Xenopus Y-box protein FRGY2 with mRNA. Role of the cold shock domain, tail domain, and selective RNA sequence recognition. The Journal of biological chemistry 271: 22706-22712.
31. Ruzanov PV, Evdokimova VM, Korneeva NL, Hershey JW, Ovchinnikov LP (1999) Interaction of the universal mRNA-binding protein, p50, with actin: a possible link between mRNA and microfilaments. Journal of cell science 112 (Pt 20): 3487-3496.
32. Eliseeva IA, Kim ER, Guryanov SG, Ovchinnikov LP, Lyabin DN (2011) Y-box-binding protein 1 (YB-1) and its functions. Biochemistry Biokhimiia 76: 1402-1433.

33. Medvedev S, Pan H, Schultz RM (2011) Absence of MSY2 in mouse oocytes perturbs oocyte growth and maturation, RNA stability, and the transcriptome. Biology of reproduction 85: 575-583.
34. Yang J, Medvedev S, Yu J, Schultz RM, Hecht NB (2006) Deletion of the DNA/RNA-binding protein MSY2 leads to post-meiotic arrest. Molecular and cellular endocrinology 250: 20-24.
35. Bouvet P, Wolffe AP (1994) A role for transcription and FRGY2 in masking maternal mRNA within Xenopus oocytes. Cell 77: 931-941.
36. Mansfield JH, Wilhelm JE, Hazelrigg T (2002) Ypsilon Schachtel, a Drosophila Y-box protein, acts antagonistically to Orb in the oskar mRNA localization and translation pathway. Development 129: 197-209.
37. Kumari P, Gilligan PC, Lim S, Tran LD, Winkler S, et al. (2013) An essential role for maternal control of Nodal signaling. eLife 2: e00683.
38. Arnold A, Rahman MM, Lee MC, Muehlhaeusser S, Katic I, et al. (2014) Functional characterization of C. elegans Y-box-binding proteins reveals tissue-specific functions and a critical role in the formation of polysomes. Nucleic acids research 42: 13353-13369.
39. Moss EG, Tang L (2003) Conservation of the heterochronic regulator Lin-28, its developmental expression and microRNA complementary sites. Developmental biology 258: 432-442.
40. Lehrbach NJ, Armisen J, Lightfoot HL, Murfitt KJ, Bugaut A, et al. (2009) LIN-28 and the poly(U) polymerase PUP-2 regulate let-7 microRNA processing in Caenorhabditis elegans. Nature structural & molecular biology 16: 1016-1020.
41. Heo I, Joo C, Cho J, Ha M, Han J, et al. (2008) Lin28 mediates the terminal uridylation of let-7 precursor MicroRNA. Molecular cell 32: 276-284.
42. Heo I, Joo C, Kim YK, Ha M, Yoon MJ, et al. (2009) TUT4 in concert with Lin28 suppresses microRNA biogenesis through pre-microRNA uridylation. Cell 138: 696-708.
43. Loughlin FE, Gebert LF, Towbin H, Brunschweiger A, Hall J, et al. (2012) Structural basis of pre-let-7 miRNA recognition by the zinc knuckles of pluripotency factor Lin28. Nature structural & molecular biology 19: 84-89.
44. Boag PR, Nakamura A, Blackwell TK (2005) A conserved RNA-protein complex component involved in physiological germline apoptosis regulation in C. elegans. Development 132: 4975-4986.
45. Yochem J, Greenwald I (1989) glp-1 and lin-12, genes implicated in distinct cell-cell interactions in C. elegans, encode similar transmembrane proteins. Cell 58: 553-563.
46. Austin J, Kimble J (1987) glp-1 is required in the germ line for regulation of the decision between mitosis and meiosis in C. elegans. Cell 51: 589-599.
47. Bagga S, Bracht J, Hunter S, Massirer K, Holtz J, et al. (2005) Regulation by let-7 and lin-4 miRNAs results in target mRNA degradation. Cell 122: 553-563.
48. Vella MC, Choi EY, Lin SY, Reinert K, Slack FJ (2004) The C. elegans microRNA let-7 binds to imperfect let-7 complementary sites from the lin-41 3'UTR. Genes & development 18: 132-137.
49. Ecsedi M, Rausch M, Grosshans H (2015) The let-7 microRNA directs vulval development through a single target. Developmental cell 32: 335-344.

50. Frokjaer-Jensen C, Davis MW, Hopkins CE, Newman BJ, Thummel JM, et al. (2008) Single-copy insertion of transgenes in Caenorhabditis elegans. Nature genetics 40: 1375-1383.
51. Sulston JEaH, H. R. (1977) Post-embryonic cell lineages of the nematode, Caenorhabditis elegans. Developmental biology 56: 110-156.
52. Koh K, Rothman JH (2001) ELT-5 and ELT-6 are required continuously to regulate epidermal seam cell differentiation and cell fusion in C. elegans. Development 128: 2867-2880.
53. Alvarez-Saavedra E, Horvitz HR (2010) Many families of C. elegans microRNAs are not essential for development or viability. Curr Biol 20: 367-373.
54. Simon DJ, Madison JM, Conery AL, Thompson-Peer KL, Soskis M, et al. (2008) The microRNA miR-1 regulates a MEF-2-dependent retrograde signal at neuromuscular junctions. Cell 133: 903-915.
55. Ambros V, Horvitz HR (1984) Heterochronic mutants of the nematode Caenorhabditis elegans. Science 226: 409-416.
56. Euling S, Ambros V (1996) Heterochronic genes control cell cycle progress and developmental competence of C. elegans vulva precursor cells. Cell 84: 667-676.
57. Hallam SJ, Jin Y (1998) lin-14 regulates the timing of synaptic remodelling in Caenorhabditis elegans. Nature 395: 78-82.
58. Johnston RJ, Hobert O (2003) A microRNA controlling left/right neuronal asymmetry in Caenorhabditis elegans. Nature 426: 845-849.
59. Shaw WR, Armisen J, Lehrbach NJ, Miska EA (2010) The conserved miR-51 microRNA family is redundantly required for embryonic development and pharynx attachment in Caenorhabditis elegans. Genetics 185: 897-905.
60. Roush S, Slack FJ (2008) The let-7 family of microRNAs. Trends in cell biology 18: 505-516.
61. Abbott AL, Alvarez-Saavedra E, Miska EA, Lau NC, Bartel DP, et al. (2005) The let-7 MicroRNA family members mir-48, mir-84, and mir-241 function together to regulate developmental timing in Caenorhabditis elegans. Dev Cell 9: 403-414.
62. Eisenmann DM, Kim SK (1997) Mechanism of activation of the Caenorhabditis elegans ras homologue let-60 by a novel, temperature-sensitive, gain-of-function mutation. Genetics 146: 553-565.
63. Johnson SM, Grosshans H, Shingara J, Byrom M, Jarvis R, et al. (2005) RAS is regulated by the let-7 microRNA family. Cell 120: 635-647.
64. Sternberg PW (2005) Vulval development. WormBook: 1-28.
65. Zisoulis DG, Lovci MT, Wilbert ML, Hutt KR, Liang TY, et al. (2010) Comprehensive discovery of endogenous Argonaute binding sites in Caenorhabditis elegans. Nature structural & molecular biology 17: 173-179.
66. Hillier LW, Reinke V, Green P, Hirst M, Marra MA, et al. (2009) Massively parallel sequencing of the polyadenylated transcriptome of C. elegans. Genome research 19: 657-666.
67. Bailey TL, Elkan C (1994) Fitting a mixture model by expectation maximization to discover motifs in biopolymers. Proceedings / International Conference on Intelligent Systems for Molecular Biology ; ISMB International Conference on Intelligent Systems for Molecular Biology 2: 28-36.

68. Lorenz R, Bernhart SH, Honer Zu Siederdissen C, Tafer H, Flamm C, et al. (2011) ViennaRNA Package 2.0. Algorithms for molecular biology : AMB 6: 26.
69. Myer VE, Fan XC, Steitz JA (1997) Identification of HuR as a protein implicated in AUUUA-mediated mRNA decay. The EMBO journal 16: 2130-2139.
70. Levine TD, Gao F, King PH, Andrews LG, Keene JD (1993) Hel-N1: an autoimmune RNA-binding protein with specificity for 3' uridylate-rich untranslated regions of growth factor mRNAs. Molecular and cellular biology 13: 3494-3504.
71. Meisner NC, Filipowicz W (2010) Properties of the regulatory RNA-binding protein HuR and its role in controlling miRNA repression. Advances in experimental medicine and biology 700: 106-123.
72. Lu YC, Chang SH, Hafner M, Li X, Tuschl T, et al. (2014) ELAVL1 modulates transcriptome-wide miRNA binding in murine macrophages. Cell reports 9: 2330-2343.
73. Chang SH, Lu YC, Li X, Hsieh WY, Xiong Y, et al. (2013) Antagonistic function of the RNA-binding protein HuR and miR-200b in post-transcriptional regulation of vascular endothelial growth factor-A expression and angiogenesis. The Journal of biological chemistry 288: 4908-4921.
74. Slack FJ, Basson M, Liu Z, Ambros V, Horvitz HR, et al. (2000) The lin-41 RBCC gene acts in the C. elegans heterochronic pathway between the let-7 regulatory RNA and the LIN-29 transcription factor. Molecular cell 5: 659-669.
75. Stadler M, Artiles K, Pak J, Fire A (2012) Contributions of mRNA abundance, ribosome loading, and post- or peri-translational effects to temporal repression of C. elegans heterochronic miRNA targets. Genome research 22: 2418-2426.
76. Slack FJ, Basson M, Liu Z, Ambros V, Horvitz HR, et al. (2000) The lin-41 RBCC gene acts in the C. elegans heterochronic pathway between the let-7 regulatory RNA and the LIN-29 transcription factor. Mol Cell 5: 659-669.
77. Stiernagle T (2006) Maintenance of C. elegans. WormBook : the online review of C elegans biology: 1-11.
78. Fraser AG, Kamath RS, Zipperlen P, Martinez-Campos M, Sohrmann M, et al. (2000) Functional genomic analysis of C. elegans chromosome I by systematic RNA interference. Nature 408: 325-330.
79. Nurrish S, Segalat L, Kaplan JM (1999) Serotonin inhibition of synaptic transmission: Galpha(0) decreases the abundance of UNC-13 at release sites. Neuron 24: 231-242.
80. Mello CC, Kramer JM, Stinchcomb D, Ambros V (1991) Efficient gene transfer in C.elegans: extrachromosomal maintenance and integration of transforming sequences. EMBO J 10: 3959-3970.
81. Billi AC, Alessi AF, Khivansara V, Han T, Freeberg M, et al. (2012) The Caenorhabditis elegans HEN1 ortholog, HENN-1, methylates and stabilizes select subclasses of germline small RNAs. PLoS genetics 8: e1002617.
82. Nolan T, Hands RE, Bustin SA (2006) Quantification of mRNA using real-time RT-PCR. Nature Protocols 1: 1559-1582.

CHAPTER 4
Future Directions

The main focus of this dissertation has been to identify and characterize factors that regulate the miRNA effector complex, miRISC. Two proteins with novel roles in regulating miRISC function have been described. Here, I will discuss future directions that may further our understanding of how CK2 and CEY-1 interact with the miRNA pathway. Investigation into the mechanism by which these factors affect miRISC activity and exploration of the regulation of their roles in the miRNA pathway are promising common themes for future research.

Future Directions for CK2

Assess the role of CK2 phosphorylation of CGH-1 in promoting miRISC assembly and target binding

We provide extensive evidence that CK2 facilitates miRISC silencing of its mRNA targets (Fig 2-2B-E). Mechanistically, our data suggest that CK2 promotes miRISC binding to its targets: the *C. elegans* miRISC Argonaute protein, ALG-1, binds substantially less of the *let-7* target, *lin-41* in samples depleted of CK2 (*kin-3* RNAi) versus the empty vector control (Fig 2-3F). However, how CK2 facilitates miRISC-target association has yet to be defined. Therefore, one future avenue of research is to investigate how CK2 promotes miRISC association with mRNA.

In *C. elegans* the interaction of CGH-1 and the TRIM-NHL protein NHL-2 is

required for efficient miRISC target silencing [1], suggesting that the loss of these co-factors disrupts miRISC effector function. We identified the miRISC cofactor CGH-1 as a CK2 substrate and provide genetic evidence that post-translational modification of CGH-1 at serine 2 (S2) by CK2 is important for its function in the miRNA pathway. We observe that strains expressing the *cgh-1::gfp* phospho-defective transgene do not rescue miRNA mutant phenotypes in the sensitized *cgh-1(ts); let-7(mg279)* background, while the wild-type transgene does (Fig 2-4 E-G). Therefore, one hypothesis is that CK2 promotes miRISC association with mRNAs through phosphorylation of CGH-1.

To examine if phosphorylation of CGH-1 by CK2 is required for CGH-1 interaction with miRISC or the miRISC co-factor NHL-2, we could perform co-immunoprecipitations of ALG-1/NHL-2 and CGH-1::GFP in strains expressing the wild-type or phospho-mutant versions of the *cgh-1::gfp* transgene in the *cgh-1(ts)* mutant background. If CK2 phosphorylation is required for CGH-1 interaction with ALG-1 or NHL-2, then we hypothesize that the phospho-defective *cgh-1::gfp* strain will have decreased association versus the wild-type *cgh-1::gfp* strain.

To determine if phosphorylation of CGH-1 by CK2 is required for miRISC target binding, we could perform RIP of ALG-1 in strains expressing the wild-type or phospho-mutant versions of the *cgh-1::gfp* transgene. These results could be compared to ALG-1 binding in samples treated with either CK2 RNAi or *cgh-1* RNAi. If CK2 phosphorylation is required for miRISC binding to targets, then we hypothesize that the phospho-defective *cgh-1::gfp* strain will have attenuated binding compared to the wild-type *cgh-1::gfp* strain.

Assess CK2 regulation through additional miRISC co-factors

Our analysis of post-dauer development suggests that CK2 function in the *C. elegans* miRNA pathway is different post-dauer than during continuous development. Post-dauer suppression of miRNA phenotypes requires CK2, but not CK2 phosphorylation of CGH-1 (Fig 2-S7B), suggesting that during post-dauer development, CK2 may have additional substrates and/or that additional factors may dictate CK2 regulation of miRISC. In support of the former, preliminary data suggests that depletion of CK2 by *kin-10* RNAi enhances the alae defects and vulval rupture of *let-7(mg279)* more than RNAi of *cgh-1* (data not shown).

In our initial search for possible CK2 substrates in miRISC, we also identified the miRISC co-factor VIG-1. Under continuous development, VIG-1 is required for silencing of a *let-7* miRNA target reporter, indicating that, like CK2 and CGH-1, VIG-1 is required for miRNA target silencing [2,3]. VIG-1 has 7 putative CK2 phosphorylation sites (Fig 4-1A). According to a published phospho-proteome dataset two of these sites, S17 and S143, are phosphorylated in vivo [4]. Our data suggest that S17, but not S143, can be phosphorylated by CK2 in vitro (Fig 4-1B-C). To determine if phosphorylation of VIG-1 by CK2 is required for miRISC function, a similar experimental strategy could be employed for VIG-1 as was used for CGH-1. Namely, the generation and phenotyping of phospho-mutant VIG-1 transgenic strains in sensitized miRNA mutant backgrounds.

Vig-1 mutants do not show striking enhancement of miRNA mutant phenotypes [2], which has led to the view that VIG-1 plays a minor, or perhaps tissue selective, role in promoting miRISC. However, nothing is known about the role of VIG-1 during post-dauer development. Thus, determining the requirement of VIG-1 and CK2

phosphorylation of VIG-1 in suppression of post-dauer miRNA mutant phenotypes may provide insight into the role of VIG-1 in the post-dauer miRNA pathway and illuminate how CK2 facilitates miRISC in a CGH-1-independent manner during post-dauer development.

One of the major technical challenges in investigating the role of the serine 2 phosphorylation site of CGH-1 was creating similarly expressed transgenic lines, since transgenes are expressed from multi-copy arrays that have been randomly integrated into the genome. However, the increasingly routine use of the CRISPR-Cas9 genome editing techniques in *C.elegans* would enable the introduction of specific mutations, deletions, and expressed epitope tags to any endogenous gene in the worm genome [5]. Our lab has successfully adopted that the CRISPR system for generating transgenics. Thus, investigating the role of VIG-1 modifications by CK2 should take advantage of this new technology to make VIG-1 phospho-mutants.

Assess co-regulation of the miRNA pathway by CK2 and PP2A

Despite considerable efforts in kinase biology, the matter of whether CK2 is constitutively active or regulated remains controversial [6]. Interestingly, *let-92*, the single *C. elegans* homolog of PP2AC, the catalytic subunit of the serine/threonine phosphatase PP2A, was identified in a genome-wide RNAi screen to identify novel miRNA pathway genes [7]. PP2A is an attractive candidate to balance CK2 kinase activity as it is thought to play an important role in establishing the balance of numerous phosphorylation-dependent processes, in so-called kinase-phosphatase cycles. Moreover, CK2 and PP2A have been reported to have antagonistic roles in Notch-mediated lateral-inhibition during *Drosophila* development [10].

The PP2A holoenzyme is composed of catalytic (C), scaffolding (A), and regulatory (B) subunits. A large number of regulatory subunits exist and function to dictate the substrate specificity of the holoenzyme [8,9]. To examine if PP2A might co-regulate miRISC with CK2, we performed a bioinformatic analysis to identify additional PP2A regulatory subunits in *C. elegans* and tested the effect of RNAi knockdown of these genes in the *let-7(n2853)* mutant. We observed robust enhancement of vulval rupture phenotypes with RNAi of the regulatory subunits encoded by *sur-6* and *pptr-1,* comparable to RNAi of miRISC core component *alg-1,* and the CK2 subunit *kin-3* (Fig 4-2). Both *sur-6* and *pptr-1* are promising candidates. *sur-6* was also identified in genetic screen for suppressors of a hyperactive mutation of the miR-84 target *let-60/RAS,* which supports a possible role for *sur-6* in regulating miRNA activity [11]. *pptr-1* regulates dauer formation through the *C. elegans* insulin/IGF-1 signaling pathway [12]. Thus, *pptr-1* could modulate the activity of CK2 during post-dauer development.

However, our data suggest that loss of either CK2 or PP2A compromise miRISC (enhance Rup). One interpretation of this result is that a balance of CK2-mediated phosphorylation is required in the miRNA pathway, with complete phosphorylation by CK2 or no phosphorylation, both resulting in defective miRISC. Therefore, an interesting avenue for future work would be to investigate the role of PP2A in the regulation of the miRNA pathway, and its relationship to the activity of CK2.

Future Directions for CEY-1

The data on CEY-1 presented in CHAPTER 3 are informative, but primarily descriptive. The current investigation of CEY-1 would be greatly enhanced by data that provide

mechanistic evidence to explain how the loss of *cey-1* dramatically suppresses phenotypes associated with the *let-7(n2853)* mutant. We propose that loss of *cey-1* ameliorates *let-7(n2853)* mutant phenotypes by affecting the translational dynamics of *lin-41* by inducing loss of polysome formation on *lin-41* and, perhaps, by increasing *let-7* miRISC access to the *lin-41* 3'UTR. Thus, future directions for this project include experiments to test this model.

Assess the effect of CEY-1 on the translational dynamics of *lin-41*

We demonstrate that loss of *cey-1* potently suppresses *let-7* mutant phenotypes (Fig 3-2 and 3-3B), yet has a relatively mild effect on *lin-41* mRNA up-regulation (Fig 3-7). Consistent with the finding that loss of *cey-1* is associated with loss of polysome formation [13], our data also suggest that CEY-1 may regulate *lin-41* at the translational level. Therefore, ribosome profiling of *lin-41*, particularly in the *let-7(n2853*) mutant, with or without *cey-1* would likely be an informative experiment. If *cey-1* mutant suppression of *let-7(n2853)* is mediated by loss of polysome formation, then loss of ribosome occupancy and loading would be expected to accompany loss of *cey-1.* Western blot analysis of LIN-41 protein levels would also provide additional evidence of altered protein levels to accompany changes in translational dynamics in the *cey-1* mutant. An interesting permutation of the ribosome profiling experiment, which would demonstrate the requirement of CEY-1 RNA binding, would be to perform ribosome profiling in the *cey-1* mutants that express either the rescuing wild-type *cey-1* transgene or the non-rescuing RNA binding defective (RNPΔ) transgene.

Assess the effect of CEY-1 binding using *lin-41* 3'UTR GFP reporters

CEY-1 binding to the *lin-41* 3'UTR has been established through CEY-1 HITS-CLIP and RIP (Fig 3-8D and 3-9). However, CEY-1 association with the *lin-41* 3'UTR could be further validated by comparing the relative GFP expression of a wild-type *lin-41* 3'UTR GFP reporter with a reporter that has the HITS-CLIP-identified CEY-1 binding sites (CBS) mutated (reporter schematics in Fig. 3-10). The reporter system could initially be tested for responsiveness to loss of CEY-1 by comparing the wild-type reporter intensity in animals fed *cey-1* RNAi versus empty vector RNAi. In both experiments, if suppression of *lin-41* up-regulation in the *cey-1; let-7* double mutant requires binding to the *lin-41* 3'UTR, then we predict that loss of CEY-1 or the CBS should result in decreased GFP intensity. A complementary approach to an analysis of GFP intensity would be to perform CEY-1 RIPs in animals expressing the wild-type and CBS *lin-41* 3'UTR reporters. If the CBS prove necessary for CEY-1 binding to *lin-41,* then altering the distance of CBS relative to ALG-1 binding sites would be one way to address if CEY-1 antagonizes *let-7* miRISC binding at sites that are overlapping with or adjacent to CEY-1 binding sites. Alternatively, if CBS appear to be unimportant for CEY-1 association then we might further explore how CEY-1 associates with its substrates, beginning with a more comprehensive motif-seeking analysis of HITS-CLIP-identified CEY-1 binding sites.

Assess the effect of CEY-1 binding antagonizing miRISC binding

Does CEY-1 antagonize miRISC binding in *let-7(n2853)*? This a particularly interesting question in light of two pieces of data: First, CEY-1 HITS-CLIP data suggest that CEY-1 binding sites on *let-7* targets, including *lin-41*, overlap or are adjacent to ALG-1 binding

sites (Fig 3-8D-G). Second, our phenotyping data indicate that *cey-1* mutants do not suppress *let-7* null lethality, unless the null is also carrying a partial *let-7* rescue plasmid (Fig 3-6D). The latter suggests that loss of *cey-1*-mediated polysome formation cannot singly account for the rescue of the *let-7(n2853)* hypomorphic phenotypes. Therefore, it may be possible that loss of *cey-1* allows the weak *let-7(n2853)* miRISC to better silence *lin-41* by increasing access to its 3'UTR binding sites.. To determine if CEY-1 binding limits miRISC association with *lin-41*, we could perform ALG-1 RIPs in animals expressing the *lin-41* 3'UTR reporter in *let-7(n2853).* If CEY-1 antagonizes miRISC binding, then animals expressing the wild-type reporter should have less *lin-41* mRNA bound by ALG-1 compared to animals expressing the CBS mutant reporter. If our hypothesis is valid, then a similar effect should be observed for the wild-type reporter in animals fed empty vector versus *cey-1* RNAi.

Assess what distinguishes CEY-1 and CEY-4 in the regulation of *let-7* activity.

Loss of either *cey-1* or *cey-4* yields a similar global reduction in mRNA levels and polysome formation [13]. However our data suggest that CEY-1 and CEY-4 are not redundant as loss of *cey-4* does not suppress the Rup phenotype of *let-7* mutants (Fig 3-2B). Therefore, what differentiates CEY-1 and CEY-4 is an intriguing avenue of investigation.

Both CEY-1 and CEY-4 are broadly expressed in soma and bind a large number of mRNAs [13]. CEY-1 and CEY-4 also both have RG-rich regions (Fig 4-3). The type I protein arginine methyltransferase PRMT-1, which catalyzes asymmetrical di-methylation of arginine residues at RG containing motifs [14] (Fig 4-3B), was reported to modify both CEY-1 and CEY-4, but no data was shown for CEY-1 [13]. We confirmed

that CEY-1 displays a *prmt-1*-dependent shift in electrophoretic mobility that is partially rescued in a strain expressing an *mcherry::prmt-1* transgene (Figure 4-3C). Methylation by PRMT-1 has been demonstrated to inhibit phosphorylation by the conserved serine/threonine kinase AKT-1/PKB [15,16]. Mining of a large-scale phospho-proteomic database [17] revealed CEY-1 has two phospho-serines located directly adjacent to RG-rich regions that match the AKT-1 recognition motif (RXXS/T) (red underline, Fig 4-3A). In contrast CEY-4 has multiple identified phosphorylation sites but none are located in putative AKT-1 motifs (Fig 4-3A). These data highlight the possibility that CEY-1 and CEY-4 may be differentially regulated by post-translational modifications that could affect their function. To preliminarily address if post-translational modification by either PRMT-1 or AKT-1 affects CEY-1 function in the *let-7* miRNA pathway we could compare the ability of our *cey-1* transgene to complement Rup suppression in the *cey-1; let-7* double mutant in animals treated with either empty vector, *prmt-1* or *akt-1* RNAi. If *prmt-1* or *akt-1* facilitate CEY-1 than we predict their knockdown will complement *cey-1; let-7* suppression and the transgene will no longer rescue. In contrast, if they antagonize or have no effect on CEY-1 function their knockdown is not expected to complement *cey-1; let-7* suppression. However, since the rescue of the *cey-1* transgene is not 100% there is a chance that we may be able to distinguish between these two possibilities.

It is also possible that CEY-1 and CEY-4 may have a subset of non-overlapping targets that are biologically significant. Therefore a careful comparison of mRNAs bound by these CEYs is required. For example, if CEY-4 does not associate with *lin-41*, then comparison of the loss of *cey-1* versus *cey-4* would be an informative experiment for

further investigation into *lin-41* translational dynamics in *let-7(n2853*). Similarly, if CEY-1 and CEY-4 both associate with *lin-41*, then *lin-41* ribosome profiling and examination of both *lin-41* mRNA and LIN-41 protein levels in *let-7(n2853*) with or without the loss of each *cey* may also provide insight into their functional differences.

Future Directions for understanding regulation of miRISC

The main focus of this dissertation has been to identify and characterize factors that regulate the miRNA effector complex, miRISC. In the process of investigating both CK2 and CEY-1, we observed interesting phenotypes during post-dauer development. As previously described, post-dauer suppression of miRNA phenotypes requires CK2, but not CK2 phosphorylation of CGH-1 (Fig 2-S7B), suggesting CK2 function in the miRNA pathway is different during continuous and post-dauer development. We also observed that *cey-1* mutant suppression of *let-7(n2853)* vulval rupture is significantly attenuated in post-dauer development (Fig 4-4). While loss of *cey-1* significantly suppresses *let-7(n2853)* Rup during both continuous and post-dauer development, Rup suppression is far less potent post-dauer, suggesting that CEY-1 antagonism of miRISC is less powerful in *let-7(n2853)* during post-dauer development.

Together these data highlight an underexplored biological context where miRISC activity is altered. During continuous development, *C. elegans* proceeds through four larval stages (L1-L4) before becoming adults. However, adverse environmental conditions promote entry into dauer quiescence, an arrested, non-aging, stress-resistant larval stage immediately after the L2 molt [18]. If conditions improve dauers resume normal development. Post-dauer cell divisions are identical to those occurring during

continuous development [19,20], suggesting that progenitor cells in dauer larvae maintain developmental potential.

Interestingly, the robustness of the dauer to developmental interruption can be partly attributed to enhanced activity of *lin-4* and *let-7* family miRNAs [21]. However, the molecular underpinnings of this enhanced activity is not well understood. Although, genetic evidence suggests that enhancement of miRNA activity occurs even without the primary miRNA Argonaute, ALG-1, as heterochronic phenotypes of *alg-1* mutants are efficiently suppressed post-dauer. One interpretation of these results is that modulatory proteins elevate the activity of the remaining ALG-2-containing miRISC [21]. Thus, identifying and characterizing the factors that affect miRISC activity in post-dauer development is a promising future direction for extending our understanding of the regulation of miRISC. Furthermore, post-dauer development can be thought of as a model to investigate the role of miRISC in cellular quiescence. In humans, stem cells are maintained in a reversible quiescent state that appears to be essential for stem cell self-renewal, and is important for cancer stem cell resistance to therapeutic intervention [22]. However, the mechanisms that regulate quiescence and the role of the miRNA pathway in this process are not fully understood. Thus, exploring the regulation of miRNA function during *C. elegans* post-dauer development could broadly inform our understanding of the role of miRNAs in the field of stem cell biology. Ultimately, findings in *C.elegans* have the potential to support ongoing efforts to develop new diagnostic, therapeutic, and preventive methods to exploit the potential of this unique cell type to benefit human health.

CONCLUSION

Post-transcriptional gene silencing by the miRNA pathway is an established paradigm in metazoan gene regulation with critical functions in diverse, essential biological processes. Mechanisms governing miRNA biogenesis and target silencing are largely established; however, significant deficits exist in our understanding of how the miRNA effector complex, miRISC, is regulated. To understand how post-translational modifications of miRISC and miRISC interaction with RNA binding proteins affect miRISC function we employed a variety of genetic and biochemical techniques to identify and characterize factors that function in each of these roles: the kinase CK2 and the RNA-binding protein CEY-1, respectively. CK2 plays a critical role in promoting miRISC binding to target mRNAs thought the phosphorylation of the conserved miRISC factor CGH-1/DDX6. CEY-1 antagonizes the silencing of *let-7* miRISC through direct association with the mRNA targets of *let-7*. While the specific aim of this dissertation was to further our understanding of conserved factors that regulate miRISC in *C. elegans*, our findings transcend their initial intent as the basic insights obtained may broadly inform efforts to decipher regulation of the miRNA pathway and the rapidly advancing field of miRNA therapeutics for treating human diseases.

Figure 4-1. VIG-1 S17 is phosphorylated by CK2 in vitro. (A) VIG-1 has 7 CK2 phosphorylation motifs. S17 and S143 have in vivo phospho-peptide coverage identified by mass spectrometry. (B) Coomassie blue (CBB) staining indicates equal protein loading in (C). (C) Full length GST-VIG-1 (WT) is phosphorylated by CK2 in vitro. VIG-1 S17A mutant, but not S143A mutant, abrogates phosphorylation signal.

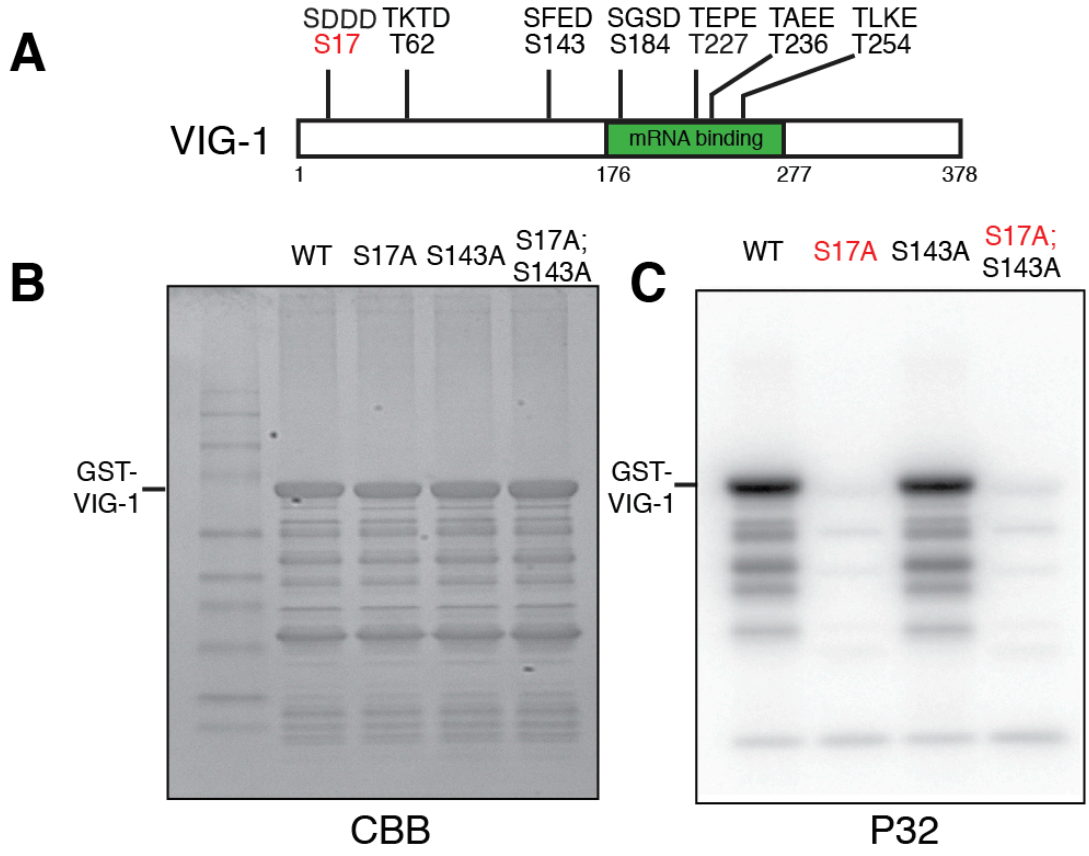

Figure 4-2. Targeted RNAi screen of *C.elegans* protein phosphatase 2A (PP2A) regulatory subunits. RNAi knockdown of *sur-6* and *pptr-1* substantially enhances vulval rupture (Rup) in *let-7(n2853)*, similar to RNAi of core miRISC Argonaute, *alg-1*, or CK2 catalytic subunit, *kin-3* (n=125).

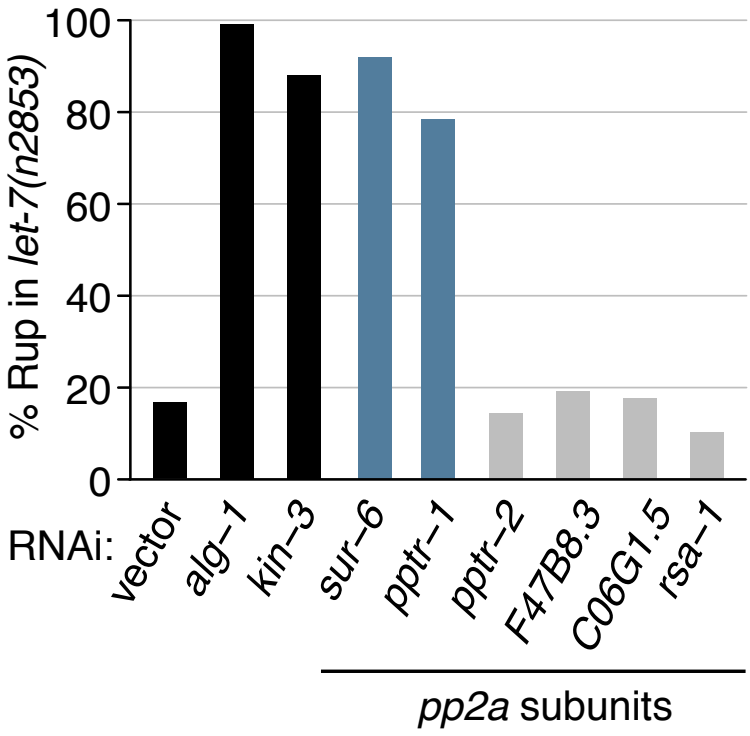

Figure 4-3. CEY-1 is modified in a *prmt-1* dependent manner and is a potential AKT-1 target. (A) CEY-1 and CEY-4 amino acid sequences with potential PRMT-1 methylation motifs (RGG, RxR, RGx or RxG) highlighted in rose. Experimentally derived post-translational modifications (PTMs) are indicated with a red asterisk. PTMs located in an AKT-1 recognition motif (RxxS/T) underlined in red. **(B)** *prmt-1* encodes a type I protein arginine methyltransferase that catalyzes asymmetrical di-methylation to arginine at RG containing motifs. **(C)** Western analysis of adult *C.elegans* lysis immunoblotted with anti-CEY-1 suggests CEY-1 displays increased electrophoretic mobility in *prmt-1(ok2710)*. Partial rescue of CEY-1 migration (red arrow) is observed in *prmt-1(ok2710)* expressing MCHERRY::PRMT-1 from an extrachromosomal array. Y-Tubulin serves as a loading control.

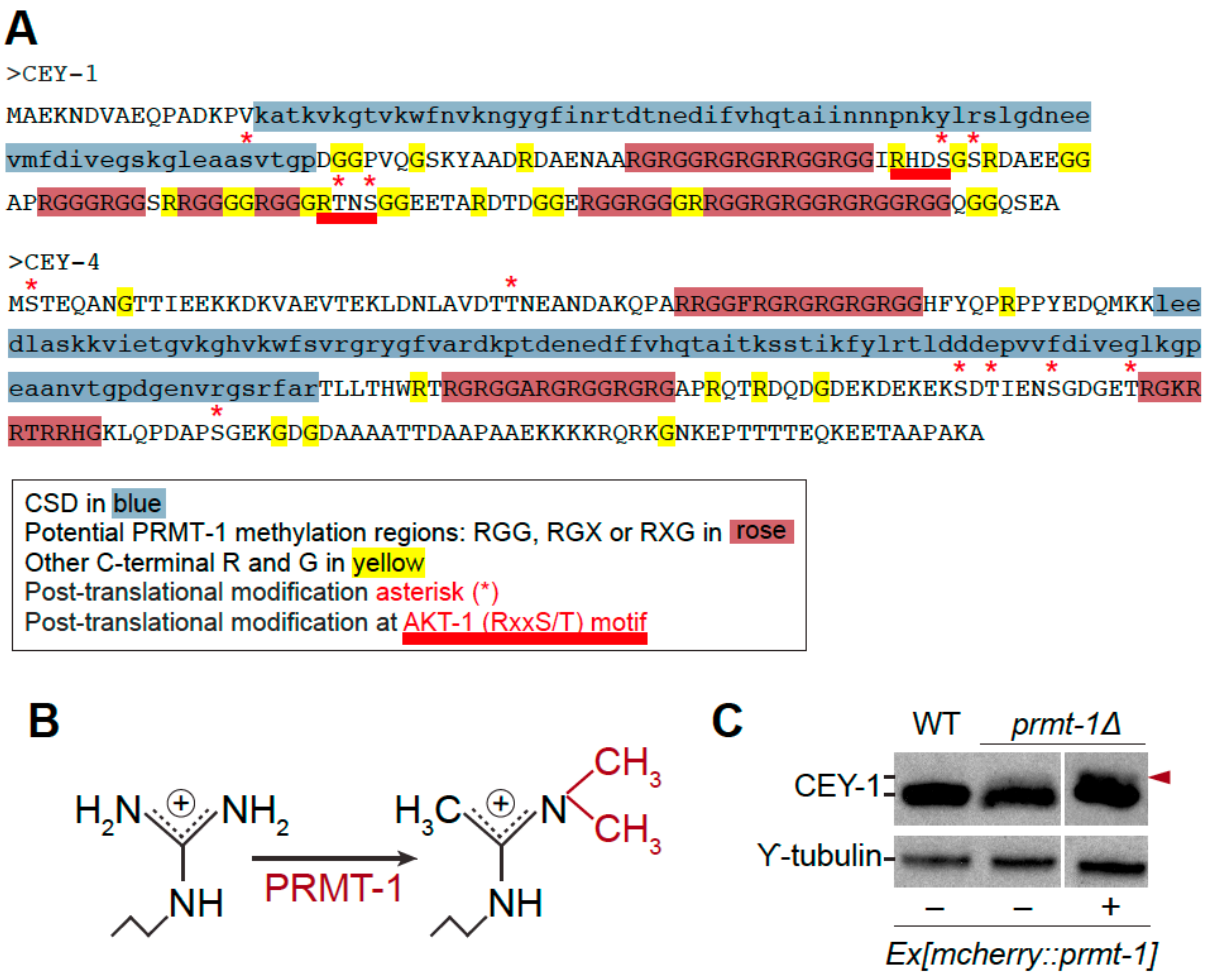

Figure 4-4. *cey-1* mutant suppression of *let-7(n2853)* Rup is significantly attenuated in post-dauer development. *cey-1(ok1805)* significantly suppresses *let-7(n2853)* Rup during continuous and post-dauer development ($p<0.001$ by Fisher's exact test, $n>365$). However Rup suppression is far less potent post-dauer.

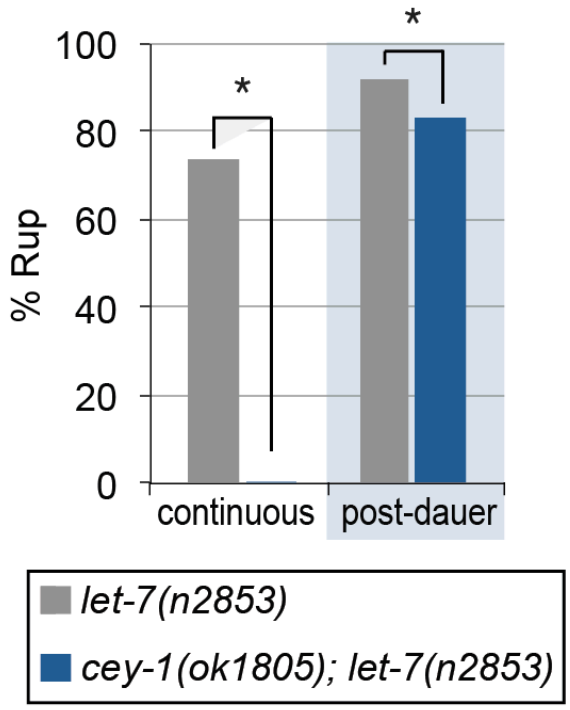

REFERENCES

1. Hammell CM, Lubin I, Boag PR, Blackwell TK, Ambros V (2009) nhl-2 Modulates microRNA activity in Caenorhabditis elegans. Cell 136: 926-938.
2. Caudy AA, Ketting RF, Hammond SM, Denli AM, Bathoorn AM, et al. (2003) A micrococcal nuclease homologue in RNAi effector complexes. Nature 425: 411-414.
3. Chan SP, Ramaswamy G, Choi EY, Slack FJ (2008) Identification of specific let-7 microRNA binding complexes in Caenorhabditis elegans. RNA 14: 2104-2114.
4. Zielinska DF, Gnad F, Jedrusik-Bode M, Wisniewski JR, Mann M (2009) Caenorhabditis elegans has a phosphoproteome atypical for metazoans that is enriched in developmental and sex determination proteins. J Proteome Res 8: 4039-4049.
5. Paix A, Wang Y, Smith HE, Lee CY, Calidas D, et al. (2014) Scalable and versatile genome editing using linear DNAs with microhomology to Cas9 Sites in Caenorhabditis elegans. Genetics 198: 1347-1356.
6. Poole A, Poore T, Bandhakavi S, McCann RO, Hanna DE, et al. (2005) A global view of CK2 function and regulation. Mol Cell Biochem 274: 163-170.
7. Parry DH, Xu J, Ruvkun G (2007) A whole-genome RNAi Screen for C. elegans miRNA pathway genes. Curr Biol 17: 2013-2022.
8. Janssens V, Longin S, Goris J (2008) PP2A holoenzyme assembly: in cauda venenum (the sting is in the tail). Trends in biochemical sciences 33: 113-121.
9. Janssens V, Goris J (2001) Protein phosphatase 2A: a highly regulated family of serine/threonine phosphatases implicated in cell growth and signalling. The Biochemical journal 353: 417-439.
10. Bose A, Kahali B, Zhang S, Lin JM, Allada R, et al. (2006) Drosophila CK2 regulates lateral-inhibition during eye and bristle development. Mechanisms of development 123: 649-664.
11. Sieburth DS, Sundaram M, Howard RM, Han M (1999) A PP2A regulatory subunit positively regulates Ras-mediated signaling during Caenorhabditis elegans vulval induction. Genes & development 13: 2562-2569.
12. Padmanabhan S, Mukhopadhyay A, Narasimhan SD, Tesz G, Czech MP, et al. (2009) A PP2A regulatory subunit regulates C. elegans insulin/IGF-1 signaling by modulating AKT-1 phosphorylation. Cell 136: 939-951.
13. Arnold A, Rahman MM, Lee MC, Muehlhaeusser S, Katic I, et al. (2014) Functional characterization of C. elegans Y-box-binding proteins reveals tissue-specific functions and a critical role in the formation of polysomes. Nucleic acids research 42: 13353-13369.
14. Bedford MT, Richard S (2005) Arginine methylation an emerging regulator of protein function. Molecular cell 18: 263-272.
15. Yamagata K, Daitoku H, Takahashi Y, Namiki K, Hisatake K, et al. (2008) Arginine methylation of FOXO transcription factors inhibits their phosphorylation by Akt. Molecular cell 32: 221-231.
16. Takahashi Y, Daitoku H, Hirota K, Tamiya H, Yokoyama A, et al. (2011) Asymmetric arginine dimethylation determines life span in C. elegans by regulating forkhead transcription factor DAF-16. Cell metabolism 13: 505-516.

17. Gnad F, Gunawardena J, Mann M (2011) PHOSIDA 2011: the posttranslational modification database. Nucleic acids research 39: D253-260.
18. Cassada RC, Russell RL (1975) The dauerlarva, a post-embryonic developmental variant of the nematode Caenorhabditis elegans. Developmental biology 46: 326-342.
19. Liu ZC, Ambros V (1991) Alternative Temporal Control-Systems for Hypodermal Cell-Differentiation in Caenorhabditis-Elegans. Nature 350: 162-165.
20. Euling S, Ambros V (1996) Reversal of cell fate determination in Caenorhabditis elegans vulval development. Development 122: 2507-2515.
21. Karp X, Ambros V (2012) Dauer larva quiescence alters the circuitry of microRNA pathways regulating cell fate progression in C. elegans. Development 139: 2177-2186.
22. Li L, Bhatia R (2011) Stem cell quiescence. Clinical cancer research : an official journal of the American Association for Cancer Research 17: 4936-4941.

APPENDIX A

The *Caenorhabditis elegans* HEN1 ortholog, HENN-1, methylates and stabilizes select subclasses of germline small RNAs

AUTHORS

Billi AC, Alessi AF*, Khivansara V, Han T, Freeberg MA, Mitani S, Kim JK

** Alessi AF contributed data in Figure A-7 C-F and Figure A-S13 C-F.*

CITATION

Billi AC, Alessi AF, Khivansara V, Han T, Freeberg M, Mitani S, Kim JK. The *Caenorhabditis elegans* HEN1 ortholog, HENN-1, methylates and stabilizes select subclasses of germline small RNAs. *PLoS Genetics* 8: e1002617 (2012).

ABSTRACT

Small RNAs regulate diverse biological processes by directing effector proteins called Argonautes to silence complementary mRNAs. Maturation of some classes of small RNAs involves terminal 2'-O-methylation to prevent degradation. This modification is catalyzed by members of the conserved HEN1 RNA methyltransferase family. In animals, Piwi-interacting RNAs (piRNAs) and some endogenous and exogenous small interfering RNAs (siRNAs) are methylated, whereas microRNAs are not. However, the mechanisms that determine animal HEN1 substrate specificity have yet to be fully resolved. In *C. elegans*, a HEN1 ortholog has not been studied, but there is evidence for methylation of piRNAs and some endogenous siRNAs. Here, we report that the worm

HEN1 ortholog, HENN-1 (*HEN* of *N*ematode), is required for methylation of *C. elegans* small RNAs. Our results indicate that piRNAs are universally methylated by HENN-1. In contrast, 26G RNAs, a class of primary endogenous siRNAs, are methylated in female germline and embryo, but not in male germline. Intriguingly, the methylation pattern of 26G RNAs correlates with the expression of distinct male and female germline Argonautes. Moreover, loss of the female germline Argonaute results in loss of 26G RNA methylation altogether. These findings support a model wherein methylation status of a metazoan small RNA is dictated by the Argonaute to which it binds. Loss of *henn-1* results in phenotypes that reflect destabilization of substrate small RNAs: dysregulation of target mRNAs, impaired fertility, and enhanced somatic RNAi. Additionally, the *henn-1* mutant shows a weakened response to RNAi knockdown of germline genes, suggesting that HENN-1 may also function in canonical RNAi. Together, our results indicate a broad role for HENN-1 in both endogenous and exogenous gene silencing pathways and provide further insight into the mechanisms of HEN1 substrate discrimination and the diversity within the Argonaute family.

AUTHOR SUMMARY

Small RNAs serve as sentinels of the genome, policing activity of selfish genetic elements, modulating chromatin dynamics, and fine-tuning gene expression. Nowhere is this more important than in the germline, where endogenous small interfering RNAs (endo-siRNAs) and Piwi-interacting RNAs (piRNAs) promote formation of functional gametes and ensure viable, fertile progeny. Small RNAs act primarily by associating with effector proteins called Argonautes to direct repression of complementary mRNAs.

HEN1 methyltransferases, which methylate small RNAs, play a critical role in accumulation of these silencing signals. In this study, we report that the 26G RNAs, a class of *C. elegans* endo-siRNAs, are differentially methylated in male and female germlines. 26G RNAs derived from the two germlines are virtually indistinguishable, except that they associate with evolutionarily divergent Argonautes. Our data support a model wherein the methylation status and, consequently, stability of a small RNA is determined by the associated Argonaute. Therefore, selective expression of Argonautes that permit or prohibit methylation may represent a new mechanism for regulating small RNA turnover. As we observe this phenomenon in the germline, it may be particularly pertinent for directing inheritance of small RNAs, which can carry information not encoded in progeny DNA that is essential for continued transgenerational genome surveillance.

INTRODUCTION

Argonautes are an evolutionarily conserved family of proteins implicated in diverse cellular processes. They function as effector proteins in the RNA-induced silencing complex (RISC), a gene regulatory complex that binds small, non-coding RNAs to target its silencing effects. Small RNAs are broadly segregated into groups that differ in their mechanisms of biogenesis and silencing, as well as in the subsets of Argonaute effectors that bind them. The microRNAs (miRNAs) are highly conserved small RNAs processed from endogenous hairpin precursors that regulate networks of mRNAs primarily through post-transcriptional repression [1,2]. The piRNAs, so named for the Piwi Argonautes that bind them, function predominantly in maintenance of germline

integrity, often through repression of repetitive transposable elements. The small interfering RNAs comprise a more heterogeneous group that includes small RNAs derived from cleavage of exogenous double-stranded RNA (exo-siRNAs) or generated endogenously (endo-siRNAs).

Chemical modification has emerged as an important theme in regulation of small RNA function (for a review, see Kim et al., 2010 [3]). Internal editing has been found to occur in select miRNA precursors through the action of ADAR (*a*denosine *d*eaminase *a*cting on *R*NA) enzymes, with consequences for miRNA processing efficiency, stability, and targeting [4,5,6,7,8]. Some siRNAs generated in fly and mouse also show evidence of editing by ADARs [9,10], but the significance of such internal editing among siRNAs is not yet known. In contrast, terminal editing through 2'-O-methylation, addition of untemplated nucleotides, or exonucleolytic trimming plays a more general role in small RNA metabolism. These terminal modifications are not unrelated. Evidence in plants and animals suggests that methylation of the 3' terminal nucleotide protects small RNAs from polyuridylation and polyadenylation, signals that direct exonucleolytic degradation [11,12,13,14,15,16]. Thus, terminal methylation plays an important role in regulating small RNA turnover. Formation of the 2'-O-methyl group is catalyzed by HEN1, a methyltransferase discovered in *Arabidopsis thaliana* that is conserved across metazoa, fungi, viridiplantae, and bacteria [17]. Although plant and animal HEN1 orthologs exhibit 40-50% amino acid similarity in the conserved methyltransferase domain [18], the proteins differ in their substrate specificity. Plant HEN1 acts on small RNAs in duplex and methylates both siRNAs and miRNAs [19,20,21]. In contrast, animal HEN1 orthologs modify only single-stranded small RNAs [22,23,24], enabling methylation of

small RNAs such as piRNAs, which are not derived from double-stranded RNA intermediates [25,26,27,28,29]. While animal piRNAs appear to be universally methylated [24,26,27,30,31,32], animal miRNAs are generally not methylated [19,26,31], and the mechanisms by which animal HEN1 orthologs discriminate between substrates are not entirely clear. HEN1 orthologs that catalyze terminal methylation of small RNAs have been characterized in mouse, fish, and fly, among other organisms [15,22,23,24,33], yet the orthologous methyltransferase in worm [18] has yet to be investigated. With its expanded Argonaute family and diverse small RNA classes, *Caenorhabditis elegans* provides an advantage for studying HEN1 substrate specificity.

Since the discovery of the founding members of the microRNA family in *C. elegans* [1,2,34], many additional classes of small RNAs have been characterized. A large-scale small RNA sequencing effort revealed a class of terminally methylated 21-nucleotide RNAs with 5' uridines [27]. These 21U RNAs were subsequently determined to represent the piRNAs of *C. elegans* based on their germline-specific expression, association with worm Piwi Argonautes PRG-1 and PRG-2, and function in transposon silencing and maintenance of temperature-dependent fertility [35,36,37,38]. Also found through small RNA cloning and deep sequencing were populations of 26- and 22-nucleotide RNAs with a 5' preference for guanosine (the 26G RNAs and 22G RNAs, respectively) that constitute the endo-siRNAs of *C. elegans* [27,39]. The 26G RNAs are primary endo-siRNAs generated in the germline to regulate spermatogenic and zygotic gene expression. They are divided into two non-overlapping subclasses named for the Argonautes that bind them: the ERGO-1 class 26G RNAs, which are generated in the maternal germline and distributed into the embryo, and the ALG-3/ALG-4 class 26G

RNAs, which are specific to the male germline and required for sperm function [40,41,42]. The 22G RNAs are composed of many small RNA classes, all of which are bound by worm-specific Argonautes (Wagos). A large population of 22G RNAs are secondary endo-siRNAs whose production by RNA-dependent RNA polymerases is triggered by the activity of 21U RNAs and 26G RNAs [36,41,42,43]; however, many other 22G RNAs are independent of these primary small RNAs [44,45]. Secondary siRNAs serve to amplify the signal of primary small RNAs to effect robust silencing. Production of 22G secondary siRNAs is also triggered by exogenously introduced dsRNAs [43,45,46,47], suggesting convergence of endogenous and exogenous RNAi pathways at the level of the secondary siRNA response.

Among *C. elegans* small RNAs, only 21U RNAs and 26G RNAs are known to be methylated [27,42]; 22G RNAs triggered by either primary endo- or exo-siRNAs appear to be unmethylated [45,46]. Although the significance of worm small RNA methylation is unknown, loss of terminal methylation has been shown to decrease stability of piRNAs in many animal models [15,22,24] and both endo- and exo-siRNAs in fly [22,48]. Methylation may therefore represent an essential step in stabilization of some classes of worm small RNAs.In this study, we characterize the *C. elegans hen1* ortholog, which has been named *henn-1* (*hen* of *n*ematode), as the name *hen-1* has already been assigned to an unrelated *C. elegans* gene. We demonstrate that HENN-1 methylates small RNAs bound by Piwi clade Argonautes: the 21U RNAs and the ERGO-1 class 26G RNAs. However, we show that 26G RNAs bound by Ago clade Argonautes ALG-3 and ALG-4 are not methylated and are therefore *henn-1*-independent. Differential methylation of 26G RNAs provides evidence for an existing model [13,22,23,49,50]

wherein evolutionarily divergent Argonautes either direct or prohibit HEN1-mediated methylation of associated small RNAs. In further support of this Argonaute-dictated methylation model, we find that small RNAs are likely methylated after associating with an Argonaute: the Argonaute ERGO-1 is required for 26G RNA methylation, but methylation is not required for ERGO-1 to bind a 26G RNA.

In the *henn-1* mutant, levels of both 21U RNAs and ERGO-1 class 26G RNAs drop precipitously after their deposition into embryo, suggesting that HENN-1-mediated methylation is essential for perdurance of the maternal small RNA load during filial development. Accordingly, the *henn-1* mutant shows enhanced somatic sensitivity to exogenous RNAi, a phenotype associated with loss of ERGO-1 class 26G RNAs. Surprisingly, however, the *henn-1* mutant germline exhibits an attenuated response to RNAi, suggesting that HENN-1 may also function in the exogenous RNAi pathway. Altogether, our study supports a role for HENN-1 in diverse small RNA pathways in *C. elegans* and offers further insight into the mechanisms governing substrate discrimination for animal HEN1 orthologs.

RESULTS

C02F5.6 Encodes the *C. elegans* HEN1 Ortholog

To examine small RNA methylation in *C. elegans*, we began by characterizing *C02F5.6*, the gene previously predicted to encode the HEN1 ortholog in worm [18]. This gene, subsequently named *henn-1*, encodes a protein that exhibits significant amino acid similarity across the conserved HEN1 methyltransferase domain relative to established members of the HEN1 family (Fig A-S1). Although two *henn-1* gene models with

differing 3' ends have been proposed, 3'RACE and protein studies using a rabbit polyclonal antibody generated against a common N-terminal HENN-1 epitope detected only the longer isoform (Fig 2.S2A, B).

To facilitate our studies of the function of HENN-1, we isolated and characterized the *henn-1(tm4477)* allele. This allele carries a deletion that encompasses *henn-1* exon four, which encodes 65% of the conserved methyltransferase domain as annotated by Kamminga et al. [15]. Sequencing of the *henn-1(tm4477)* mRNA indicates that loss of exon four activates a cryptic splice donor site in the third intron, resulting in an extended third exon that encodes a premature termination codon (Fig A.S2B). The *henn-1(tm4477)* mRNA is readily detected by RT-PCR but does not produce a detectable protein product (Fig 2.S2A) or exhibit methyltransferase activity (see below), suggesting that *henn-1(tm4477)* (hereafter, *henn-1*) represents a functional null allele.

HENN-1 Terminally Methylates and Stabilizes *C. elegans* piRNAs

Like piRNAs in fly [22,23,32], mouse [30,31], and zebrafish [26], the *C. elegans* 21U RNAs are terminally methylated [27], but the factor catalyzing this modification has not yet been identified. To determine if 21U RNA methylation depends on *henn-1*, we assessed methylation status using the β-elimination assay [51]. A small RNA molecule whose terminal nucleotide has been 2'-O-methylated is resistant to this treatment, whereas the cis-diols of an unmodified 3' terminal nucleotide are oxidized by sodium periodate, rendering the nucleotide susceptible to β-elimination under basic conditions. The resulting size difference can be resolved on a polyacrylamide gel to determine methylation status. All 21U RNAs examined were found to be terminally methylated in a

henn-1-dependent manner (Fig A-1A, A-S3A), whereas a control miRNA was not methylated in either wild-type or *henn-1* mutant animals (Fig 2A-1B). Although 21U RNAs are still detectable in the *henn-1* mutant, the abundance of the full-length species is visibly decreased for some 21U RNAs; this correlates with the appearance of putative degradation products of unmethylated, unprotected 21U RNAs. To demonstrate that loss of 21U RNA methylation in the *henn-1* mutant is specifically due to the absence of *henn-1*, we used the Mos1-mediated single copy insertion technique [52] to introduce a *henn-1::gfp* transgene driven by the promoter of the polycistronic mRNA that encodes *henn-1* (*xkSi1*) or by the germline-specific *pie-1* promoter (*xkSi2*) into the *henn-1* mutant (Fig A-S2C). Both endogenous and germline-specific expression of *henn-1::gfp* restore 21U RNA methylation in the *henn-1* mutant (Fig A-1A).

To investigate the relationship between terminal methylation and piRNA accumulation, we used Taqman RT-qPCR to assess 21U RNA levels in wild-type and *henn-1* mutant animals across development at 25°C. Importantly, the Taqman stem-loop RT primer is capable of distinguishing between full-length and terminally degraded small RNAs [53]. For example, the *let-7e* miRNA differs from *let-7a* only in the absence of the final nucleotide and U > G substitution at the ninth nucleotide, a position likely not represented in the stem-loop Taqman primer. Absence of this final nucleotide decreases detection of *let-7e* by the *let-7a* Taqman assay by more than a thousandfold [53]. *henn-1* mutant embryo and early larva show dramatically reduced detection of female germline-enriched piRNA 21UR-1848 (Fig A-2A), consistent with decreased embryonic detection for some 21U RNAs observed by northern blot (Figs A-1A, A-S3A). 21U RNA levels recover to wild-type in late larval stages, coincident with the onset of

germline proliferation and de novo 21U RNA biosynthesis; however, in gravid animals at 56 hours, 21UR-1848 levels in the *henn-1* mutant have declined to less than 50% of those observed in wild-type (P=0.0005; two-tailed *t*-test). Eight additional 21U RNAs examined show a similar pattern (Fig A-S4). These data suggest that *henn-1* is dispensable for piRNA biogenesis but essential for robust inheritance of piRNAs. Parallel analysis of miR-1 and several additional miRNAs across development shows that effects of loss of *henn-1* are specific to its substrates and not due to generalized small RNA dysregulation in the *henn-1* mutant (Figs A-2B, A-S5).

HENN-1 Plays a Minor Role in piRNA-mediated Germline Regulation

We next sought to determine the extent to which decreased abundance of piRNAs in the *henn-1* mutant compromises activity of the piRNA pathway. Unlike in fly, where many selfish genetic elements are desilenced in the absence of piRNAs [32], *C. elegans* at present has only a single established molecular readout for piRNA pathway function: increased expression of transposase mRNA from *Tc3*, a Tc1/mariner family transposon [35,36]. Two 21U RNAs have been found to map to *Tc3*, but both map in the sense direction and thus are unlikely to act directly in *Tc3* repression via canonical RNAi mechanisms [35,36]. Rather, 21U RNAs likely mediate their repressive effects through triggering production of secondary siRNAs, 22G RNAs, that engage worm-specific Argonautes (Wagos) to effect *Tc3* gene silencing [36,45]. We therefore identified a 22G RNA that shows complete antisense complementarity to *Tc3* and can be classified as a Wago-dependent, 21U RNA-dependent secondary siRNA based on its total depletion both in the MAGO12 mutant, which lacks all Wagos, and in the *prg-1(n4357); prg-*

2(n4358) double mutant, which lacks piRNAs [36,45]. Levels of this 22G RNA in the *henn-1* mutant are reduced by 44% in embryo but not significantly altered in hatched L1 larva (Fig A-S6A). This suggests that the low embryonic and early larval levels of 21U RNAs in the *henn-1* mutant are still sufficient to trigger production of secondary siRNAs, although to a lesser degree than in wild-type.

Consistent with the modest effect of loss of *henn-1* on accumulation of piRNA-triggered secondary siRNAs, *henn-1* mutant animals exhibit only a small increase (35% in starved L1 larva, 25% in L1 larva fed for 4 hours at 25°C) in *Tc3* transposase mRNA levels relative to wild-type (Fig A-2C). This is not unexpected due to the poor coincidence of the time intervals corresponding to piRNA dysregulation in the *henn-1* mutant and *Tc3* sensitivity to 21U RNAs; the *henn-1* mutant shows the greatest disparity in piRNA levels in early larval development, whereas *Tc3* levels are most sensitive to piRNAs in germline and embryo (Fig A-2A, C). These findings suggest that HENN-1 is not strictly required for piRNA target repression, but contributes to robust silencing of *Tc3*.

In addition to *Tc3* dysregulation, loss of *prg-1* also results in a temperature-sensitive sterility phenotype [38,43]. To determine if the *henn-1* mutant also exhibits a fertility defect, we assessed fertility at 20°C and 25°C. At 20°C, brood size of the *henn-1* mutant does not differ significantly from that of wild-type. In contrast, *henn-1* mutant animals maintained at 25°C exhibit a 25% decrease in brood size relative to wild-type (P=0.0059; two-tailed *t*-test) that can be rescued by germline expression of *henn-1::gfp* from the *xkSi2* transgene (Fig A-S7). The impaired fertility of the *henn-1* mutant is consistent with abnormal fertility phenotypes associated with loss of HEN1

methyltransferase activity in other animals. Loss of *HEN1* in *Tetrahymena thermophila* depletes Piwi-interacting RNAs called scan RNAs, impairing DNA elimination and, consequently, the viability of progeny [24]. The zebrafish *hen1* mutant fails to maintain a female germline, resulting in an exclusively male population [15]. Nevertheless, we cannot conclude that the temperature-sensitive fertility defect of the *henn-1* mutant is due exclusively to compromise of the 21U RNA pathway.

ERGO-1 and ALG-3/ALG-4 Class 26G RNAs Are Differentially Methylated by HENN-1

26G RNAs were reported to be methylated in the first *C. elegans* small RNA deep sequencing study [27]. Subsequent studies concluded that the species assessed was an ERGO-1 class 26G RNA [40]. Consistent with these data, we found that ERGO-1 class 26G RNAs, found in female germline and embryo, are methylated. As was the case for piRNAs, this methylation occurs in a *henn-1*-dependent manner (Figs A-3A, A-S3B). Surprisingly, however, ALG-3/ALG-4 class 26G RNAs, specific to the male germline, showed no evidence of methylation even in wild-type animals (Figs A-3B, A-S3C). One potential explanation for this observation would be that female germline small RNAs are universally methylated, whereas male germline small RNAs are not. To explore this possibility, we assessed 21U RNAs in male and female germlines. Both were methylated (Fig A-3C), indicating that differential 26G RNA methylation cannot be explained simply by a lack of methyltransferase functionality in the male germline.

Because the two classes of 26G RNAs bind unique Argonautes in male and female germlines, we hypothesized that the Argonaute ERGO-1 might direct methylation of

26G RNAs. To address this question, we sought to assess methylation of an ERGO-1 class 26G RNA in the absence of ERGO-1. As 26G RNAs are dramatically depleted in the absence of their respective Argonautes [40], we queried published wild-type and *ergo-1(tm1860)* gravid adult deep sequencing libraries [42] to identify an ERGO-1 class 26G RNA that still accumulates to levels sufficient for visualization by northern blotting in the *ergo-1(tm1860)* mutant. 26G-O1, an extremely abundant ERGO-1 class 26G RNA, is present at roughly 0.5% wild-type levels in the *ergo-1(tm1860)* mutant, but still abundant enough to detect by northern blotting. Consistent with our hypothesis that ERGO-1 is required for 26G RNA methylation, we found that 26G-O1 is unmethylated in the *ergo-1(tm1860)* mutant embryo (Fig A-4A). We next asked the converse question: Is 26G RNA methylation required for association with ERGO-1? We immunopurified ERGO-1 complexes from wild-type and *henn-1* mutant embryo lysates (Fig A-4B) and extracted RNA. In both wild-type and *henn-1* mutant samples, ERGO-1 class 26G RNAs are readily detected (Fig A-4C), indicating that ERGO-1 effectively binds both methylated and unmethylated 26G RNAs. Taken together, these data suggest that 26G RNAs bind ERGO-1 and are subsequently methylated by HENN-1.

To test whether HENN-1-mediated methylation is required to maintain levels of all substrate small RNAs, we assessed ERGO-1 class 26G RNAs for defects in accumulation in the *henn-1* mutant. Loss of *henn-1* has more severe consequences for this class of small RNAs than are observed for 21U RNAs: ERGO-1 class 26G RNA 26G-O3 fails to accumulate to wild-type levels at any stage of development, although the disparity is less pronounced in adulthood, during peak 26G RNA biogenesis (Fig A-5A). For comparison, we assayed levels of ALG-3/ALG-4 class 26G RNA 26G-S5

across the developmental window during which it is readily detected by Taqman RT-qPCR. Levels of 26G-S5 are similar in the *henn-1* mutant relative to wild-type (Fig A-5B), consistent with the idea that HENN-1 is required for accumulation of ERGO-1 class 26G RNAs but dispensable for that of ALG-3/ALG-4 class 26G RNAs. Analysis of seven additional ERGO-1 class 26G RNAs and two additional ALG-3/ALG-4 class 26G RNAs corroborated these observations (Figs A-S8, A-S9).

HENN-1 Contributes Minimally to ERGO-1 Class 26G RNA Target Silencing

To determine the effect of loss of *henn-1* on the silencing of ERGO-1 class 26G RNA targets, we assayed levels of a panel of mRNAs targeted by ERGO-1 class 26G RNAs for desilencing in *henn-1* mutant animals. During time points at which ERGO-1 class 26G RNAs are abundant, only modest upregulation of some, but not all, targets was detected; furthermore, no single target shows consistent desilencing in the *henn-1* mutant (Fig A-5C, S10A). This is not unexpected, however, as the targets themselves vary in both expression and sensitivity to small RNA-mediated silencing across development [40]. To determine the specificity of this effect, two non-targets were examined in parallel. The maximal upregulation for either non-target does not exceed the maximal upregulation observed for any target, suggesting that the upregulation of ERGO-1 class 26G RNA targets in the *henn-1* mutant may be a consequence of 26G RNA depletion (Figs A-5C, A-S10B). This connection is supported by our observation that a Wago-dependent and ERGO-1 class 26G RNA-dependent secondary siRNA that presumably enhances target silencing also shows defects in accumulation in embryo (Fig A-S6B). The effect is modest, indicating that, as observed for the piRNA pathway,

the depleted pool of ERGO-1 class 26G RNAs in the *henn-1* mutant is still sufficient for triggering fairly robust production of secondary siRNAs. Nevertheless, in an accompanying manuscript, Montgomery et al. observe that HENN-1 is required for silencing activity of a similar secondary siRNA upon a sensor transgene [54], suggesting that this pathway may indeed be compromised by loss of *henn-1*.

The Soma of the *henn-1* Mutant Exhibits Enhanced Sensitivity to Exogenous RNAi

ALG-3/ALG-4 class 26G RNAs are restricted to the male germline, and their mRNA targets are enriched for genes involved in spermatogenesis [40]. Accordingly, loss of ALG-3/ALG-4 class 26G RNAs results in male-associated sterility at non-permissive temperatures due to defects in sperm activation that are thought to arise from target dysregulation [41]. ERGO-1 class 26G RNAs, in contrast, are dispensable for fertility and target mostly poorly conserved and incompletely annotated genes, many of which reside in duplicated regions of the genome [42]. It is therefore not unexpected that the *ergo-1(tm1860)* mutant, which lacks ERGO-1 class 26G RNAs, exhibits no overt phenotypes that can be traced to target dysregulation. Rather, the *ergo-1(tm1860)* mutant exhibits an *e*nhanced *R*NA*i* sensitivity (Eri) phenotype that is attributed to effects of loss of the ERGO-1-dependent small RNAs themselves; presumably, depletion of ERGO-1 class 26G RNAs and dependent secondary siRNAs liberates limiting RNAi factors shared between the endogenous and exogenous RNAi pathways [43,55,56].

To determine whether loss of *henn-1* depletes ERGO-1 class 26G RNAs sufficiently to produce an Eri phenotype, as observed in the *ergo-1* mutant, we subjected L1 larvae

from a panel of strains to feeding RNAi targeting various genes in the soma or germline. In order to expose subtle differences in RNAi sensitivity, we modulated the degree of knockdown, attenuating the dose of dsRNA trigger by diluting the bacterial RNAi clone with a bacterial clone harboring empty vector. RNAi of the somatic gene *lir-1* causes larval arrest and lethality in wild-type animals at full strength, but dilution 1:1 with empty vector largely eliminates the effect. In contrast, the *eri-1(mg366)* mutant, which lacks 26G RNAs, is affected severely by even dilute *lir-1* RNAi. The *henn-1* mutant also shows dramatically increased sensitivity to *lir-1* feeding RNAi relative to wild-type (Fig A-6A, B). A *henn-1; eri-1* double mutant, however, shows RNAi sensitivity that is virtually identical to that of the single *eri-1* mutant, suggesting that the Eri phenotype of each allele likely stems from the same defect, namely, loss of ERGO-1 class 26G RNAs. While the somatic Eri phenotype of the *henn-1* mutant shows partial rescue by the germline-specific *henn-1::gfp* transgene *xkSi2*, *henn-1::gfp* expression under the native promoter from transgene *xkSi1* rescues wild type RNAi sensitivity completely in the *henn-1* mutant (Fig A-6B). These findings suggest that loss of *henn-1* in both germline and soma contributes to the Eri phenotype of the *henn-1* mutant. The *henn-1* mutant exhibits a similar somatic Eri response to RNAi of *dpy-13* and *lin-29* (Fig A-S11).

The Germline of the *henn-1* Mutant Exhibits Decreased Sensitivity to Exogenous RNAi

While the somatic Eri phenotype of the *henn-1* mutant was expected, knockdown of genes required for germline development or embryogenesis revealed that, incongruously, the *henn-1* mutant maternal germline exhibits an *R*NAi *de*fective (Rde)

phenotype. Animals subjected to *pos-1* RNAi lay dead embryos because maternally loaded *pos-1* mRNA is required for specifying cell fate of many tissues during embryonic development [57]. On *pos-1* RNAi diluted 1:2 with empty vector (1/3 strength), knockdown in wild-type animals is still sufficiently robust to reduce average brood size to fewer than five offspring per animal. *henn-1* mutant animals at this dilution, however, produce an average brood greater than tenfold that of wild-type, suggesting that loss of *henn-1* confers resistance to RNAi-mediated knockdown of this maternally deposited mRNA (Fig A-6C). A lesser but statistically significant effect was observed for RNAi of the germline-expressed transcripts *par-1*, *par-2*, *pie-1*, and *glp-1* (Fig A-S12). Sensitivity to *pos-1* RNAi is effectively rescued by either endogenous or germline-specific expression of *henn-1::gfp*, likely due to the fact that both transgenes are expressed in germline.

HENN-1 is Expressed in Both Germline and Soma

HEN1 orthologs appear to be restricted to the germline in vertebrates [15,33]; however, we observe phenotypes in both the germline and soma of the *henn-1* mutant that suggest broader activity. To investigate expression of HENN-1 in *C. elegans*, we assessed *henn-1* mRNA and protein levels throughout development. *henn-1* mRNA levels are lowest in young larva and increase as the germline proliferates, peaking in gravid adult (Figs A-7A, A-S13A). Germline-deficient *glp-4(bn2)* adult hermaphrodites show approximately a 50% reduction in *henn-1* mRNA levels relative to wild-type (Fig A-S13B), indicating that *henn-1* mRNA is expressed in both germline and soma. Embryonic levels of *henn-1* are high but decrease rapidly; this pattern suggests that,

unlike in zebrafish [15], *henn-1* mRNA may be maternally deposited into the embryo. HENN-1 protein is detectable throughout development and in both hermaphrodite and male adults (Fig A-7B).

We next assessed the distribution of HENN-1::GFP fusion protein expressed from *xkSi1*, the rescuing *henn-1::gfp* transgene driven by the endogenous promoter, in the *henn-1* mutant background. Although single copy transgene expression levels are too low for direct visualization by fluorescence microscopy, HENN-1::GFP is readily detected using a mouse monoclonal anti-GFP antibody. Whole-mount immunostaining of transgenic L4 larvae reveals that HENN-1::GFP is expressed broadly in diverse somatic tissues and germline (Fig A-S13C). Non-transgenic larvae show no signal, indicating that detection of HENN-1::GFP is specific. In extruded gonads of *xkSi1; henn-1* hermaphrodites, HENN-1::GFP is detected throughout the germline. Notably, the proximal oocytes show cytoplasmic and intense nucleoplasmic HENN-1::GFP expression (Fig A-7C). Although nucleoplasmic enrichment is lost following fertilization, HENN-1::GFP is also abundant in embryo, with ubiquitous expression prior to gastrulation (Fig A-S13D). HENN-1::GFP is also expressed throughout the germline of *xkSi1; henn-1* males (Fig A-7D). During sperm maturation, we detect enrichment of HENN-1::GFP in residual bodies, but we cannot definitively conclude that it is excluded from sperm (Fig A-7D, inset). In wild-type animals, studies of endogenous HENN-1 using the rabbit polyclonal antibody generated against an N-terminal HENN-1 epitope corroborate the above findings, although the signal is more difficult to detect (Fig A-7E). Staining in the *henn-1* mutant yields no signal for anti-GFP and anti-HENN-1 antibodies (Fig A-7F); this demonstrates that detection of transgenic and endogenous HENN-1

proteins is specific. Together, these data define an expression pattern consistent with a role for HENN-1 in modifying small RNAs in both male and female germlines as well as in soma.

The 21U RNAs and 26G RNAs appear to be significantly stable only in the presence of their respective Argonaute proteins [35,36,40]; accordingly, the localization patterns of the Argonaute proteins reflect the distribution of the different classes of small RNAs. We therefore wanted to compare the expression patterns of HENN-1 and the 26G RNA-binding Argonautes to determine whether the small RNA substrate specificity of HENN-1 could be explained by differential access to Argonaute-bound small RNAs. ERGO-1, which binds methylated 26G RNAs, is abundant in embryo [42], and its transcript is enriched during oogenesis [58], but its localization has not yet been reported. We assessed the staining pattern of ERGO-1 in hermaphrodite gonad and embryo using a polyclonal antibody generated against a C-terminal ERGO-1 epitope. ERGO-1 expression in the hermaphrodite germline begins at pachytene exit and persists in embryo (Fig A-S13D, E). ERGO-1 shows cytoplasmic enrichment both in germline and embryo, suggesting that the cytoplasmic pool of HENN-1 may act in methylating 26G RNAs bound by ERGO-1. This interaction may, however, be transient, as we were unable to identify HENN-1 by mass spectrometry of immunopurified ERGO-1 complexes, nor could we detect ERGO-1 in immunopurified HENN-1::GFP complexes by western blot (data not shown). Notably, both HENN-1 and ERGO-1 remain abundant in early embryo (Fig A-S13D). This is consistent with the proposed existence of a somatic endo-siRNA pathway that promotes continued biosynthesis of ERGO-1 class 26G RNAs after fertilization [59].

We next assessed co-localization of HENN-1 and ALG-3. ALG-3 and its close paralog, ALG-4, bind unmethylated 26G RNAs, and their transcripts are enriched during spermatogenesis [58]. In the male gonad, a rescuing *gfp::alg-3* transgene was reported to express in the proximal male germline, with localization to P granules beginning at late pachytene [41]. During sperm maturation, GFP::ALG-3 is relegated to residual bodies. Dual immunostaining of GFP::ALG-3 and endogenous HENN-1 demonstrates a large region of overlap (Fig A-S13F), but HENN-1 does not appear to localize to P granules. This does not explain why ALG-3/ALG-4 class 26G RNAs are not methylated, because it is likely that HENN-1 can access P granules transiently: PRG-1 localizes predominantly to P granules [35,37], and the PRG-1-bound piRNAs are methylated. This is in contrast to zebrafish Hen1, which carries a poorly conserved C-terminal domain (Fig A-S1) that directs localization of Hen1 to nuage, perinuclear granules similar to *C. elegans* P granules, to methylate piRNAs [15].

DISCUSSION

Differential 26G RNA Methylation Supports an Argonaute-Dictated Methylation Model

We have shown that HENN-1 is essential for methylating select classes of *C. elegans* small RNAs, namely, 21U RNAs and ERGO-1 class 26G RNAs. As is the case in other animals, small RNAs in *C. elegans* that associate with Piwi clade Argonautes require HENN-1 for maintenance of wild-type levels. Ago clade Argonaute-associated microRNAs and ALG-3/ALG-4 class 26G RNAs, in contrast, are HENN-1-independent (Fig A-S14A). It has been proposed that spatial and temporal regulation of HEN1

ortholog expression may contribute to small RNA substrate specificity in metazoans [24]. However, our immunostaining studies indicate that HENN-1 is coexpressed in the same tissues and subcellular compartments as Argonautes ERGO-1, PRG-1, and ALG-3 and their respective small RNAs (Figs A-7, A-S13). Therefore, differences in gross subcellular localization cannot explain the failure of ALG-3/ALG-4 class 26G RNAs to be methylated. Furthermore, although the two subclasses of 26G RNAs are generated in different germlines from non-overlapping targets, their sequences exhibit no obvious distinguishing characteristics that might account for their non-uniform methylation status. One model of small RNA methylation posits that animal HEN1 orthologs only methylate small RNAs bound by Argonautes [15,22,23,24,49]. In support of this, work in fly shows that siRNA methylation requires assembly of DmAgo2 RISC [22,50], and in vitro studies using lysate from a silkworm ovary-derived cell line show that methylation of synthetic RNA only occurs after the longer substrate is bound by a Piwi protein and trimmed to piRNA size [60]. This model predicts that all 26G RNAs are bound as unmethylated species by either ERGO-1 in the female germline or ALG-3/ALG-4 in the male germline and subsequently methylated or not, respectively. This is consistent with our findings in vivo that ERGO-1 is required for methylation of 26G RNAs (Fig A-4A) and associates with 26G RNAs of either methylation status (Fig A-4C). It has been further proposed that the identity of the Argonaute determines whether bound small RNAs are methylated [22,23,49,50]. An elegant illustration of this is provided by fly miR-277, which associates with both Ago1, the canonical fly miRNA Argonaute, and Ago2, which binds methylated siRNAs [61]. The miR-277 pool contains both methylated and unmethylated species. Depletion of Ago2 in cell culture results in loss of methylated miR-277, whereas Ago1

depletion results in a completely methylated miR-277 population [22]. Similarly, fly hairpin derived hp-esiRNAs sort into Ago1 and Ago2, but accumulate mainly in Ago2 because only hp-esiRNAs bound by Ago2 are methylated and therefore protected against degradation triggered by their extensive target complementarity [50]. In *C. elegans*, the model of Argonaute-dictated methylation can be invoked to explain the disparate methylation of the 26G RNAs: in the male germline, only ALG-3/ALG-4 are expressed, resulting in an unmethylated male 26G RNA population, whereas exclusive expression of ERGO-1 in the female germline and embryo directs methylation of female and zygotic 26G RNAs. This raises the intriguing possibility that selective expression of Argonautes that permit or prevent methylation could represent a new mechanism for differentially regulating small RNA turnover.

It is important to note that our results do not definitively exclude an alternative model wherein 26G RNAs are methylated prior to association with Argonautes and subsequently bound by ALG-3/ALG-4 only if unmethylated or by ERGO-1 only if methylated. In this model, HEN1 would methylate 26G RNAs in both germlines, but degradation of labile unbound siRNAs would result in a purely unmethylated or methylated population of 26G RNAs in male and female germlines, respectively. Because 26G RNAs assessed in embryo are fully methylated (Figs A-3A, A-S3B), such a mechanism would require that ERGO-1 exhibit very unfavorable kinetics for association with unmethylated small RNAs. We do not find this to be the case, as ERGO-1 binds some 26G RNAs with similar efficiency when methylated and unmethylated (Fig A-4C). Our data therefore provide stronger evidence for a model of Argonaute-dictated methylation of small RNAs.

Possible Advantages for Selective Methylation of Small RNAs

Differential germline expression of Argonautes could have evolved in *C. elegans* because of advantages conferred by selective stabilization of female germline 26G RNAs. Unlike ALG-3/ALG-4 class 26G RNAs, which appear to function exclusively during sperm development [40,41], ERGO-1 class 26G RNAs exert much of their influence during embryonic and larval development, well beyond initiation of their biogenesis in the hermaphrodite germline [40]. Accordingly, their targets are depleted of germline-enriched genes [40,59]. The oocyte contributes the vast majority of the initial zygotic cellular contents; therefore, methylation of 26G RNAs originating in the female germline may ensure robust inheritance and perdurance of primary small RNAs. Methylation of 26G RNAs in the male germline would likely not significantly increase their representation in sperm or zygote, as ALG-3/ALG-4 are relegated to residual bodies during spermatogenesis and exert effects in mature sperm only indirectly through dependent secondary 22G RNAs [41]. Nonetheless, it would be interesting to express ERGO-1 ectopically in sperm and determine whether ALG-3/ALG-4 class small RNAs are methylated. Such a strategy may reveal unexpected consequences related to inappropriate methylation and stabilization of ALG-3/ALG-4 class 26G RNAs.

Role of HENN-1 in the Balance Between Endo- and Exo-RNAi

In the absence of *henn-1*, we show that response to RNAi-mediated knockdown is enhanced for somatic genes (Figs A-6A,B, A-S11). This is likely due to destabilization of ERGO-1 class 26G RNAs in the *henn-1* mutant, which reduces competition with primary

exo-siRNAs for stimulating secondary siRNA activity mediated by somatic Argonautes such as SAGO-1 and SAGO-2 [43,55]. While germline-specific expression of *henn-1::gfp* only partially rescues this somatic Eri phenotype, *henn-1* mutant animals rescued with an endogenous *henn-1::gfp* transgene, which drives both somatic and germline expression, show wild-type RNAi sensitivity. Under the model of competing endo- and exo-RNAi pathways, this suggests that HENN-1-mediated methylation of ERGO-1 class 26G RNAs in the germline alone cannot maintain small RNA levels sufficient to sequester an appropriate proportion of the limiting RNAi factors. It is possible that ERGO-1 class 26G RNA biogenesis continues in embryo and larva, as previously suggested [59], and that high concentrations of HENN-1 are necessary for continued stabilization of these small RNAs. Such a model would be consistent with our characterization of the distributions of HENN-1 and ERGO-1, both of which are still detected in abundance in developing embryo (Fig A-S13D, E).

While the majority of the phenotypes observed in the *henn-1* mutant can be attributed to destabilization of endogenous small RNA substrates, the germline Rde phenotype suggests a role for HENN-1 in exogenous RNAi. It is unclear why HENN-1 is dispensable for robust exogenous RNAi in the soma but required in the germline. While this may be an indirect effect, as suggested in concurrent work by Kamminga et al. [62], one possible explanation is that HENN-1 stabilizes primary exo-siRNAs or dependent 22G secondary siRNAs. There is support in fly for methylation of exo-siRNAs and transgenic hairpin-derived siRNAs [22,63], but this has not yet been demonstrated in *C. elegans*. 22G RNAs triggered by primary exo-siRNAs appear not to be methylated [47], consistent with our and others' observations that Wago-dependent 22G RNAs from

diverse endogenous sources are unmethylated (Figs A-3A, A-S3B, and [45]). The methylation status of worm primary exo-siRNAs has not been definitively established, although a 22-nucleotide siRNA generated from a transgene encoding a perfect hairpin was not found to be methylated [46].

Structural Differences in Ago and Piwi Clade Argonautes May Dictate HEN1 Substrate Specificity

All Argonautes contain two signature domains, PAZ and Piwi [64]. The Piwi domain, unique to Argonautes, adopts an RNase H-like configuration and serves as the catalytic core of RISC [65,66]. The PAZ domain recognizes and anchors the 3' end of the small RNA [67,68]. Comparison of Piwi and Ago clade Argonautes reveals that Piwi proteins contain a small insertion in their PAZ domains in a loop connecting two β strands [69]. Crystal structures of a human Piwi Argonaute PAZ domain suggest that this insertion results in the formation of a more spacious binding pocket capable of accommodating the 2'-O-methyl group of a piRNA. Interactions between the methyl group and hydrophobic residues lining the pocket confer a threefold to sixfold higher binding affinity for 2'-O-methyl than 2'-OH [69]. In *C. elegans*, only PRG-1/PRG-2 and ERGO-1 show evidence of a PAZ domain insertion (Fig A-S14B), consistent with their designation as Piwi clade Argonautes and association with methylated small RNAs.

In spite of their shared classification, ERGO-1 exhibits far less homology than PRG-1/PRG-2 to mammalian and insect Piwi proteins (Fig A-S14A) [43]. Similarly, among worm, fly, and human Argonautes, DmAgo2 and *C. elegans* Argonaute RDE-1 are among the most divergent members of their clades [43]. In fact, so divergent is RDE-1

that its cladistics are ambiguous, with our and other published alignments variably assigning it to each of the three clades (Fig A-S14A and [43,70]). Both DmAgo2 and RDE-1 bind exo-siRNAs, although only the former has been shown to permit methylation [22]. Interestingly, both lack the insertion found in Piwi Argonaute PAZ domains (Fig A-S14B). The absence of this insertion in DmAgo2 suggests that it is not required for association with methylated small RNAs, raising the possibility that RDE-1 too may permit methylation of associated small RNAs. If HENN-1 does not methylate RDE-1-bound small RNAs, it is unclear what specific role HENN-1 plays in exo-RNAi in the germline. Nevertheless, its dual functions in endogenous and exogenous RNAi place HENN-1 in the company of DCR-1 and the Wago proteins at the intersection between these two RNAi pathways.

MATERIALS AND METHODS

***C. elegans* Strains.** *C. elegans* were maintained according to standard procedures. The Bristol strain N2 was used as the standard wild-type strain. The alleles used in this study, listed by chromosome, are: unmapped: *neIs23[unc-119(+) GFP::ALG-3]*; LGI: *glp-4(bn2)*, *prg-1(tm872)*; LGII: *xkSi1[PC30A5.3::henn-1::gfp::henn-1 3'UTR cb-unc-119(+)] II, xkSi2[Ppie-1::henn-1::gfp::tbb-2 3'UTR cb-unc-119(+)] II*; LGIII: *rde-4(ne301), henn-1(tm4477)*; LGIV: *eri-1(mg366)*, *fem-1(hc17)*, *him-8(e1489)*; LGV: *ergo-1(tm1860)*. The *neIs23[unc-119(+) GFP::ALG-3]* strain was generously provided by Craig Mello (University of Massachusetts, Worcester, MA).

RNA Sample Preparation. For embryo samples, L1 larvae were grown at 20°C until gravid. Embryos were isolated using sodium hypochlorite solution; an aliquot of embryos was allowed to hatch overnight at room temperature to determine viability. For male samples, synchronized *him-8(e1489)* L1 larvae were grown at 20°C for 72-75 hours. Males were isolated by filtering through 35 µm mesh [71]. For female samples, synchronized *fem-1(hc17)* L1 larvae were plated and grown at 25°C for 52 hours. For time course samples, synchronized wild-type (N2) and *henn-1(tm4477)* L1 larvae were grown at 25°C until gravid; embryos were extracted and harvested for RNA or hatched overnight at room temperature and then grown at 25°C for the specified number of hours before harvest. The *prg-1(tm872)* time course samples were prepared in the same way, except that animals were grown for the first generation at 20°C to evade temperature-sensitive sterility. Samples were processed by either three rounds of freeze/thaw lysis or two rounds of homogenization for 15 sec using the Tissue Master-125 Watt Lab Homogenizer (Omni International) and the RNA was extracted in TriReagent (Ambion) following the vendor's protocol, with the following alterations: RNA was precipitated in isopropanol for one hour at -80°C; RNA was pelleted by centrifugation at 4°C for 30 min at 20,000 x g; the pellet was washed three times in 75% ethanol; the pellet was resuspended in water.

β-elimination Assay for Small RNAs and Northern Blot Analysis. For detection of small RNAs, 10 or 40 µg of total RNA were β-eliminated as described [51]; control samples were processed in parallel without sodium periodate. Northern blot analysis was performed as described [72]. In brief, 5 or 10 µg of β-eliminated total RNA were

resolved on 17.5% or 20% denaturing Urea-PAGE gels (SequaGel, National Diagnostics) and transferred to Hybond-NX membrane (Amersham). 21 and 26 nt synthetic RNAs were run as size markers and visualized in tandem with rRNA by ethidium bromide staining. Pre-hybridization/hybridization and washes were performed at 48°C or 50°C. Oligonucleotides corresponding to the antisense sequences of the small RNAs (Table A-S1) were synthesized and end-labeled with [α-^{32}P]-dATP using the miRNA StarFire kit (Integrated DNA Technologies).

RNAi Sensitivity Assay. To test the response to exogenous RNAi, bacterial clones from the Ahringer RNAi library [73] were diluted with bacteria harboring the empty vector *L4440* to achieve a level of RNAi sensitivity that allowed us to differentiate the RNAi responses in the strains examined. To determine *lir-1* RNAi sensitivity, the *lir-1* RNAi bacterial clone diluted with *L4440* bacterial clone at a 1:1 or 1:2 ratio (1/2 or 1/3 strength) was used; >50 L1 larvae were plated per plate and the number of total animals assayed per plate was determined at day two after plating; the percent of animals exhibiting the larval arrest phenotype was determined at 70 hours at 20°C. Sensitivity to RNAi of *dpy-13* and *lin-29* was also assessed using this method, where animals subjected to *dpy-13* RNAi were imaged at 70 hours and those subjected to *lin-29* RNAi were evaluated for the absence of protruding vulva or bursting phenotype. For *pos-1* RNAi, synchronized L1 larvae were singled onto plates with *pos-1* RNAi diluted with empty vector at a 1:2 ratio (1/3 strength) that had been induced overnight at 25°C. Animals were grown at 20°C for six days and progeny were counted. Sensitivity to RNAi of *pie-1*, *par-1*, and *par-2* was assessed similarly at the indicated dilutions with 4 plates

of 4 P_0 animals per strain. Sensitivity to *glp-1* RNAi was determined at the indicated dilutions by plating 4 plates of >50 L1 larvae per strain per gene and scoring for the absence of oocytes and embryos in both arms of the germline at 70 hours at 20°C. For all RNAi sensitivity assays, data are representative of at least two independent experiments.

Fertility Assay. To determine brood size, synchronized L1 larvae from gravid adults grown at 20°C or shifted to 25°C for two generations were singled onto plates with OP50 and grown to adulthood at their respective temperatures. Once egg-laying began, animals (N ≥ 13 per strain) were transferred to fresh plates daily until the supply of fertilized eggs was exhausted. Progeny of the singled parents were counted as late larvae/adults. Results are representative of two independent experiments.

Quantitative RT-PCR. Taqman small RNA probes were synthesized by Applied Biosystems (Table A-S2) [74]. For each reaction, 50 ng of total RNA were converted into cDNA using Multiscribe Reverse Transcriptase (Applied Biosystems). The resulting cDNAs were analyzed by a Realplex thermocycler (Eppendorf) with TaqMan Universal PCR Master Mix, No AmpErase UNG (Applied Biosystems). We could not identify a small RNA whose levels were consistent across development for use in normalization. Therefore, to preserve the developmental profile of each of the small RNA assessed, back transformation was used to calculate relative small RNA levels from qRT-PCR cycle numbers. As a control for RNA quality, miR-1 Taqman assays were run in parallel for all samples excluding the ERGO-1 RNA immunoprecipitation samples, in which

miRNAs are absent. For quantification of mRNA levels, 100 ng of total RNA were converted into cDNA with Multiscribe Reverse Transcriptase (Applied Biosystems) following the vendor's protocol with the following changes: 25 units of RT and 7.6 units of RNAse OUT (Invitrogen) were used per reaction. cDNAs were analyzed using Power Sybr Green PCR Master Mix (Applied Biosystems) (primers, Table A-S3). Relative mRNA levels were calculated based on the $\Delta\Delta 2C_t$ method [75] using *eft-2* for normalization. For all qPCR, 40 cycles of amplification were performed; reactions whose signals were not detected were therefore assigned a cycle number of 40. All results presented are the average values of independent calculations from biological triplicates unless indicated. To determine average upregulation of ERGO-1 26G RNA targets in *henn-1* relative to wild-type (Fig A-5C), the mean was calculated for all of the ratios generated by dividing each *henn-1* biological replicate by each wild-type biological replicate.

3' RACE. 3' RACE was performed using the 3' RACE System for Rapid Amplification of cDNA ends (Invitrogen) according to the manufacturer's protocol. *henn-1* gene-specific primer (5' GCAGTATGTCGCCTCCAAGTAGAT 3') was used to amplify *henn-1* 3' ends from cDNA generated from embryo. Product corresponding to only the seven-exon gene model of *henn-1* was observed, consistent with detection of a single protein isoform corresponding to this model on western blot analysis.

Plasmids and Transgenic Strains. The endogenous *henn-1::gfp* reporter construct *(xkSi1)* was generated by introducing the following fragments into pCFJ151:

endogenous promoter of the *henn-1*-containing operon CEOP3488 [76] (3.9 kb PCR fragment immediately upstream of the *C30A5.3* start codon), *henn-1* genomic coding region (1.8 kb PCR fragment with mutated termination codon), *gfp* coding region (0.9 kb fragment with multiple synthetic introns and termination codon), and *henn-1* endogenous 3'UTR (1.1 kb PCR fragment immediately downstream of *henn-1* termination codon). The germline-only *henn-1::gfp* reporter construct (*xkSi2)* was generated as above with the following substitutions: CEOP3488 operon promoter was replaced with the *pie-1* promoter (A-4 kb PCR fragment immediately upstream of *pie-1* start codon) and *henn-1* endogenous 3'UTR was replaced with the *C36E8.4* 3'UTR (0.3 kb PCR fragment downstream of *C36E8.4*). Constructs were cloned into the pCFJ151 vector, confirmed by sequencing, and used to generate single-copy integrated transgenes via the MosSCI technique [52]. Gene fusion products of the expected size were specifically detected by western blot with both anti-HENN-1 and anti-GFP antibodies.

Generation of Antibodies. Synthetic antigenic peptides were conjugated to KLH and each was used to immunize two rabbits (Proteintech). Antisera were subsequently affinity purified using Affi-Gel 15 gel (Bio-Rad). Antigenic peptide sequences are as follows: N-terminal HENN-1 peptide with N-terminal added cysteine (CTYVEAYEQLEIALLEPLDR), C-terminal ERGO-1 peptide (CEVNKDMNVNEKLEGMTFV).

Western Blot Analysis. Proteins immobilized on Immobilon-FL transfer membrane (Millipore) were probed with anti-HENN-1 rabbit polyclonal antibody (1:2000), anti-γ-tubulin rabbit polyclonal antibody (LL-17) (Sigma) (1:2000), or anti-ERGO-1 rabbit polyclonal antibody (1:1000). Peroxidase-AffiniPure goat anti-rabbit IgG secondary antibody was used at 1:10000 (Jackson ImmunoResearch Laboratories) for detection using Pierce ECL Western Blotting Substrate (Thermo Scientific).

Isolation of ERGO-1-associated RNAs. Wild-type, *henn-1*, or *eri-1(mg366)* embryos isolated from gravid adults grown at 20°C were frozen in liquid nitrogen and homogenized with a Mixer Mill MM 400 ball mill homogenizer (Retsch) Homogenates were suspended in lysis buffer (50 mM HEPES (pH 7.4), 1 mM EGTA, 1 mM $MgCl_2$, 100 mM KCl, 10% glycerol, 0.05% NP-40 treated with a Complete, Mini, EDTA-free Protease Inhibitor Cocktail tablet (Roche Applied Sciences)) and clarified by centrifugation at 12,000 x g for 12 minutes at 4°C. Aliquots of homogenate were reserved as crude lysate for western blot to confirm that immunoprecipitations were performed in lysates of equivalent protein concentration (2 mg/mL). For immunoprecipitations, embryo homogenates were incubated at 4°C for one hour with 75 μg anti-ERGO-1 rabbit polyclonal antibody conjugated to Dynabeads® Protein A (Invitrogen), after which the beads were washed (500 mM Tris-HCl (pH 7.5), 200 mM KCl, 0.05% NP-40) and associated proteins were eluted with 200 μL glycine. Three quarters of each eluate were precipitated overnight at 4°C in trichloroacetic acid, pelleted, washed with acetone, and resuspended for western blot analysis. The remaining eluate was treated with 2 mg/ml Proteinase K (Roche) and incubated at 37°C

for 30 minutes. RNA was isolated from the eluate by incubation with TriReagent and processed as described above. RNA pellets were resuspended in 10 μL water and 5 μL were used for each Taqman RT reaction.

Immunostaining. Primary antibodies were applied according to the following specifications: anti-GFP mouse monoclonal antibody 3E6 (Invitrogen) was diluted 1:1500 to detect HENN-1::GFP and 1:200 to detect ALG-3::GFP; anti-ERGO-1 rabbit polyclonal was diluted 1:200; and anti-HENN-1 rabbit polyclonal antibody was preabsorbed as described [77] with *henn-1(tm4477)* mutant extract and diluted 1:200. Alexa Fluor 555 goat anti-rabbit IgG and Alexa Fluor 488 goat anti-mouse IgG (Molecular Probes) secondary antibodies were diluted 1:500. All antibodies were diluted in 0.5% bovine serum albumin (Sigma). For immunostaining of gonads and embryos, synchronized gravid hermaphrodites or adult males grown at 20°C were dissected on Superfrost Plus positively charged slides (Fisherbrand) with 27 G x 1/2 inch BD PrecisionGlide needles (Becton, Dickinson and Company) as described by Chan and Meyer in WormBook [78] Protocol 21 with 1.5% paraformaldehyde (Sigma). Slides were incubated with primary antibodies overnight at 4°C and with secondary antibodies for three hours at room temperature. Slides were mounted with VECTASHIELD Mounting Medium with DAPI (Vector Laboratories). For whole-worm immunostaining, synchronized late L4 larvae grown at 20°C were transferred to subbed slides [77] in M9, fixed for six minutes in 1.5% paraformaldehyde, freeze-cracked, and incubated for 15 minutes in ice cold methanol. After fixation, slides were processed as above. Images were captured on an Olympus BX61 epifluorescence compound microscope with a

Hamamatsu ORCA ER camera using Slidebook 4.0.1 digital microscopy software (Intelligent Imaging Innovations) and processed using ImageJ.

AUTHOR CONTRIBUTIONS

The initial discovery of differential methylation of 26G RNAs in male and female germlines is credited to TH. ACB and JKK conceived and designed all subsequent experiments. ACB performed the experiments and analyses in Figs A-1, A-2, A-3, A-4A, A-5, A-6, A-7A,B, A-S1, A-S2, A-S3, A-S4, A-S5, A-S6, A-S7, A-S8, A-S9, A-S10, A-S11, A-S12, A-S13A-B, A-S14. ACB generated the transgenic strains analyzed in Figs A-7C,D,F and A-S13C-E. AFA performed the experiments in Figs A-7C-F and A-S13C-F. VK performed the experiments in Fig A-4B,C. MF identified species for design of Taqman small RNA assays. SM isolated the *henn-1* deletion strain. ACB wrote the manuscript. ACB and JKK edited the manuscript.

ACKNOWLEDGMENTS

We thank Patrick Hu, Chi Zhang, and Sylvia Fischer for helpful comments on the manuscript. We thank Carolyn Philips for advice on immunostaining. We also thank the *Caenorhabditis* Genetics Center for *C. elegans* for strains.

Figure A-1. Methylation of 21U RNAs Requires *C. elegans* HEN1 Ortholog HENN-1. A) HENN-1 is required for 21U RNA methylation. Endogenous (*xkSi1*) and germline-specific (*xkSi2*) expression of *henn-1::gfp* rescue 21U RNA methylation in *henn-1(tm4477)* mutant embryo. Total embryo RNA of the indicated genotypes was β-eliminated (βe +) or control treated (βe -) and probed for piRNA 21UR-429A- *prg-1(tm872)* lacks 21U RNAs and is included as a negative control. Below, ethidium bromide staining of 5.8S rRNA is shown. Additional 21U RNA northern blots are shown in Fig A-S3A. B) *C. elegans* miRNAs are unmethylated. Total embryo RNA was probed for miR-1. Variable intensity of 5.8S rRNA bands in embryo indicates unequal loading.

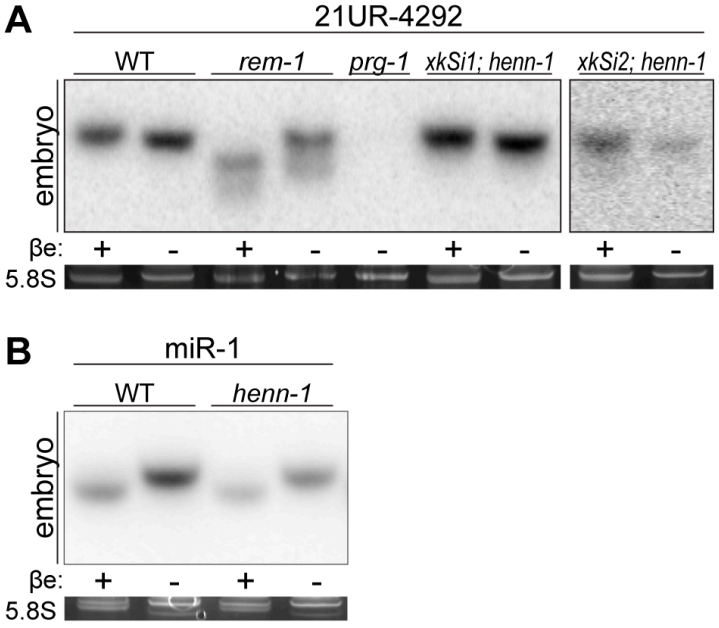

Figure A-2. HENN-1 Stabilizes 21U RNAs. A) Loss of *henn-1* impairs 21U RNA accumulation in adult, embryo, and early larva. Levels of 21UR-1848 were assayed by Taqman qPCR in embryo and every four hours across development of wild-type and *henn-1(tm4477)* mutant animals at 25°C. Standard deviation is shown for biological triplicates. Taqman qPCR data for eight additional 21U RNAs are shown in Fig A-S4. B) Effects of loss of *henn-1* are restricted to its small RNA substrates. Levels of miR-1 across development were assayed by Taqman qPCR. Standard deviation is shown for biological triplicates. Additional Taqman qPCR data for miRNAs are shown in Fig A-S5. C) Loss of *henn-1* impairs *Tc3* transposase silencing primarily in early L1 larva. *Tc3* transposase mRNA levels were assayed by qPCR across development and normalized to mRNA levels of *eft-2*, an abundantly expressed housekeeping gene. *prg-1(tm872)* lacks 21U RNAs and is included as a positive control for *Tc3* upregulation. Significant zero and four hour time points are expanded at right (*: P=0.0251; **: P=0.0250, two-tailed *t*-test). Standard deviation is shown for biological triplicates. E, embryo; hr, hour.

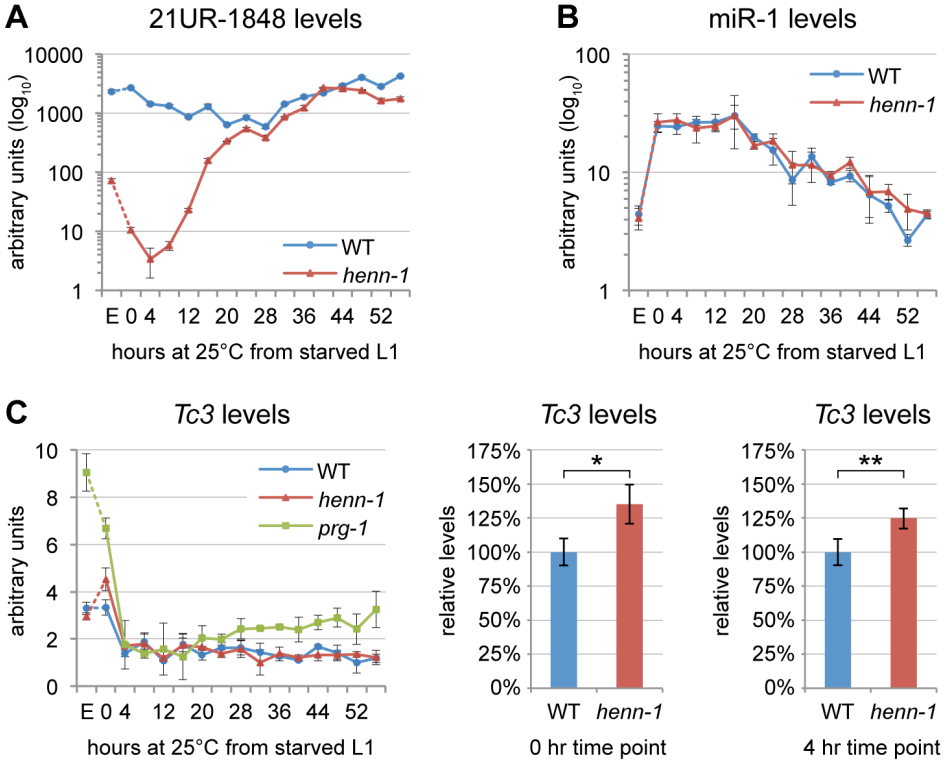

Figure A-3. HENN-1 Selectively Methylates ERGO-1 Class 26G RNAs in an ERGO-1-dependent Manner. A) HENN-1 is required for ERGO-1 class 26G RNA methylation and stability. Total β-eliminated (βe +) or control treated (βe -) embryo RNA of the indicated genotypes was probed for ERGO-1 class 26G RNA 26G-O7. *eri-1(mg366)* lacks 26G RNAs and is included as a negative control. Asterisk indicates signal corresponding to cross-hybridization with unmethylated 22G RNAs. Below, ethidium bromide staining of 5.8S rRNA. Additional ERGO-1 class 26G RNA northern blots are shown in Fig A-S3B. B) ALG-3/ALG-4 class 26G RNAs are unmethylated. Total *him-8(e1489)* male RNA was probed for ALG-3/ALG-4 class 26G RNA 26G-S5. An additional ALG-3/ALG-4 class 26G RNA northern blot is shown in Fig A-S3C. C) 21U RNAs are methylated in a HENN-1-dependent manner in both female and male germlines. Total RNA of the indicated genotypes from *fem-1(hc17)* female or *him-8(e1489)* male was probed for female germline-enriched piRNA 21UR-4292 or male germline-enriched piRNA 21UR-5941, respectively.

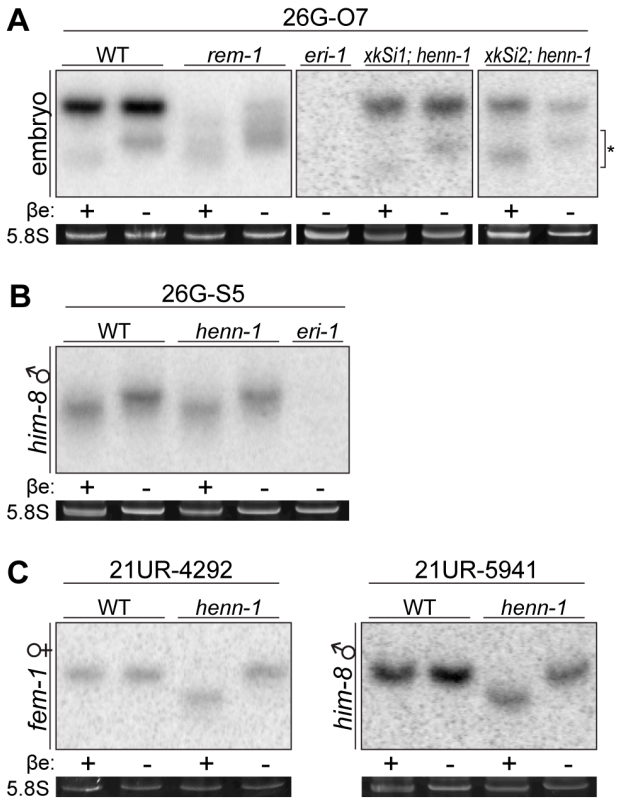

Figure A-4. ERGO-1 is Required for Methylation of 26G RNAs. A) ERGO-1 class 26G RNA 26G-O1 is unmethylated in the absence of ERGO-1. Total embryo wild-type (5 µg) or *ergo-1(tm1860)* (10 µg) β-eliminated (βe +) or control treated (βe -) RNA was probed for 26G-O1. B) Anti-ERGO-1 rabbit polyclonal antibody immunoprecipitates ERGO-1 complexes. ERGO-1 complexes were immunopurified from lysates of equalized protein concentration extracted from wild-type, *henn-1(tm4477)* mutant, or *eri-1(mg366)* mutant embryo. Aliquots of lysates and immunoprecipitates (RNA IP) were probed with anti-ERGO-1 antibody. *ergo-1(tm1860)* mutant lysate was run in parallel to ensure specificity of ERGO-1 detection (data not shown). C) ERGO-1 binds methylated and unmethylated 26G RNAs. Taqman RT-qPCR for the indicated ERGO-1 class 26G RNAs was performed on samples described in B. The *eri-1(mg366)* mutant lacks 26G RNAs and serves as a negative control to demonstrate specificity of 26G RNA detection by Taqman assay. Standard deviation is shown for technical duplicates. Results are representative of two independent RNA immunoprecipitation experiments.

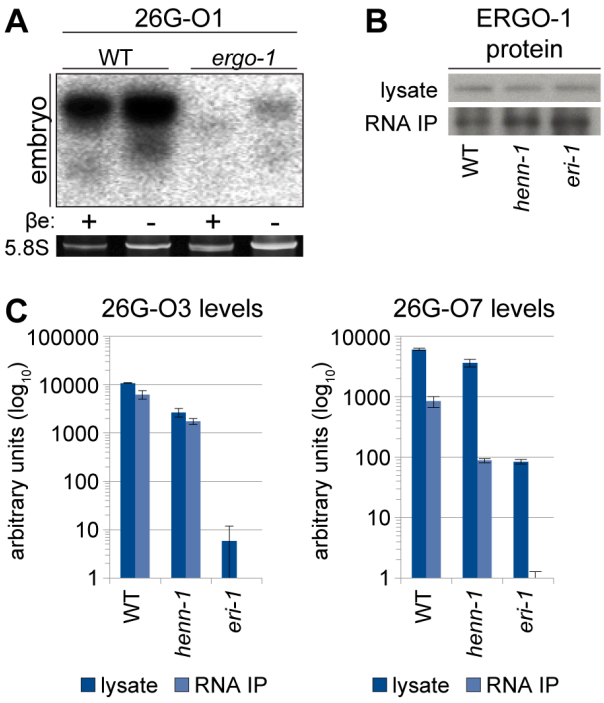

Figure A-5. HEN1 Stabilizes ERGO-1 Class, but Not ALG-3/ALG-4 Class, 26G RNAs. A) Loss of *henn-1* impairs ERGO-1 class 26G RNA accumulation at all stages. Levels of ERGO-1 class 26G RNA 26G-O3 were assayed by Taqman qPCR across development of wild-type and *henn-1(tm4477)* mutant animals at 25°C. Standard deviation is shown for biological triplicates. Taqman qPCR data for seven additional ERGO-1 class 26G RNAs are shown in Fig A-S8. B) ALG-3/ALG-4 class 26G RNAs are *henn-1*-independent. Levels of ALG-3/ALG-4 class 26G RNA 26G-S5 were assayed across the period of development in which ALG-3/ALG-4 class 26G RNAs are readily detectable. Standard deviation is shown for biological triplicates. Taqman qPCR data for two additional ALG-3/ALG-4 class 26G RNAs are shown in Fig A-S9. C) Loss of *henn-1* may result in modest, sporadic defects in ERGO-1 class 26G RNA target silencing. Levels of eight target and two non-target mRNAs were assayed across development of wild-type and *henn-1(tm4477)* mutant animals at 25°C and normalized to *eft-A*. Expression in the *henn-1(tm4477)* mutant relative to wild-type is represented according to the red-green color scheme indicated in the right panel. Raw data is shown in Fig A-S10. E, embryo.

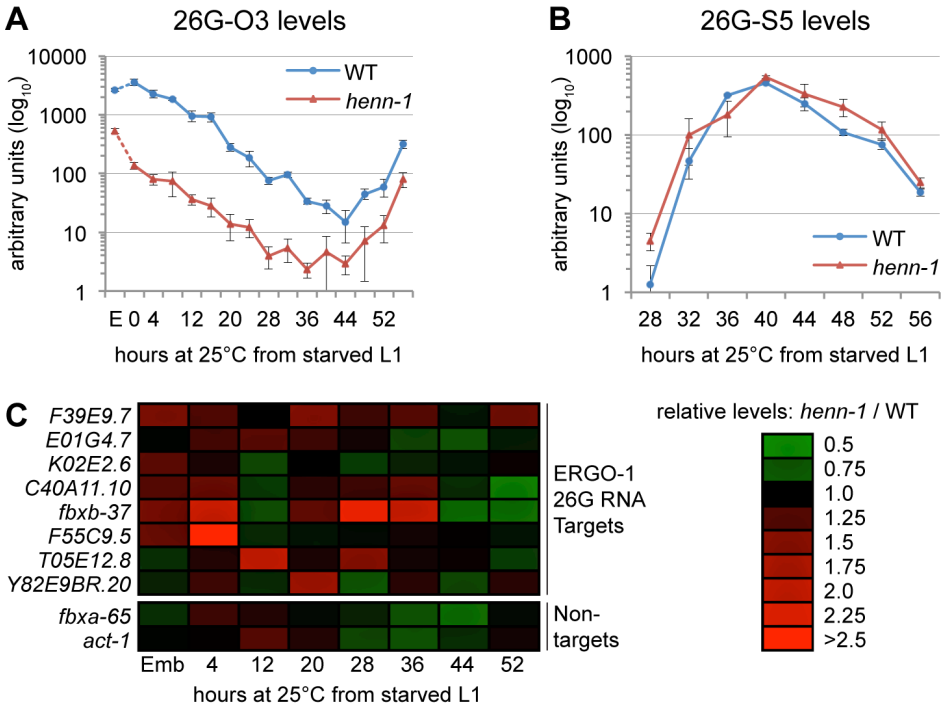

Figure A-6. The *henn-1* Mutant Exhibits Opposite RNAi Sensitivity Phenotypes in Soma and Germline. A) *henn-1(tm4477)* mutant animals exhibit mildly enhanced somatic RNAi. Animals of the indicated genotype were plated as L1 larvae on *lir-1* feeding RNAi diluted 1:1 with empty vector (1/2 strength) and grown for 70 hours at 20°C. Data is quantified in part B. RNAi sensitivity data for knockdown of two additional somatic transcripts are shown in Fig A-S11. B) Endogenous expression of *henn-1::gfp* from *xkSi1* rescues somatic RNAi sensitivity. Percent of animals reaching full size on *lir-1* feeding RNAi of the indicated strength at 70 hours is plotted. N = 8 plates of >50 animals per strain. Standard deviation is shown. C) *henn-1(tm4477)* mutant animals exhibit defective germline RNAi. Brood size of animals plated at 20°C as L1 larvae on *pos-1* feeding RNAi diluted 1:2 with empty vector is plotted. N ≥ 13 animals per strain. Mean and standard deviation are shown. RNAi sensitivity data for knockdown of four additional germline transcripts are shown in Fig A-S12. Alleles used in this figure: *eri-1(mg366)*, *prg-1(tm872)*, *rde-4(ne301)*.

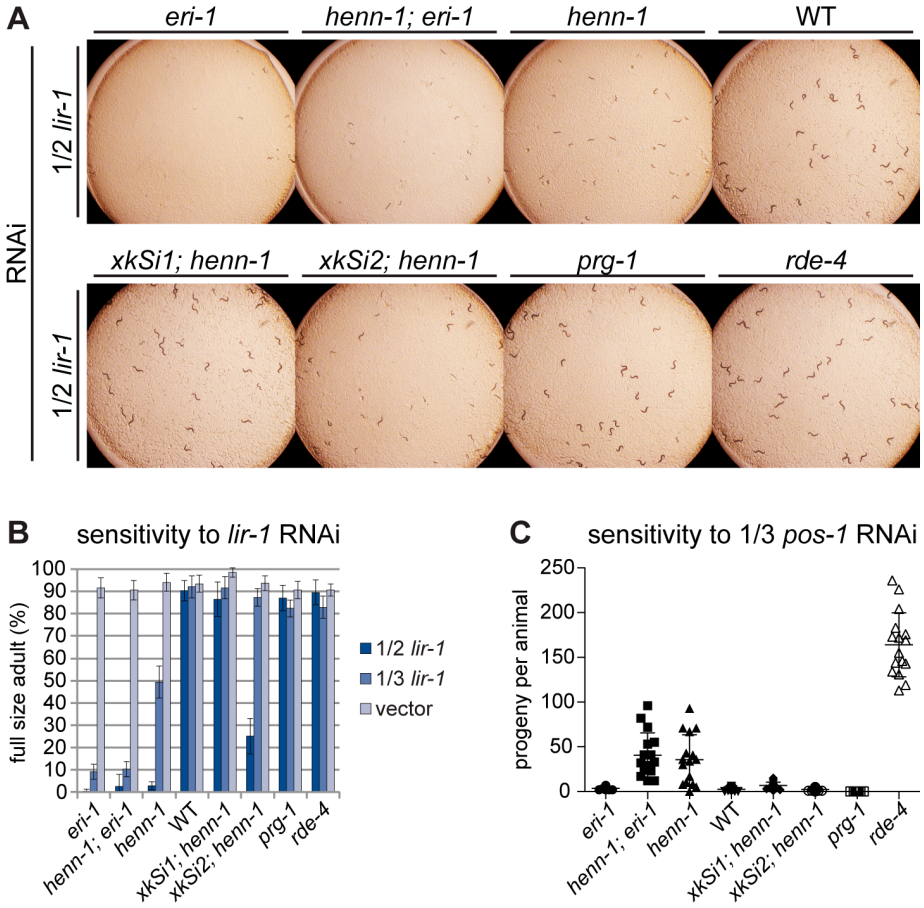

Figure A-7. HENN-1 is Broadly Expressed in *C. elegans* Germline. A) The *henn-1* mRNA expression profile is consistent with germline enrichment. Levels of *henn-1* mRNA were assayed throughout development and normalized to *eft-2* mRNA. Standard deviation is shown for biological triplicates. Non-normalized levels are shown in Fig A-S13A. B) HENN-1 is detected at all stages of development and in male. Lysates from animals of the indicated stages were probed with anti-HENN-1 rabbit polyclonal antibody. C) HENN-1 is abundant in hermaphrodite proximal germline and enriched in proximal oocyte nucleoplasm (inset). Extruded gonads of *xkSi1; henn-1(tm4477)* adult hermaphrodites were stained with anti-GFP mouse monoclonal and anti-HENN-1 rabbit polyclonal antibodies. D) HENN-1 is detectable in male proximal and distal gonad, with enrichment in residual bodies during spermatid maturation (inset). Extruded gonads of *xkSi1; henn-1(tm4477)* adult males were stained with anti-GFP and anti-HENN-1 antibodies. E) Expression of endogenous HENN-1 mirrors expression of HENN-1::GFP from transgene *xkSi1*. Extruded gonads of wild-type animals were stained with anti-HENN-1 antibody. F) Detection of HENN-1 proteins by immunostaining is specific. Extruded gonads of *henn-1(tm4477)* mutant animals were stained with anti-GFP and anti-HENN-1 antibodies. E, embryo.

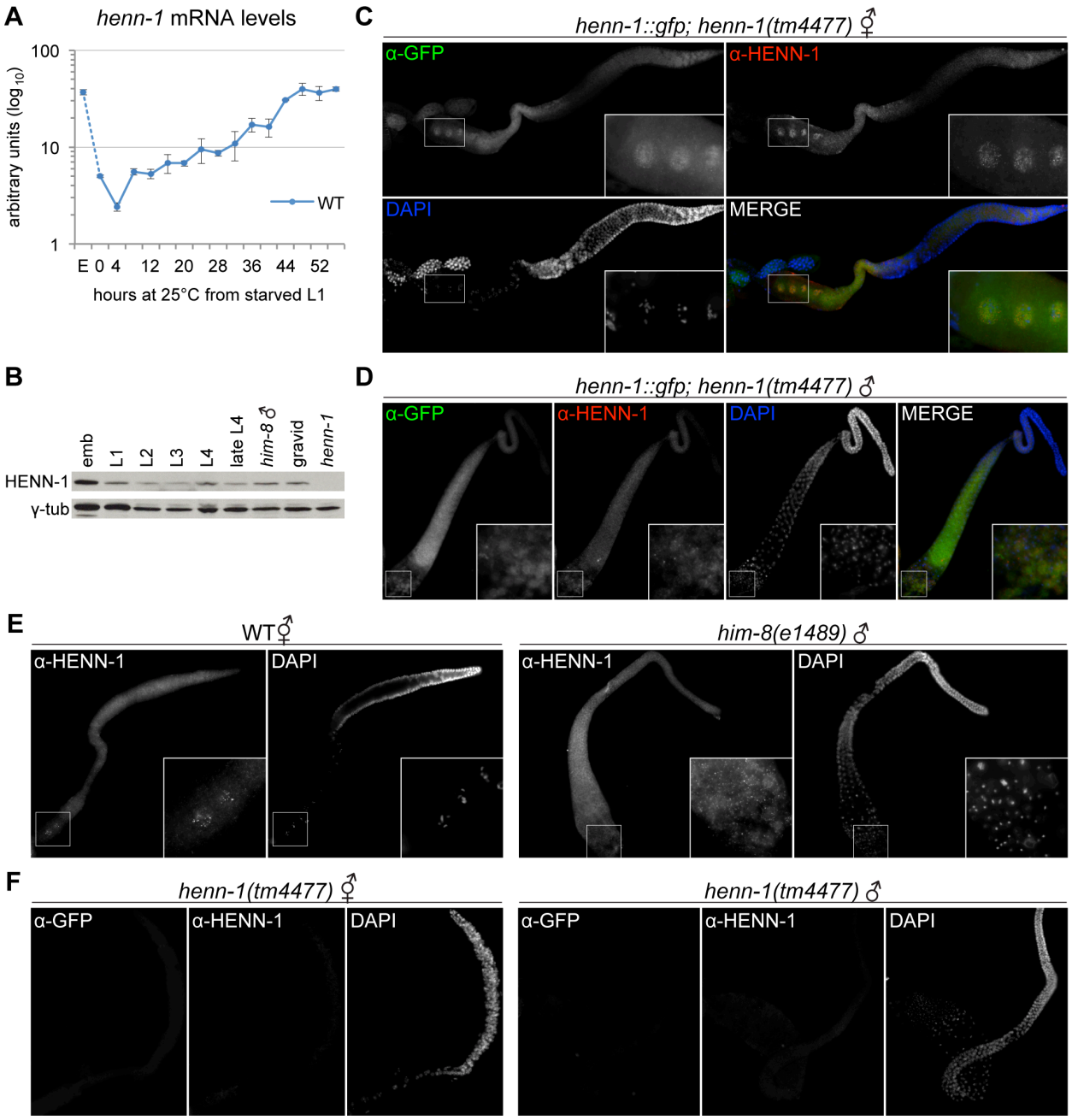
A
henn-1 mRNA levels
100
10
1
arbitrary units (log10)
WT
E 0 4 12 20 28 36 44 52
hours at 25°C from starved L1
B
emb
L1
L2
L3
L4
late L4
him-8 ♂
gravid
henn-1
HENN-1
γ-tub
C
henn-1::gfp; henn-1(tm4477) ♀
α-GFP
α-HENN-1
DAPI
MERGE
D
henn-1::gfp; henn-1(tm4477) ♂
α-GFP
α-HENN-1
DAPI
MERGE
E
WT ♀
α-HENN-1
DAPI
him-8(e1489) ♂
α-HENN-1
DAPI
F
henn-1(tm4477) ♀
α-GFP
α-HENN-1
DAPI
henn-1(tm4477) ♂
α-GFP
α-HENN-1
DAPI

Figure A-S1. Alignment of HEN1 Orthologs. A) *C. elegans* HENN-1 bears the conserved HEN1 methyltransferase domain. Protein sequences of HEN1 orthologs from *Caenorhabditis elegans* (NP_741250.1), *Drosophila melanogaster* (NP_610732.1), *Danio rerio* (NP_001017842.1), *Mus musculus* (NP_079999.2), *Homo sapiens* (NP_001096062.1), and *Arabidopsis thaliana* (NP_567616.1) were aligned using T-Coffee [79,80] with default parameters. The resulting multiple sequence alignment was cropped to show the conserved HEN1 methyltransferase domain (underlined in red) and the C terminus. Significant alignment was not observed for the N terminus. B) Conservation of the HEN1 methyltransferase domain of HENN-1 is comparable to that of other orthologs. Percent identity was calculated using ClustalW (version 2.1; http://www.ebi.ac.uk/Tools/msa/clustalw2/) [81,82] with default parameters to perform pairwise alignments of the conserved HEN1 methyltransferase domains as defined in Fig A-S1A.

S1A

```
C.elegans          -------ddheqrknffqpplqvqrnsfvkntlmefkrssqidisrlavmgcgemslekgiceylgsfgtin 146
D.melanogaster     -------tkmtetgitfdppvyeqrycatiqiledarw--kdqikkvvefgcaemrffqlmrri-etieh--  71
D.rerio            ------------tatpfspplymqryqfvidyvkt------yrprkvidfgcaecc1kklkfhrngiql--  53
M.musculus         --------vspekvirfkpplykqryqfvrdlvdr------hepkkvadlgcgdakllkllkiy-pciql--  74
H.sapiens          --------vpretaiqfkpplyrqryqfvknlvdq------hepkkvadlgcgdtsllrllkvn-pciel--  73
A.thaliana         llgvkgpseermeaaffkpplskqrveyalkhire------ssastlvdfgcgsgslldslldyptslqt-- 740
conservation                     *.**:  **   . . :            :  :**..  :   :      :

C.elegans          vlsvdidepslsigqqllgkaesiflrkhlernaeilavetglp-vlmrsyvgdilepdhrfadvdaivsme 217
D.melanogaster     iglvdidksllmrnltsvnplvsdyirs------------rasp-lkvqilqgnvadsseelrdtdaviaie 130
D.rerio            lvgvdinsvvllkrmhslaplvsdylqp------------sdgp-ltielyqgsvmerepctkgfdlvtcve 112
M.musculus         lvgvdineeklhsnghrlspylgefvkp------------rdld-ltvtlyhgsvverdsrllgfdlitcie 133
H.sapiens          lvgvdinedklrwrgdslapflgdflkp------------rdln-ltitlyhgsvverdsrllgfdlitcie 132
A.thaliana         iigvdispkglaraakmlhvk----lnk------------eacnvksatlydgsilefdsrlhdvdigtcle 796
conservation       :  ***.   *      :       :.                          *.: : .    . *   .:*

C.elegans          vvehiplpnakkfvenvlgtlmprififstpnheynavfgm--------------epgefrhgdhkfemnrk 275
D.melanogaster     liehvyddvlakipvnifgfmqpklvvfstpnsdfnviftrfn----------pllpngfrhedhkfewsrd 192
D.rerio            liehleleeverfsevvfgymapgavivttpnaefnpllpg--------------l-rgfrnyghkfewtra 169
M.musculus         liehldsddlarfpdvvfgylspamvvistpnaefnplfpt--------------v--tlrdadhkfewsrm 189
H.sapiens          liehldsgdlarfpevvfgylspsmivistpnsefnplfps--------------v--tlrdsdhkfewtrm 188
A.thaliana         viehmeedqacefgekvlslfhpkllivstpnyefntilqrstpetqeennsepqlp-kfrnhdhkfewtre 867
conservation       ::**:      .:   ::. : *  .:.:*** ::* ::                    :*. .**** .*

C.elegans          efsnwleelsirfphyqidpphyigmtrgyenlsgasqaavcrlqvdlnt---------t-lpqevtpyemv 337
D.melanogaster     efknwclgivekypnymfsltgvgnppkeyesvgpvsqiaifvrkdmlemqlvnplvskpnidkesipykli 264
D.rerio            efqtwahrvcreh-gysvqftgvgeaaghwrdvgfctqiavfqrnfdgvn---rsms-n-aehlepsvyrll 235
M.musculus         efqtwalhvancy-nyrveftgvgtppagsehvgyctqigvftknggkls---kpsv---sqqcdqhvykpv 254
H.sapiens          efqtwalyvanry-dysveftgvgeppagaenvgyctqigifrknggkat---escl---seqhdqhvykav 253
A.thaliana         qfnqwasklgkrh-nysvefsgvggs--gevepgfasqiaifrreassve---n-----va-essmqpykvi 927
conservation       :*. *   :   .  * .. .           .  :* .:   :                   .   *. :

C.elegans          g--hlpcrlgsrliaynlvkeafldw------le---------------------------------kie 366
D.melanogaster     htveypfyvdtrtekeklwtevqielqrfkrqfe---------------------------------sse 301
D.rerio            yrvvypslcdnniyqktlinevlyeaqhlrqqwlirenmnnnahfy--------spp--lmealhhgaegna 297
M.musculus         yttsypslqqekvlkfvlvgelliqvdrlrlryqrmlrdrekdrgpkpgdmdscpaphlllgavfteaekar 326
H.sapiens          fttsypslqqerffklvlvnevsqqveslrvshlprrkeqagergdkpkdiggskapvpcfgpvftevekak 325
A.thaliana         we---------------------------------------------------------------------- 929
conservation

C.elegans          lqeheprtdgyspywifnvqnil--h---hlkapv---------sfaltidek-va-ikyi-qgmtsrkvha 421
D.melanogaster     ieeg--t-yq--dtcnmpiafll--drlehvgatkerieelll-ennltvenecvlivssdqesews--dpy 363
D.rerio            ceq-qpv-yqqggiicvplarvwscprvqalcgslqrlrekllledervr--------m-------------- 345
M.musculus         ies-spkpfcegekfyiplqrlltypklhrlcadedrvrsli-ad-svc--------l-------------- 373
H.sapiens          ien-sptpfcvgdkffvplqrllaypklnrlcaneemmrsvi-ad-sip--------l-------------- 372
A.thaliana         ---------------------------------------------------------------------- 929
conservation

C.elegans          eys-hgf-ngivi---------lqmhskeelikt----------------------vqdntl          450
D.melanogaster     kfsdrssqddalv----------dqeqeeerwd----------------------qgpes           391
D.rerio            -----sadgsalnlpaddddnveeeeeeeeeenqqnvkavsgavnnmeedwdrelgsygde          402
M.musculus         -----ssdgsavv--------------------------------vdlhnswdy---rpeen          395
H.sapiens          -----ssdgsavv--------------------------------adlrnyfde----qfef          393
A.thaliana         ------------------------wkkedvek-----------------------kktdl          942
conservation
```

S1B

	C.e.	D.m.	D.r.	M.m.	H.s.
A.t	27%	22%	33%	33%	35%
H.s	23%	34%	50%	77%	
M.m	22%	35%	47%		
D.r.	18%	32%			
D.m.	23%				

% identity between HEN1 ortholog methyltransferase domains

Figure A-S2. *C02F5.6* Alleles and Transgenes. A) anti-HENN-1 polyclonal antibody recognizes a single ~52 kD HENN-1 isoform in wild-type embryo lysate; no protein product is detected in *henn-1(tm4477)* embryo lysate. B) *C02F5.6* (*henn-1*) gene structure showing the encoded N-terminal epitope for generating the anti-HENN-1 rabbit polyclonal antibody, conserved HEN1 domain (pink), and deletion region for the *henn-1(tm4477)* allele (red underline). Aberrant splicing of *henn-1(tm4477)* mRNA is diagrammed below. Activation of a cryptic splice donor site in the *henn-1(tm4477)* mRNA produces a premature termination codon (STOP). C) Diagrams of *xkSi1* (endogenous expression) and *xkSi2* (germline-only expression) *henn-1::gfp* transgenes. Transgenes were inserted as single copies on chromosome II via the MosSCI technique [52].

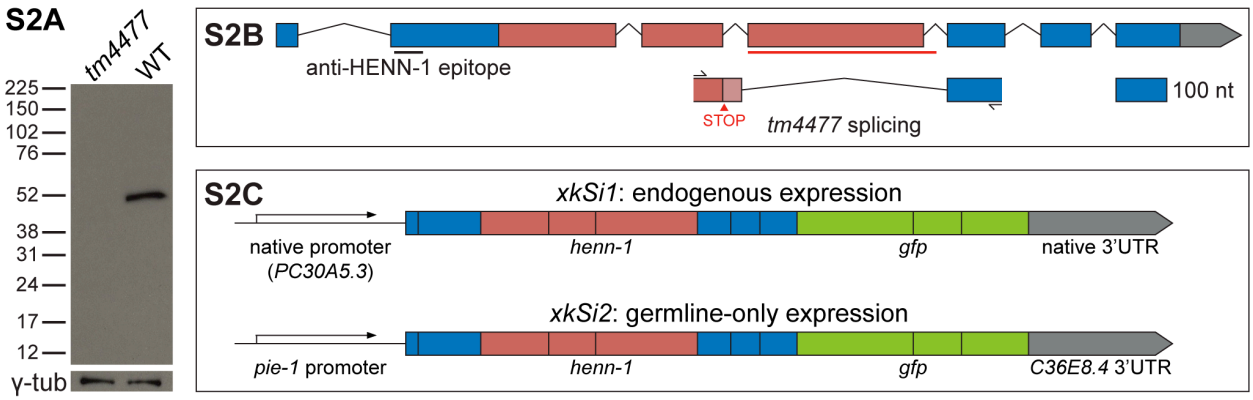

Figure A-S3. Methylation Status of Additional Small RNAs. A) Additional 21U RNAs show HENN-1-dependent methylation. β-eliminated (βe +) or control treated (βe -) embryo RNA of the indicated genotypes was probed for the specified 21U RNAs. Below, ethidium bromide staining of 5.8S rRNA. *prg-1(tm872)* lacks 21U RNAs and is included as a negative control. B) Additional ERGO-1 class 26G RNAs show HENN-1-dependent methylation in embryo RNA. *eri-1(mg366)* lacks 26G RNAs and is included as a negative control. C) ALG-3/ALG-4 class 26G RNA 26G-S7 shows absence of methylation in *him-8(e1489)* male RNA.

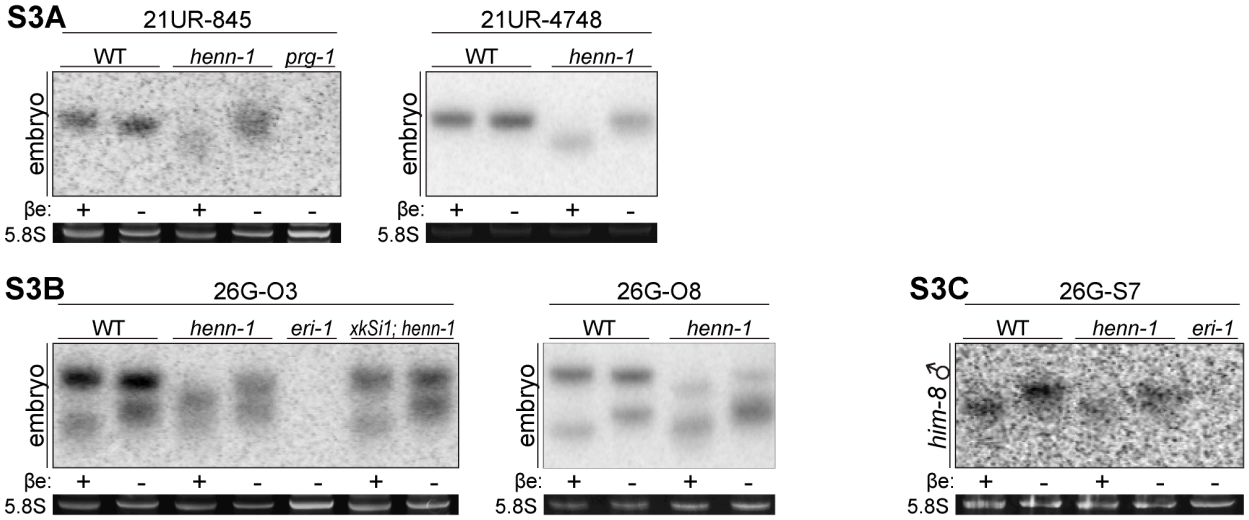

Figure A-S4. Diverse 21U RNAs Exhibit HENN-1 Dependence in Early Development and Adulthood. A) A panel of additional 21U RNAs exhibit significant defects in accumulation in the *henn-1(tm4477)* mutant. 21U RNA levels were assayed by Taqman qPCR in wild-type and *henn-1(tm4477)* mutant animals at the indicated developmental time points. Standard deviation is shown for biological triplicates. B) 21U RNAs are generally depleted in the *henn-1(tm4477)* mutant relative to wild-type in embryo, early larva, and gravid adult. Abundance in *henn-1(tm4477)* mutant relative to wild-type was calculated for the 21U RNAs shown in A) and Fig A-2A and the average was plotted for each time point to illustrate the general effect of loss of *henn-1*. C) 21U RNA Taqman assays specifically detect piRNAs. 21U RNA and miRNA levels were assayed in *prg-1(tm872)* mutant embryo biological duplicates. Fold levels relative to wild-type embryo are plotted. E, embryo.

S4A

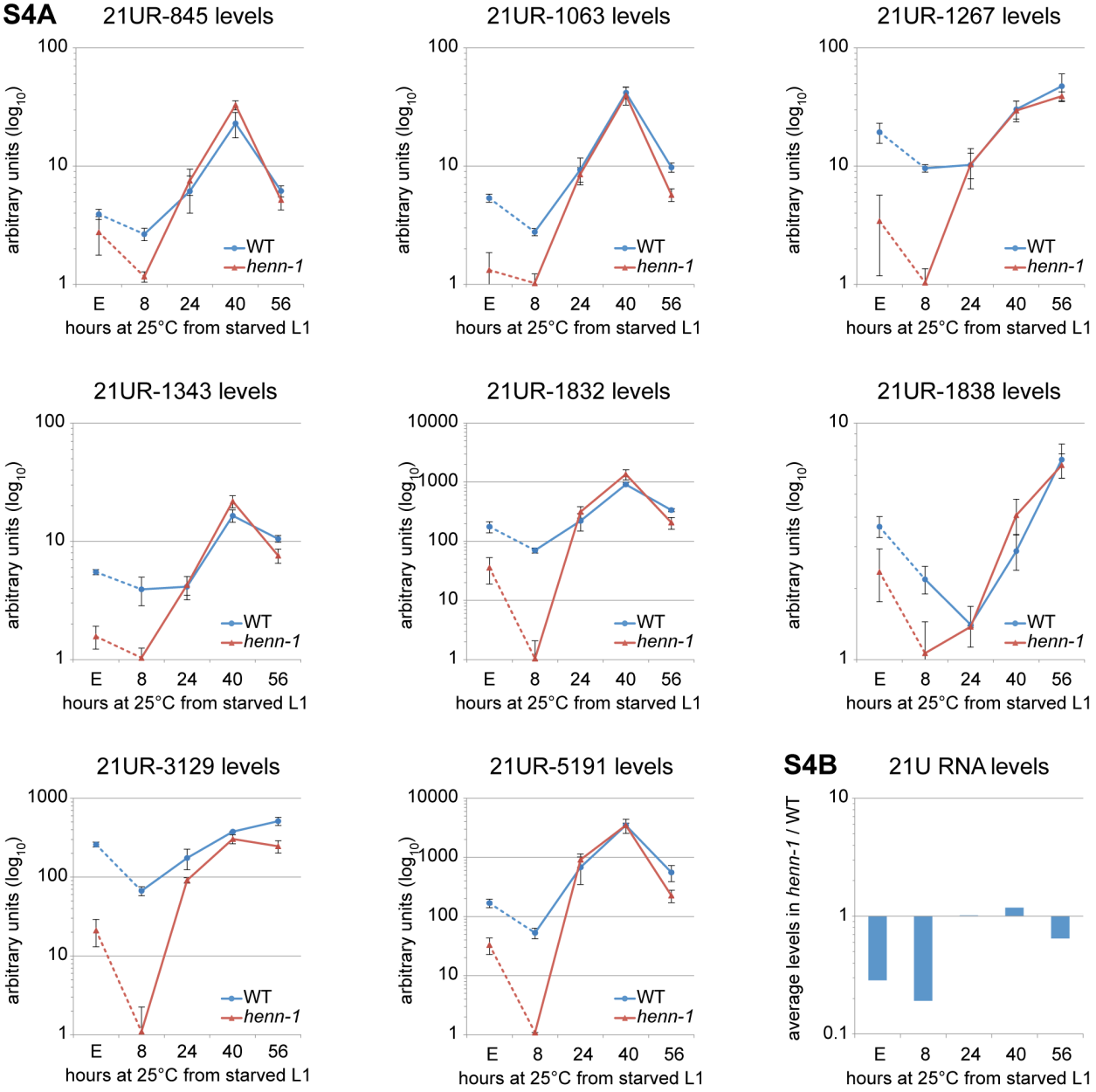
21UR-845 levels
21UR-1063 levels
21UR-1267 levels
21UR-1343 levels
21UR-1832 levels
21UR-1838 levels
21UR-3129 levels
21UR-5191 levels
arbitrary units (log10)
WT
henn-1
E 8 24 40 56
hours at 25°C from starved L1

S4B

21U RNA levels
average levels in henn-1 / WT
E 8 24 40 56
hours at 25°C from starved L1

S4C

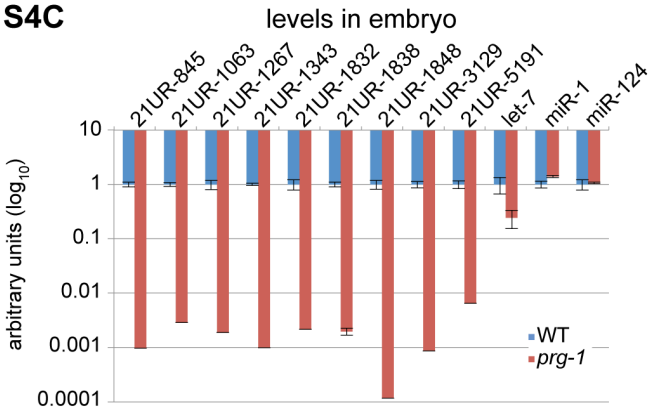
levels in embryo
21UR-845
21UR-1063
21UR-1267
21UR-1343
21UR-1832
21UR-1838
21UR-1848
21UR-3129
21UR-5191
let-7
miR-1
miR-124
arbitrary units (log10)
WT
prg-1

Figure A-S5. miRNAs Do Not Exhibit HENN-1 Dependence. A) miRNAs are generally unaffected in the *henn-1(tm4477)* mutant. miRNA levels were assayed by Taqman qPCR in wild-type and *henn-1(tm4477)* mutant animals at the developmental time points assessed in Fig A-S4. Standard deviation is shown for biological triplicates. B) miRNAs are not generally depleted in the *henn-1(tm4477)* mutant relative to wild-type. Abundance in *henn-1(tm4477)* mutant relative to wild-type was calculated for the miRNAs shown in A) and the average was plotted for each time point to illustrate the general effect of loss of *henn-1*. E, embryo.

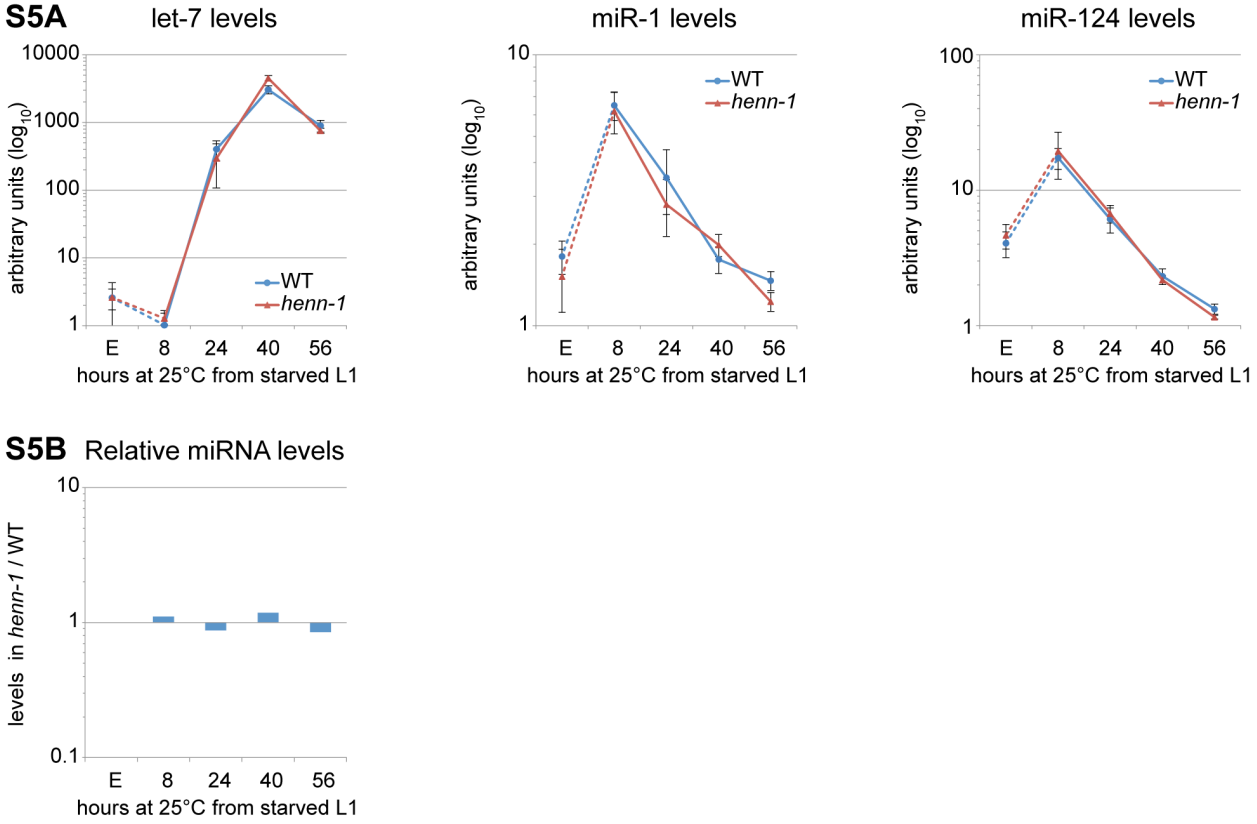

Figure A-S6. HENN-1 Dependence of Substrate-dependent Secondary siRNAs. A) Levels of a Wago-dependent, 21U RNA-dependent 22G RNA targeting *Tc3* are decreased in *henn-1(tm4477)* mutant embryo (P=0.0064; two-tailed *t*-test). Standard deviation is shown for biological triplicates. B) Levels of a Wago-dependent, ERGO-1 class 26G RNA-dependent 22G RNA targeting *E01G4.7* are decreased in *henn-1(tm4477)* mutant embryo (P=0.044; two-tailed *t*-test). Standard deviation is shown for biological triplicates.

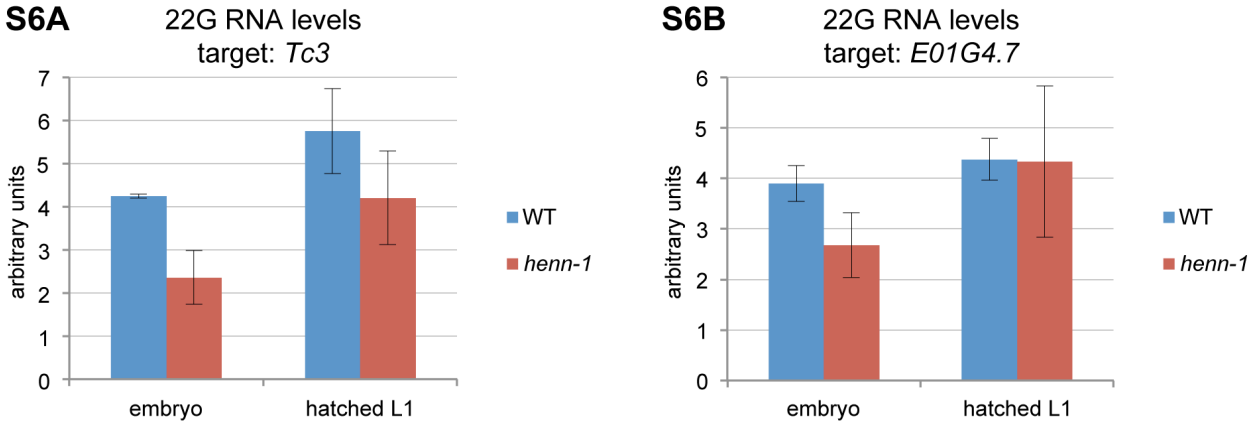

Figure A-S7. *henn-1* Contributes to Robust Fertility at Elevated Temperatures. *henn-1(tm4477)* mutant animals exhibit a modest fertility defect at 25°C that is rescued by germline-specific expression of *henn-1::gfp* from transgene *xkSi2*. Progeny per animal cultured at 20°C or shifted to 25°C for three generations is plotted for animals of the indicated genotype. Differences between *henn-1(tm4477)* mutant and wild-type or *xkSi2; henn-1(tm4477)* transgenic rescue strain are statistically significant (*: P=0.0059; **: P=0.0130, two-tailed *t*-test). N ≥ 13 animals per strain. Mean and standard deviation are shown.

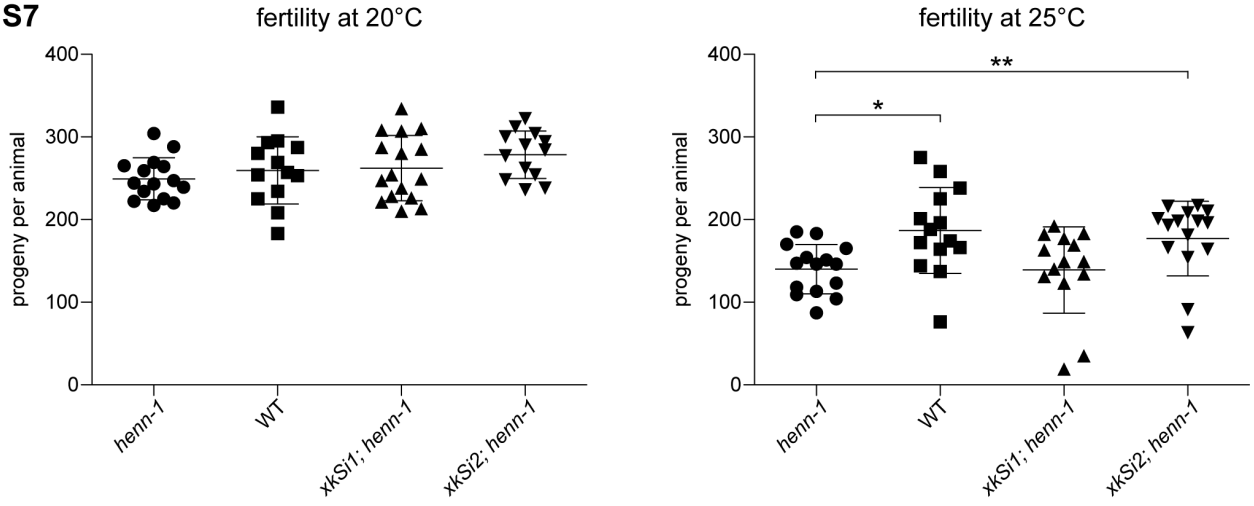

Figure A-S8. Many ERGO-1 Class 26G RNAs Exhibit HENN-1 Dependence throughout Development. A) A panel of additional ERGO-1 class 26G RNAs exhibit significant defects in accumulation in the *henn-1(tm4477)* mutant. ERGO-1 class 26G RNA levels were assayed by Taqman qPCR in wild-type and *henn-1(tm4477)* mutant animals at the indicated developmental time points. Standard deviation is shown for biological triplicates. B) ERGO-1 class 26G RNAs are generally depleted in the *henn-1(tm4477)* mutant relative to wild-type throughout development. Abundance in *henn-1(tm4477)* mutant relative to wild-type was calculated for the 26G RNAs shown in A) and Fig A-5A and the average was plotted for each time point to illustrate the general effect of loss of *henn-1*. C) ERGO-1 class 26G RNA Taqman assays specifically detect ERI-1-dependent small RNAs. ERGO-1 class 26G RNA and miRNA levels were assayed in *eri-1(mg366)* mutant embryo biological duplicates. Fold levels relative to wild-type embryo are plotted. E, embryo.

S8A

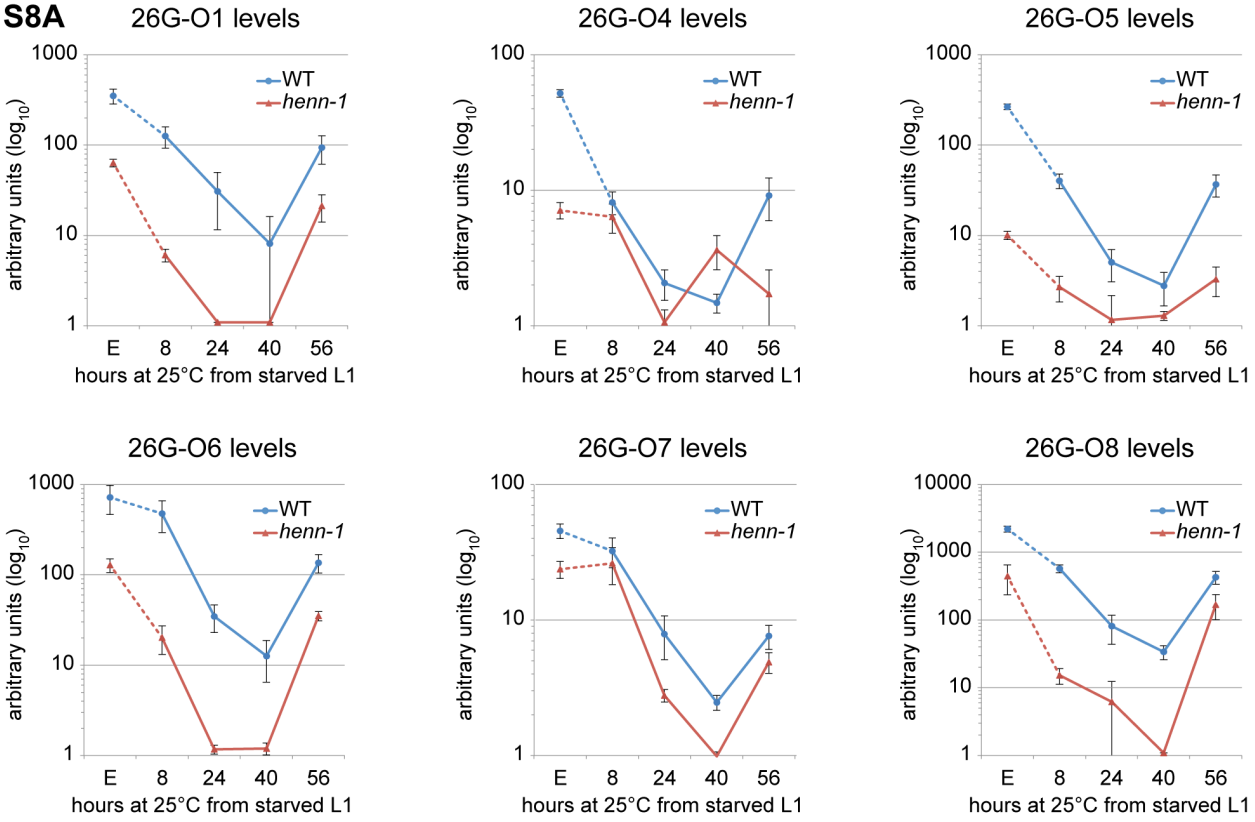
26G-O1 levels
26G-O4 levels
26G-O5 levels
26G-O6 levels
26G-O7 levels
26G-O8 levels
26G-O9 levels
WT
henn-1
arbitrary units (log10)
hours at 25°C from starved L1
E
8
24
40
56

S8B

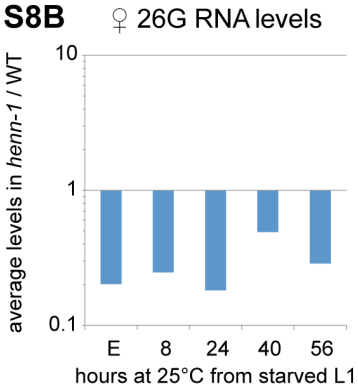
♀ 26G RNA levels
average levels in henn-1 / WT
hours at 25°C from starved L1

S8C

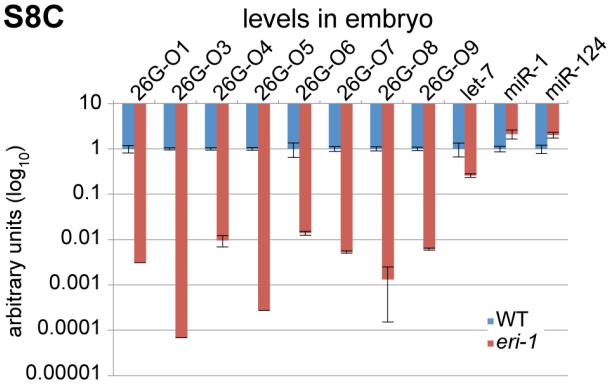
levels in embryo
26G-O1
26G-O3
26G-O4
26G-O5
26G-O6
26G-O7
26G-O8
26G-O9
let-7
miR-1
miR-124
arbitrary units (log10)
WT
eri-1

Figure A-S9. ALG-3/ALG-4 Class 26G RNAs Do Not Exhibit HENN-1 Dependence. A) Additional ALG-3/ALG-4 class 26G RNAs do not exhibit significant defects in accumulation in the *henn-1(tm4477)* mutant. ALG-3/ALG-4 class 26G RNA levels were assayed by Taqman qPCR in wild-type and *henn-1(tm4477)* mutant animals at the indicated developmental time points. Standard deviation is shown for biological triplicates. B) ALG-3/ALG-4 class 26G RNAs are generally unchanged in the *henn-1(tm4477)* mutant relative to wild-type during their peak expression. Abundance in *henn-1(tm4477)* mutant relative to wild-type was calculated for the 26G RNAs shown in A) and Fig A-5B and the average was plotted for each time point to illustrate the general effect of loss of *henn-1*. C) ALG-3/ALG-4 class 26G RNA Taqman assays specifically detect ERI-1-dependent small RNAs. ALG-3/ALG-4 class 26G RNA and miRNA levels were assayed in *eri-1(mg366); him-8(e1489)* mutant male biological duplicates. Fold levels relative to wild-type male are plotted. D) miRNAs are generally unaffected in the *henn-1(tm4477)* mutant. miRNA levels were assayed by Taqman qPCR in wild-type and *henn-1(tm4477)* mutant animals at the developmental time points assessed in A. Standard deviation is shown for biological triplicates. B) miRNAs are not generally depleted in *henn-1(tm4477)* mutant relative to wild-type animals. Abundance in *henn-1(tm4477)* mutant relative to wild-type was calculated for the miRNAs shown in D) and the average was plotted for each time point to illustrate the general effect of loss of *henn-1*.

S9A

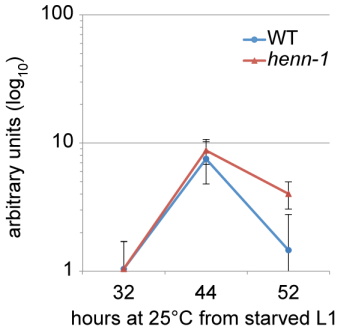

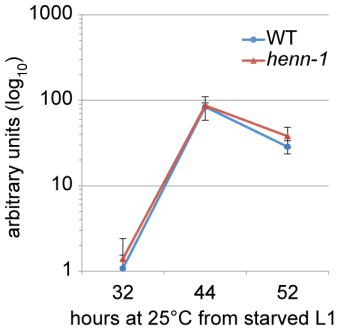

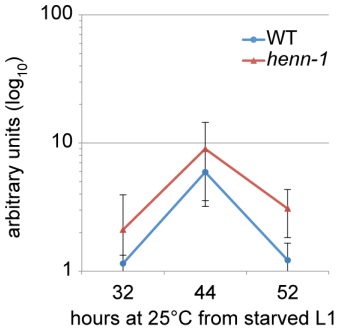

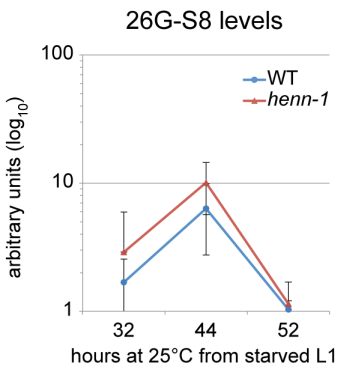

S9B

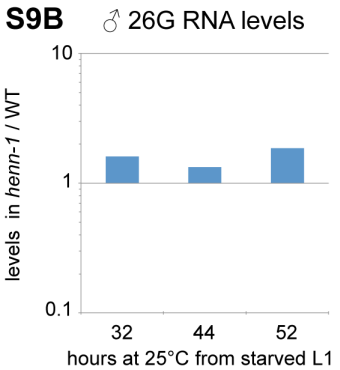

S9C

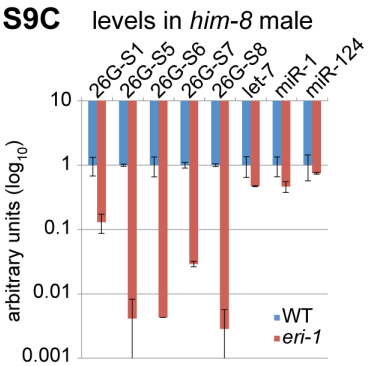

S9D

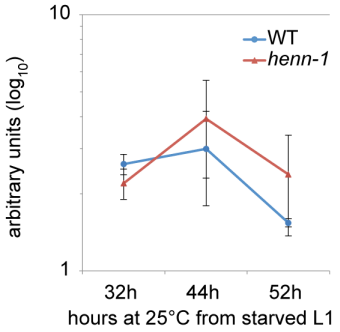

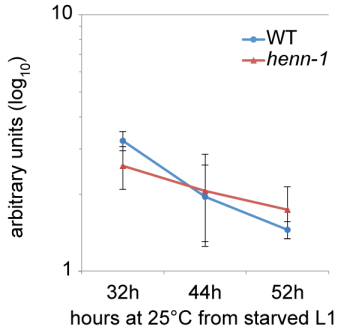

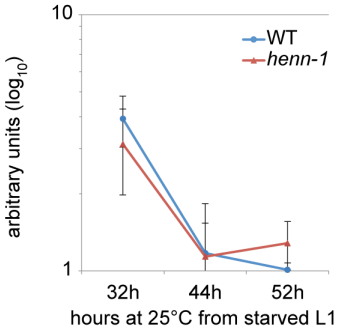

S9E

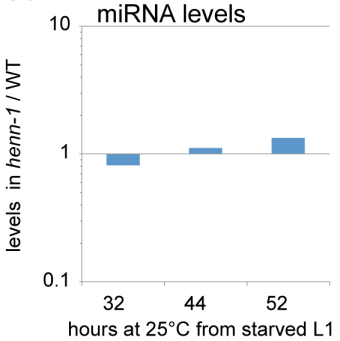

Figure A-S10. The *henn-1(tm4477)* Mutant Does Not Exhibit Significant Upregulation of ERGO-1 Class 26G RNA Target mRNAs. A) ERGO-1 class 26G RNA target mRNAs show only sporadic HENN-1 dependence. Data is summarized in Fig A-5C. Levels of eight ERGO-1 class 26G RNA targets were assayed across development of wild-type and *henn-1(tm4477)* mutant animals at 25°C and normalized to mRNA levels of *eft-2*, an abundantly expressed housekeeping gene. Standard deviation is shown for biological triplicates. B) Non-target mRNAs do not show upregulation in the *henn-1(tm4477)* mutant relative to wild-type. Levels of two non-target mRNAs were assayed across development of wild-type and *henn-1(tm4477)* mutant animals at 25°C and normalized to *eft-2*. Standard deviation is shown for biological triplicates. E, embryo.

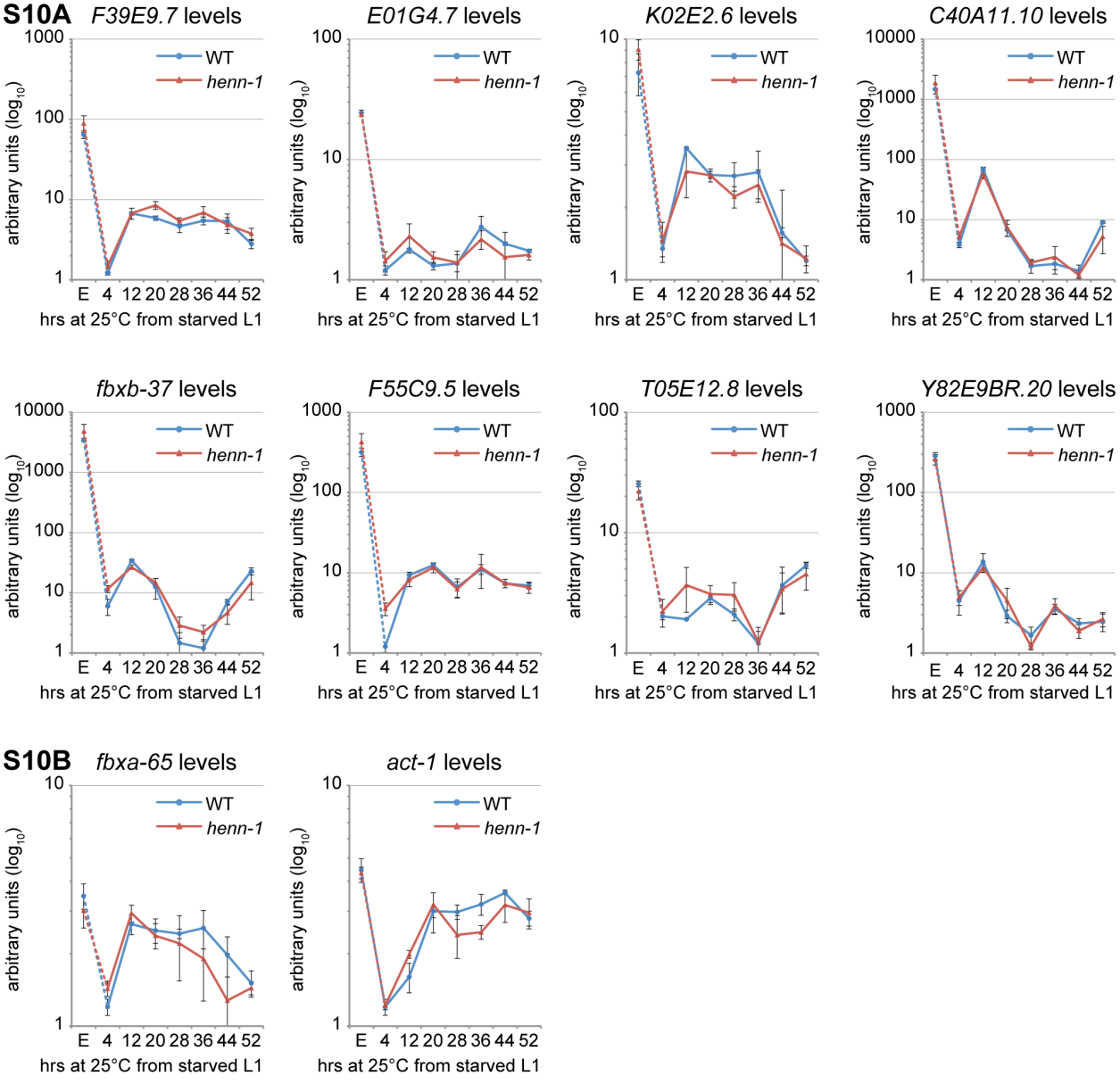

Figure A-S11. The *henn-1(tm4477)* Mutant Exhibits a Mild but General Somatic Eri Phenotype. A) *henn-1(tm4477)* mutant animals are weakly somatic Eri to RNAi knockdown of *dpy-13*. Animals of the indicated genotypes were plated as L1 larvae on *dpy-13* feeding RNAi diluted 1:2 or 1:5 (1/3 or 1/6 strength) with empty vector and grown for 90 hours at 20°C. *eri-1(mg366)* and *rde-4(ne301)* are included as controls. B) *henn-1(tm4477)* mutant animals are weakly somatic Eri to RNAi knockdown of *lin-29*. Animals of the indicated genotypes were plated as L1 larvae on *lin-29* feeding RNAi diluted 1:2 (1/3 strength) or 1:5 (1/6 strength) with empty vector and grown for 70 hours at 20°C. Percent of animals reaching full size without exhibiting protruding vulva or bursting is plotted. N = 4 plates of >50 animals per strain. Mean and standard deviation are shown.

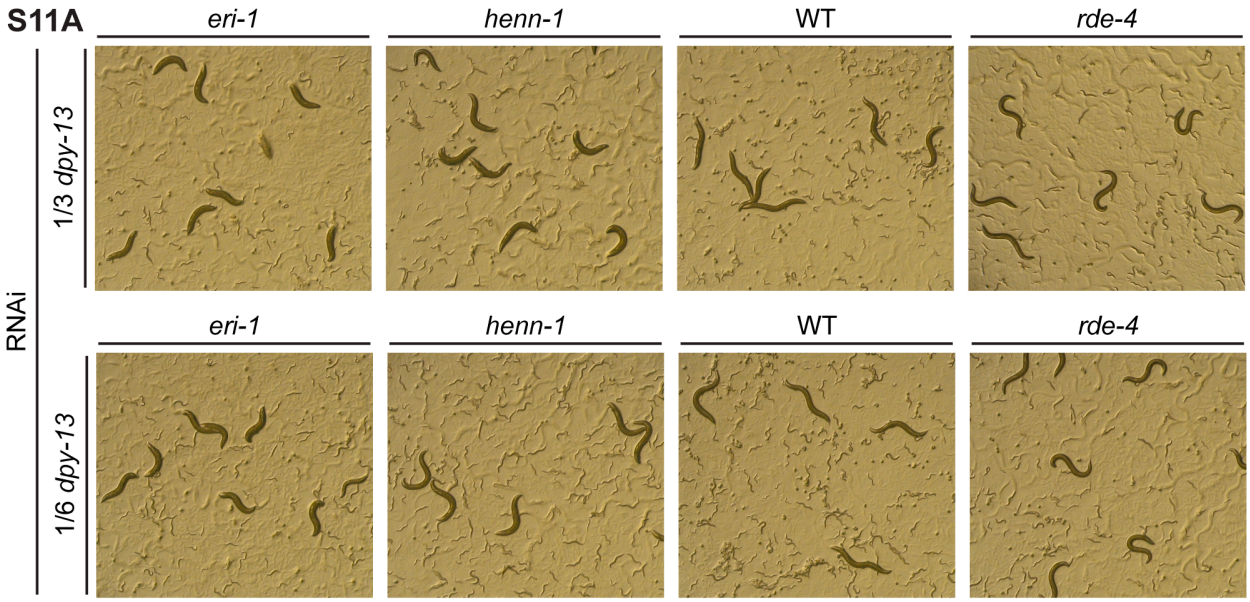

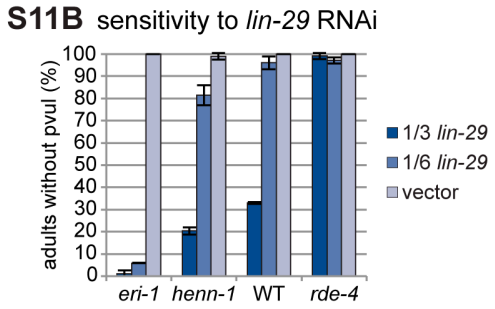

Figure A-S12. The *henn-1(tm4477)* Mutant Exhibits a General Germline Rde Phenotype. A) *henn-1(tm4477)* mutant animals are Rde to RNAi knockdown of germline genes. Animals of the indicated genotypes were plated as L1 larvae on *par-1*, *par-2*, or *pie-1* feeding RNAi diluted to the indicated strengths with empty vector and grown for 6 days at 20°C. Brood size averaged to the number of P_0 L1s per plate is plotted. N = 4 plates of 4 P_0 animals per strain. Mean and standard deviation are shown. *: P=0.0234; **: P=0.0028; ***: P=0.0151; ****: P=0.0098, two-tailed *t*-test. B) *henn-1(tm4477)* mutant animals are weakly Rde to RNAi knockdown of germline development gene *glp-1*. Animals of the indicated genotypes were plated as L1 larvae on *glp-1* feeding RNAi and grown for 70 hours at 20°C. Percent of animals failing to develop both arms of the germline is plotted. *rde-4(ne301)* is included as a control. N = 4 plates of >50 animals per strain. Mean and standard deviation are shown. †: P=0.0424, two-tailed *t*-test.

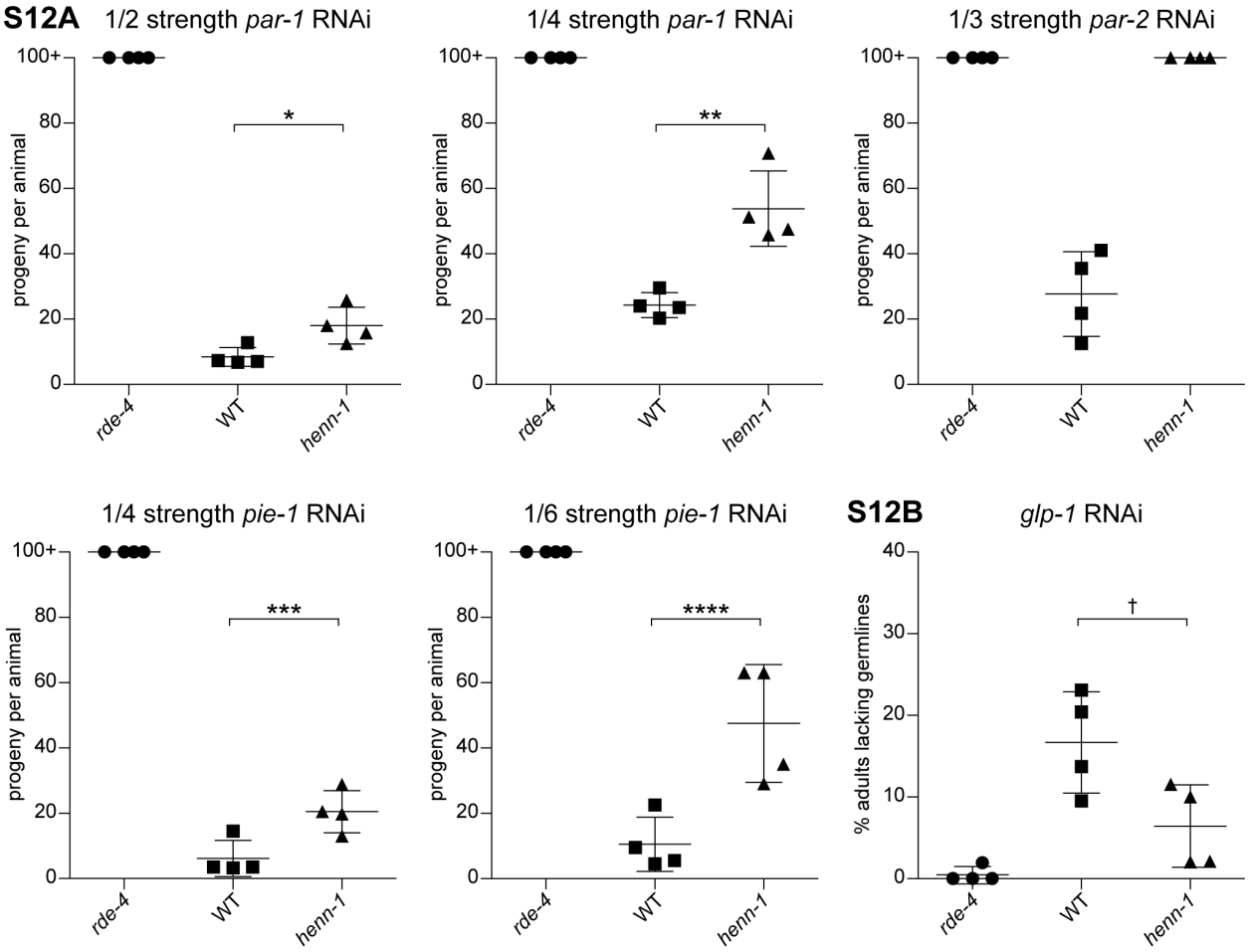

Figure A-S13. HENN-1 is Broadly Expressed in the Germline and Soma. A) *henn-1* mRNA is highly expressed throughout development. Non-normalized *henn-1* mRNA levels are plotted relative to *eft-2* mRNA levels. The expression profile of *henn-1* is largely unaffected by normalization to *eft-2* (as shown in Fig A-7A). B) *henn-1* is expressed in germline and soma. Levels of *henn-1* mRNA were assayed in wild-type and *glp-4(bn2)* mutant animals grown for 56 hours at 25°C. C) HENN-1::GFP is broadly expressed in both germline and somatic tissues. HENN-1::GFP was detected in *xkSi1; henn-1(tm4477)* L4 larva but not wild-type control larva using anti-GFP mouse monoclonal antibody. D) ERGO-1 and HENN-1::GFP are generally abundant in early embryo; specificity of anti-ERGO-1 antibody in embryo is shown on right. E) ERGO-1 shows cytoplasmic enrichment in the hermaphrodite proximal germline. Extruded gonads of *xkSi1; henn-1(tm4477)* adult hermaphrodite were stained with anti-GFP and anti-HENN-1 antibodies. Staining of *ergo-1(tm1860)* mutant demonstrates specificity of anti-ERGO-1 antibody (right). F) GFP::ALG-3 expression overlaps with that of HENN-1 (inset: residual bodies). Extruded gonads of *gfp::alg-3* transgenic adult males were stained with anti-GFP and anti-HENN-1 antibodies. E, embryo.

S13A relative mRNA levels

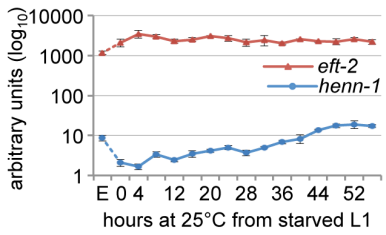

S13B *henn-1* levels at 25°C

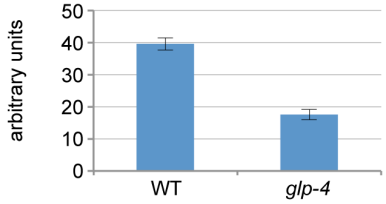

S13C

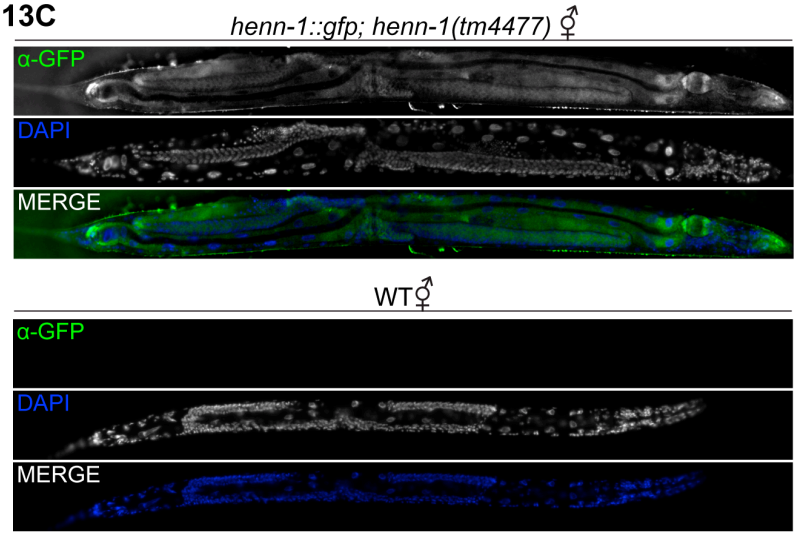

S13D

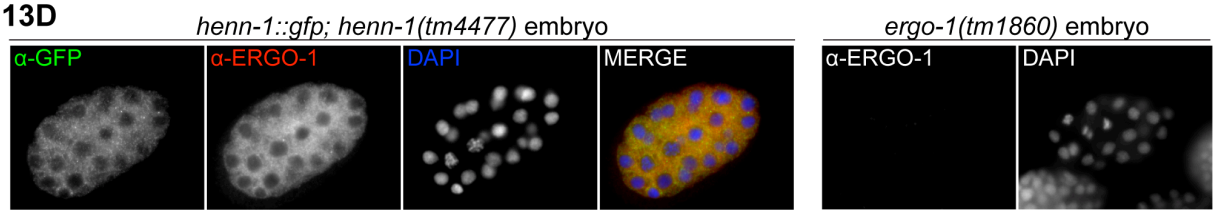

S13E

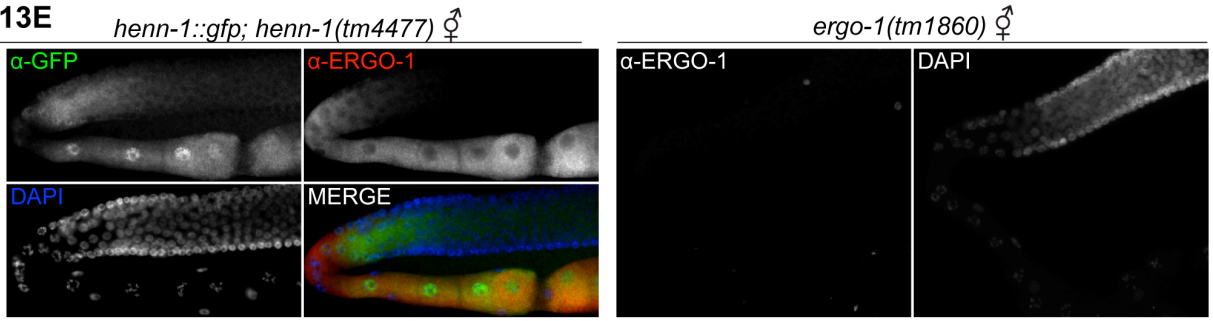

S13F

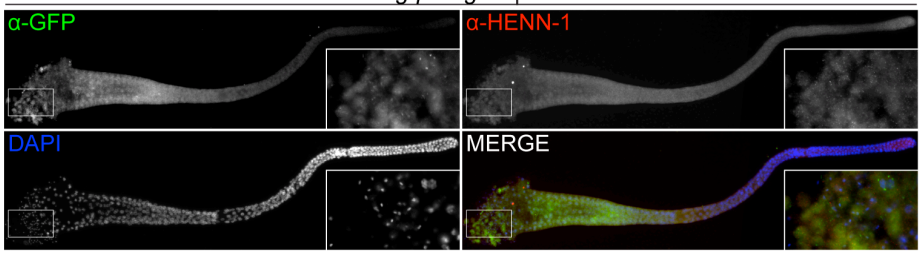

Figure A-S14: Comparison of *C. elegans* Argonautes. A) Phylogram of human, fly, and worm Argonautes shows divergence of CeERGO-1, CeRDE-1, and DmAgo2 relative to other members of their clades. Multiple sequence alignment of the longest annotated RefSeq protein sequences was performed using ClustalW with default parameters and visualized using Phylodendron (version 0.8d; http://www.es.embnet.org/Doc/phylodendron/). Scale, 0.1: 0.1 substitutions per site. B) Only Piwi clade Argonautes bear the characteristic PAZ domain insertion. Multiple sequence alignment of select Argonautes was performed using ClustalW with default parameters and cropped to show the context of the PAZ domain insertion between strands β6 and β7 as annotated by Tian et al. [69]. For each Argonaute, methylation status (MET) of associated small RNAs is indicated at right (Yes, methylated; No, not methylated). Sources: HsAGO1, [68,69] and by analogy to mouse [31]; DmAgo1, [19]; CeALG-1, [19]; CeALG-3, this study; HsPIWIL1, [69] and by analogy to mouse [30,31]; DmPiwi, [31,32]; CePRG-1, [27] and this study, DmAgo2, [9,22]; CeERGO-1, [27,42] and this study.

S14A

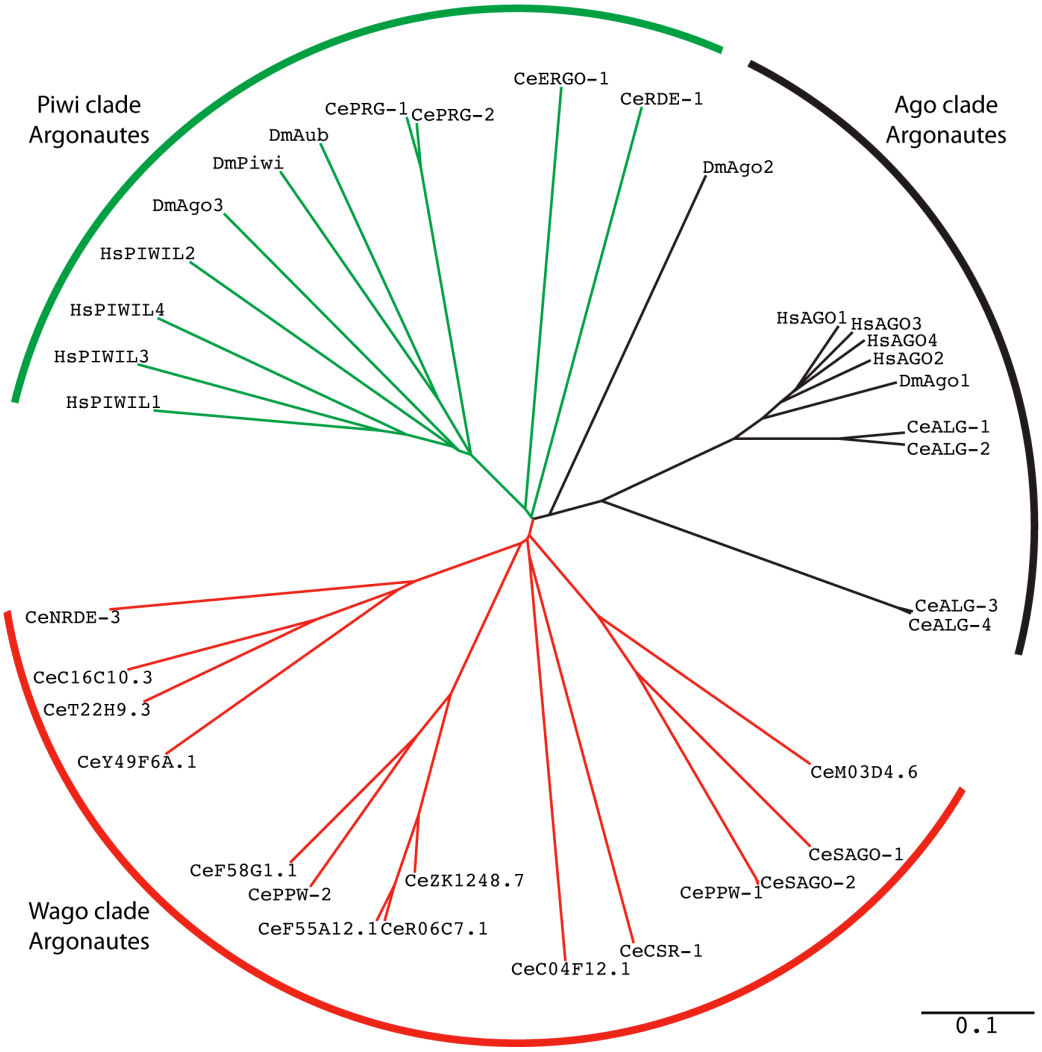

S14B

			β5 α3 β6 β7 β8		MET
HsAGO1	NP_036331.1	307	VECTVAQYFKQKYNLQLKYPHLPCLQVG---------QEQKHTYLPLEVCNIVAGQRCIK	352	No
DmAgo1	NP_725341.1	418	VECTVAKYFLDKYRMKLRYPHLPCLQVG---------QEHKHTYLPLEVCNIVAGQRCIK	463	No
CeALG-1	NP_510322.2	452	IECTVAKYFYDKYRIQLKYPHLPCLQVG---------QEQKHTYLPPEVCNIVPGQRCIK	497	No
CeALG-3	NP_502218.1	440	VVCSVADYFSEKYG-PLKYPKLPCLHVG---------PPTRNIFLPMEHCLIDSPQKYNK	484	No
HsPIWIL1	NP_004755.2	346	SEVSFLEYYRKQYNQEITDLKQPVLVSQPKRRRGPGGTLPGPAMLIPELCYLTG-LTDKM	397	Yes
DmPiwi	NP_476875.1	328	RDISFVEYYLTKYNIRIRDHNQPLLISK-NRDKALKTNASELVVLIPELCRVTG-LNAEM	378	Yes
CePRG-1	NP_492121.1	288	QSITLKEYFKNQYGIEITVDDQPIIISEGKPKQP--GEPPQVSYIVPELCFPTG-LTDEM	337	Yes
DmAgo2	NP_648775.1	682	KKVTIASYFHSRNY-PLKFPQLHCLNVG---------SSIKSILLPIELCSIEEGQALNR	723	Yes
CeERGO-1	NP_503362.2	485	VELTVADYYLQKYNIRLRYPNLPCVLKKAPEQCG----NKHSAMPLELVSYIVVPTRYGG	541	Yes
CeRDE-1	NP_741611.1	380	KYDTTLFKIYEENKKFIEFPHLPLVKVKS--------GAKEYAVPMEHLEVHEKPQRYKN	427	?

Table A-S1. Oligonucleotides for Northern Blot Analysis. Oligonucleotides corresponding to the antisense sequences of small RNAs were synthesized by Integrated DNA Technologies and used for small RNA detection by northern blot.

Small RNA target	Probe sequence
cel-miR-1	5’ TACATACTTCTTTACATTCCA /3StarFire/ 3’
21UR-845	5’ TTCGAGTTCTTGCTTTCCTGA /3StarFire/ 3’
21UR-4292	5’ CCATTCTTTGTCACCCTCGTA /3StarFire/ 3’
21UR-4748	5’ TAGCCAGTACTCTACGTTGTA /3StarFire/ 3’
21UR-5941	5’ ATTAACCGTTCGTGCCCCGAA /3StarFire/ 3’
26G-O1	5' TTGAAAATAATCTACCGTTTCTGAGC /3StarFire/ 3'
26G-O3	5' AAAAGTATCCGACTTTCGAGTTTGTC /3StarFire/ 3'
26G-O7	5’ TTCCACGATCAGAAGGGATGTCACTC /3StarFire/ 3’
26G-O8	5’ TGCTGCGAAAACTGTGGATTTCCTAC /3StarFire/ 3’
26G-S5	5' TACCATGTCGCTCACTGCTGATCCAC /3StarFire/ 3'
26G-S7	5' CGATGATCATATTCTACTTCATTTTC /3StarFire/ 3'

Table A-S2. Small RNA Sequences for Taqman Probe Design. Sequences of the indicated small RNAs were submitted to Applied Biosystems for Taqman small RNA probe design and synthesis.

Small RNA	**Sequence (5' to 3')**
let-7	TGAGGTAGTAGGTTGTATAGTT
miR-1	TGGAATGTAAAGAAGTATGTA
miR-124	TAAGGCACGCGGTGAATGCCA
21UR-845	TCAGGAAAGCAAGAACTCGAA
21UR-1063	TGAGCGCATTTGTATACACTG
21UR-1267	TAGGAACGAAATGAACAAAAT
21UR-1343	TGAAGGAAGAGTACGAAACTT
21UR-1832	TTTAACAAATGACGGTAAATC
21UR-1838	TTGTTCTTCGTTCGGTCCAAA
21UR-1848	TAAAGGCAGAATTTTATCAAC
21UR-3129	TGTATGTAAAACTTTACGGCA
21UR-5191	TGTAAAAAGTTTTTTGATGTA
22G targeting *Tc3*	GAATCAGAACCAGTCTGGAGAT
22G targeting *E01G4.7*	GAGTGACATCCCTTCTGATCGT
26G-O1	GCTCAGAAACGGTAGATTATTTTCAA
26G-O3	GACAAACTCGAAAGTCGGATACTTTT
26G-O4	GAGGGGATAAGAGCTCGTCCGATGGC
26G-O5	GATGGGAATGCAGAAGAAAAGAGGGG
26G-O6	GTAGAAGGATTCATCTGGCATTTCAT
26G-O7	GAGTGACATCCCTTCTGATCGTGGAA
26G-O8	GATGAATCGTCGATAGAAAGACAAAC
26G-O9	GTAGGAAATCCACAGTTTTCGCAGCA
26G-S1	GCTATGGAGGACGAGAATACATAATT
26G-S5	GTGGATCAGCAGTGAGCGACATGGTA
26G-S6	GACTCTTCGACTTCGGCATTTGCGGA
26G-S7	GAAGAACGAAAATTTGAAGATGTATA
26G-S8	GAAAATGAAGTAGAATATGATCATCG

Table A-S3. Primers for RT-qPCR. RT-qPCR primers for detection of the indicated gene targets were synthesized by Integrated DNA Technologies.

Gene target	Forward (5' to 3')	Reverse (5' to 3')
act-1	CCAGGAATTGCTGATCGTATGCAGAA	TGGAGAGGGAAGCGAGGATAGA
C40A11.10	AATGGCTCCTTGAAAAGATCG	TACATTTCCGCCACGTTGAAA
E01G4.7	GCACAAGGTTTCGTTCTTGGTG	AGTGACATCCCTTCTGATCG
eft-2	TGTGTTTCCGGAGTGTGTGT	CCATCGTCGTCTCCGTAAGT
F39E9.7	CCCAGTGGCCCAATTAAACG	GCACAAGGTTTCGTTCTTGGTG
F55C9.5	ACCATTGGAGCACGTAAATCAA	GGTCCTAATAATAAAGTTGCGTCG
fbxa-65	ACTTACAAGGATCAAGAAAAGCG	CCTTGACCGCTATTCCGAGAAA
fbxb-37	CATAAGTCCTGGAAGCCATACTCC	ATCTTTCGATACGATGTATGTTCG
K02E2.6	CAGTGGTACAAGTGGGAGTAAACG	AATTGGCAAGTAACTGATTCCG
rem-1	GGAAGAGGGATGTGTTCAACG	TTCCAGTGCTGATGCGATCATA
ssp-16	GTCATCAAACAACAATGAGTACCG	GCTCCAGCAGTGCGAGTGAT
T05E12.8	TTCCATTTGAGGATTTTGCTACG	ATTATTTGGATGGCAGCCGATG
Tc3	GAGCGTTCACGGAGAAGAAG	AATAGTCGCGGGTTGAGTTG
Y82E9BR.20	CTCCCGCTTTCTTGATGTATTG	AGTCCGAACTCATCCAAAGCAG

REFERENCES

1. Lee RC, Feinbaum RL, Ambros V (1993) The C. elegans heterochronic gene lin-4 encodes small RNAs with antisense complementarity to lin-14. Cell 75: 843-854.
2. Wightman B, Ha I, Ruvkun G (1993) Posttranscriptional regulation of the heterochronic gene lin-14 by lin-4 mediates temporal pattern formation in C. elegans. Cell 75: 855-862.
3. Kim Y-K, Heo I, Kim VN (2010) Modifications of small RNAs and their associated proteins. Cell 143: 703-709.
4. Kawahara Y, Zinshteyn B, Sethupathy P, Iizasa H, Hatzigeorgiou AG, et al. (2007) Redirection of silencing targets by adenosine-to-inosine editing of miRNAs. Science 315: 1137-1140.
5. Kawahara Y, Megraw M, Kreider E, Iizasa H, Valente L, et al. (2008) Frequency and fate of microRNA editing in human brain. Nucleic Acids Research 36: 5270-5280.
6. Kawahara Y, Zinshteyn B, Chendrimada TP, Shiekhattar R, Nishikura K (2007) RNA editing of the microRNA-151 precursor blocks cleavage by the Dicer-TRBP complex. EMBO Rep 8: 763-769.
7. Yang W, Chendrimada TP, Wang Q, Higuchi M, Seeburg PH, et al. (2006) Modulation of microRNA processing and expression through RNA editing by ADAR deaminases. Nat Struct Mol Biol 13: 13-21.
8. Hundley HA, Bass BL (2010) ADAR editing in double-stranded UTRs and other noncoding RNA sequences. Trends in biochemical sciences 35: 377-383.
9. Kawamura Y, Saito K, Kin T, Ono Y, Asai K, et al. (2008) Drosophila endogenous small RNAs bind to Argonaute 2 in somatic cells. Nature 453: 793-797.
10. Nejepinska J, Malik R, Filkowski J, Flemr M, Filipowicz W, et al. (2012) dsRNA expression in the mouse elicits RNAi in oocytes and low adenosine deamination in somatic cells. Nucleic Acids Research 40: 399-413.
11. Shen B, Goodman HM (2004) Uridine addition after microRNA-directed cleavage. Science 306: 997.
12. van Wolfswinkel JC, Claycomb JM, Batista PJ, Mello CC, Berezikov E, et al. (2009) CDE-1 affects chromosome segregation through uridylation of CSR-1-bound siRNAs. Cell 139: 135-148.
13. Ameres SL, Horwich MD, Hung J-H, Xu J, Ghildiyal M, et al. (2010) Target RNA-directed trimming and tailing of small silencing RNAs. Science 328: 1534-1539.
14. Ibrahim F, Rymarquis LA, Kim EJ, Becker J, Balassa E, et al. (2010) Uridylation of mature miRNAs and siRNAs by the MUT68 nucleotidyltransferase promotes their degradation in Chlamydomonas. Proc Natl Acad Sci U S A 107: 3906-3911.
15. Kamminga LM, Luteijn MJ, den Broeder MJ, Redl S, Kaaij LJ, et al. (2010) Hen1 is required for oocyte development and piRNA stability in zebrafish. EMBO J 29: 3688-3700.
16. Li J, Yang Z, Yu B, Liu J, Chen X (2005) Methylation protects miRNAs and siRNAs from a 3'-end uridylation activity in Arabidopsis. Curr Biol 15: 1501-1507.
17. Tkaczuk KL, Obarska A, Bujnicki JM (2006) Molecular phylogenetics and comparative modeling of HEN1, a methyltransferase involved in plant microRNA biogenesis. BMC Evol Biol 6: 6.

18. Park W, Li J, Song R, Messing J, Chen X (2002) CARPEL FACTORY, a Dicer homolog, and HEN1, a novel protein, act in microRNA metabolism in Arabidopsis thaliana. Curr Biol 12: 1484-1495.
19. Yu B, Yang Z, Li J, Minakhina S, Yang M, et al. (2005) Methylation as a crucial step in plant microRNA biogenesis. Science 307: 932-935.
20. Yang Z, Ebright YW, Yu B, Chen X (2006) HEN1 recognizes 21-24 nt small RNA duplexes and deposits a methyl group onto the 2' OH of the 3' terminal nucleotide. Nucleic Acids Res 34: 667-675.
21. Vilkaitis G, Plotnikova A, Klimasauskas S (2010) Kinetic and functional analysis of the small RNA methyltransferase HEN1: the catalytic domain is essential for preferential modification of duplex RNA. RNA 16: 1935-1942.
22. Horwich MD, Li C, Matranga C, Vagin V, Farley G, et al. (2007) The Drosophila RNA methyltransferase, DmHen1, modifies germline piRNAs and single-stranded siRNAs in RISC. Curr Biol 17: 1265-1272.
23. Saito K, Sakaguchi Y, Suzuki T, Siomi H, Siomi MC (2007) Pimet, the Drosophila homolog of HEN1, mediates 2'-O-methylation of Piwi- interacting RNAs at their 3' ends. Genes Dev 21: 1603-1608.
24. Kurth HM, Mochizuki K (2009) 2'-O-methylation stabilizes Piwi-associated small RNAs and ensures DNA elimination in Tetrahymena. RNA 15: 675-685.
25. Brennecke J, Aravin AA, Stark A, Dus M, Kellis M, et al. (2007) Discrete small RNA-generating loci as master regulators of transposon activity in Drosophila. Cell 128: 1089-1103.
26. Houwing S, Kamminga LM, Berezikov E, Cronembold D, Girard A, et al. (2007) A role for Piwi and piRNAs in germ cell maintenance and transposon silencing in Zebrafish. Cell 129: 69-82.
27. Ruby JG, Jan C, Player C, Axtell MJ, Lee W, et al. (2006) Large-scale sequencing reveals 21U-RNAs and additional microRNAs and endogenous siRNAs in C. elegans. Cell 127: 1193-1207.
28. Girard A, Sachidanandam R, Hannon GJ, Carmell MA (2006) A germline-specific class of small RNAs binds mammalian Piwi proteins. Nature 442: 199-202.
29. Lau NC, Seto AG, Kim J, Kuramochi-Miyagawa S, Nakano T, et al. (2006) Characterization of the piRNA complex from rat testes. Science 313: 363-367.
30. Kirino Y, Mourelatos Z (2007) Mouse Piwi-interacting RNAs are 2'-O-methylated at their 3' termini. Nat Struct Mol Biol 14: 347-348.
31. Ohara T, Sakaguchi Y, Suzuki T, Ueda H, Miyauchi K (2007) The 3' termini of mouse Piwi-interacting RNAs are 2'-O-methylated. Nat Struct Mol Biol 14: 349-350.
32. Vagin VV, Sigova A, Li C, Seitz H, Gvozdev V, et al. (2006) A distinct small RNA pathway silences selfish genetic elements in the germline. Science 313: 320-324.
33. Kirino Y, Mourelatos Z (2007) The mouse homolog of HEN1 is a potential methylase for Piwi-interacting RNAs. RNA 13: 1397-1401.
34. Reinhart BJ, Slack FJ, Basson M, Pasquinelli AE, Bettinger JC, et al. (2000) The 21-nucleotide let-7 RNA regulates developmental timing in Caenorhabditis elegans. Nature 403: 901-906.

35. Batista PJ, Ruby JG, Claycomb JM, Chiang R, Fahlgren N, et al. (2008) PRG-1 and 21U-RNAs interact to form the piRNA complex required for fertility in C. elegans. Mol Cell 31: 67-78.
36. Das PP, Bagijn MP, Goldstein LD, Woolford JR, Lehrbach NJ, et al. (2008) Piwi and piRNAs act upstream of an endogenous siRNA pathway to suppress Tc3 transposon mobility in the Caenorhabditis elegans germline. Mol Cell 31: 79-90.
37. Wang G, Reinke V (2008) A C. elegans Piwi, PRG-1, regulates 21U-RNAs during spermatogenesis. Current biology : CB 18: 861-867.
38. Cox DN, Chao A, Baker J, Chang L, Qiao D, et al. (1998) A novel class of evolutionarily conserved genes defined by piwi are essential for stem cell self-renewal. Genes & development 12: 3715-3727.
39. Ambros V, Lee RC, Lavanway A, Williams PT, Jewell D (2003) MicroRNAs and other tiny endogenous RNAs in C. elegans. Curr Biol 13: 807-818.
40. Han T, Manoharan AP, Harkins TT, Bouffard P, Fitzpatrick C, et al. (2009) 26G endo-siRNAs regulate spermatogenic and zygotic gene expression in Caenorhabditis elegans. Proc Natl Acad Sci U S A 106: 18674-18679.
41. Conine CC, Batista PJ, Gu W, Claycomb JM, Chaves DA, et al. (2010) Argonautes ALG-3 and ALG-4 are required for spermatogenesis-specific 26G-RNAs and thermotolerant sperm in Caenorhabditis elegans. Proc Natl Acad Sci U S A 107: 3588-3593.
42. Vasale JJ, Gu W, Thivierge C, Batista PJ, Claycomb JM, et al. (2010) Sequential rounds of RNA-dependent RNA transcription drive endogenous small-RNA biogenesis in the ERGO-1/Argonaute pathway. Proc Natl Acad Sci U S A 107: 3582-3587.
43. Yigit E, Batista PJ, Bei Y, Pang KM, Chen CC, et al. (2006) Analysis of the C. elegans Argonaute family reveals that distinct Argonautes act sequentially during RNAi. Cell 127: 747-757.
44. Zhang C, Montgomery TA, Gabel HW, Fischer SE, Phillips CM, et al. (2011) mut-16 and other mutator class genes modulate 22G and 26G siRNA pathways in Caenorhabditis elegans. Proceedings of the National Academy of Sciences of the United States of America 108: 1201-1208.
45. Gu W, Shirayama M, Conte D, Jr., Vasale J, Batista PJ, et al. (2009) Distinct argonaute-mediated 22G-RNA pathways direct genome surveillance in the C. elegans germline. Mol Cell 36: 231-244.
46. Sijen T, Steiner FA, Thijssen KL, Plasterk RHA (2007) Secondary siRNAs result from unprimed RNA synthesis and form a distinct class. Science 315: 244-247.
47. Pak J, Fire A (2007) Distinct populations of primary and secondary effectors during RNAi in C. elegans. Science 315: 241-244.
48. Okamura K, Chung WJ, Ruby JG, Guo H, Bartel DP, et al. (2008) The Drosophila hairpin RNA pathway generates endogenous short interfering RNAs. Nature 453: 803-806.
49. Huang Y, Ji L, Huang Q, Vassylyev DG, Chen X, et al. (2009) Structural insights into mechanisms of the small RNA methyltransferase HEN1. Nature 461: 823-827.
50. Ameres SL, Hung J-H, Xu J, Weng Z, Zamore PD (2011) Target RNA-directed tailing and trimming purifies the sorting of endo-siRNAs between the two Drosophila Argonaute proteins. RNA 17: 54-63.

51. Yang Z, Vilkaitis G, Yu B, Klimasauskas S, Chen X (2007) Approaches for studying microRNA and small interfering RNA methylation in vitro and in vivo. Meth Enzymol 427: 139-154.
52. Frokjaer-Jensen C, Davis MW, Hopkins CE, Newman BJ, Thummel JM, et al. (2008) Single-copy insertion of transgenes in Caenorhabditis elegans. Nat Genet 40: 1375-1383.
53. Chen C, Ridzon DA, Broomer AJ, Zhou Z, Lee DH, et al. (2005) Real-time quantification of microRNAs by stem-loop RT-PCR. Nucleic Acids Res 33: e179.
54. Montgomery TA, Rim Y-S, Zhang C, Dowen RH, Phillips CM, et al. (2012) PIWI associated siRNAs and piRNAs specifically require the *Caenorhabditis elegans* HEN1 ortholog henn-1. PLoS Genetics.
55. Duchaine TF, Wohlschlegel JA, Kennedy S, Bei Y, Conte D, Jr., et al. (2006) Functional proteomics reveals the biochemical niche of C. elegans DCR-1 in multiple small-RNA-mediated pathways. Cell 124: 343-354.
56. Lee RC, Hammell CM, Ambros V (2006) Interacting endogenous and exogenous RNAi pathways in Caenorhabditis elegans. RNA 12: 589-597.
57. Tabara H, Hill RJ, Mello CC, Priess JR, Kohara Y (1999) pos-1 encodes a cytoplasmic zinc-finger protein essential for germline specification in C. elegans. Development 126: 1-11.
58. Reinke V, Gil IS, Ward S, Kazmer K (2004) Genome-wide germline-enriched and sex-biased expression profiles in Caenorhabditis elegans. Development 131: 311-323.
59. Gent JI, Lamm AT, Pavelec DM, Maniar JM, Parameswaran P, et al. (2010) Distinct phases of siRNA synthesis in an endogenous RNAi pathway in C. elegans soma. Molecular Cell 37: 679-689.
60. Kawaoka S, Izumi N, Katsuma S, Tomari Y (2011) 3' end formation of PIWI-interacting RNAs in vitro. Molecular Cell 43: 1015-1022.
61. Forstemann K, Horwich MD, Wee L, Tomari Y, Zamore PD (2007) Drosophila microRNAs are sorted into functionally distinct argonaute complexes after production by dicer-1. Cell 130: 287-297.
62. Kamminga LM, van Wolfswinkel J, Luteijn MJ, Kaaij LJ, Bagjin MP, et al. (2012) Differential impact of the Hen1 homolog HENN-1 on 21U and 26G RNAs in the germline of *Caenorhabditis elegans*. PLoS Genetics.
63. Pelisson A, Sarot E, Payen-Groschene G, Bucheton A (2007) A novel repeat-associated small interfering RNA-mediated silencing pathway downregulates complementary sense gypsy transcripts in somatic cells of the Drosophila ovary. Journal of Virology 81: 1951-1960.
64. Cerutti L, Mian N, Bateman A (2000) Domains in gene silencing and cell differentiation proteins: the novel PAZ domain and redefinition of the Piwi domain. Trends Biochem Sci 25: 481.
65. Liu J, Carmell MA, Rivas FV, Marsden CG, Thomson JM, et al. (2004) Argonaute2 is the catalytic engine of mammalian RNAi. Science 305: 1437-1441.
66. Song JJ, Smith SK, Hannon GJ, Joshua-Tor L (2004) Crystal structure of Argonaute and its implications for RISC slicer activity. Science 305: 1434-1437.
67. Lingel A, Simon B, Izaurralde E, Sattler M (2004) Nucleic acid 3'-end recognition by the Argonaute2 PAZ domain. Nat Struct Mol Biol 11: 576-577.

68. Ma JB, Ye K, Patel DJ (2004) Structural basis for overhang-specific small interfering RNA recognition by the PAZ domain. Nature 429: 318-322.
69. Tian Y, Simanshu DK, Ma JB, Patel DJ (2011) Structural basis for piRNA 2'-O-methylated 3'-end recognition by Piwi PAZ (Piwi/Argonaute/Zwille) domains. Proceedings of the National Academy of Sciences 108: 903.
70. Boland A, Huntzinger E, Schmidt S, Izaurralde E, Weichenrieder O (2011) Crystal structure of the MID-PIWI lobe of a eukaryotic Argonaute protein. Proceedings of the National Academy of Sciences of the United States of America 108: 10466-10471.
71. L'Hernault SW, Roberts TM (1995) Cell biology of nematode sperm. Methods in cell biology 48: 273-301.
72. Pall GS, Hamilton AJ (2008) Improved northern blot method for enhanced detection of small RNA. Nature protocols 3: 1077-1084.
73. Kamath RS, Fraser AG, Dong Y, Poulin G, Durbin R, et al. (2003) Systematic functional analysis of the Caenorhabditis elegans genome using RNAi. Nature 421: 231-237.
74. Chen C, Ridzon DA, Broomer AJ, Zhou Z, Lee DH, et al. (2005) Real-time quantification of microRNAs by stem-loop RT-PCR. Nucleic Acids Research 33: e179.
75. Nolan T, Hands RE, Bustin SA (2006) Quantification of mRNA using real-time RT-PCR. Nature Protocols 1: 1559-1582.
76. Allen MA, Hillier LW, Waterston RH, Blumenthal T (2011) A global analysis of C. elegans trans-splicing. Genome research 21: 255-264.
77. Crittenden S, Kimble J (2009) Preparation and immunolabeling of Caenorhabditis elegans. Cold Spring Harbor protocols 2009: pdb prot5216.
78. Girard LR, Fiedler TJ, Harris TW, Carvalho F, Antoshechkin I, et al. (2007) WormBook: the online review of Caenorhabditis elegans biology. Nucleic Acids Research 35: D472-475.
79. Notredame C, Higgins DG, Heringa J (2000) T-Coffee: A novel method for fast and accurate multiple sequence alignment. Journal of molecular biology 302: 205-217.
80. Poirot O, O'Toole E, Notredame C (2003) Tcoffee@igs: A web server for computing, evaluating and combining multiple sequence alignments. Nucleic Acids Research 31: 3503-3506.
81. Larkin MA, Blackshields G, Brown NP, Chenna R, McGettigan PA, et al. (2007) Clustal W and Clustal X version 2.0. Bioinformatics 23: 2947-2948.
82. Goujon M, McWilliam H, Li W, Valentin F, Squizzato S, et al. (2010) A new bioinformatics analysis tools framework at EMBL-EBI. Nucleic Acids Research 38: W695-699.